OGP

Model based assessment of underwater noise from an airgun array soft-start operation

Report No. 451
February 2011

International Association of Oil & Gas Producers

OGP Publications

Global experience

The International Association of Oil & Gas Producers has access to a wealth of technical knowledge and experience with its members operating around the world in many different terrains. We collate and distil this valuable knowledge for the industry to use as guidelines for good practice by individual members.

Consistent high quality database and guidelines

Our overall aim is to ensure a consistent approach to training, management and best practice throughout the world.

The oil and gas exploration and production industry recognises the need to develop consistent databases and records in certain fields. The OGP's members are encouraged to use the guidelines as a starting point for their operations or to supplement their own policies and regulations which may apply locally.

Internationally recognised source of industry information

Many of our guidelines have been recognised and used by international authorities and safety and environmental bodies. Requests come from governments and non-government organisations around the world as well as from non-member companies.

Model based assessment of underwater noise from an airgun array soft-start operation

OGP Report No: 451
February 2011

Foreword

Geological surveys using marine seismic techniques are widely used in the oil & gas industry to detect and quantify accumulations of oil & gas in rock formations and, where hydrocarbon deposits are present in economically viable quantities, to assist through the life of the field in ensuring optimal recovery of the reserves. Seismic surveys are also used to study structures in shallower sediments and rock formations in preparing the ground for deployment and maintenance of facilities including platforms, pipelines and subsea installations.

Seismic data are typically acquired using a number of 'air-guns' that collectively provide a source of acoustic energy. High pressure compressed air is released from an array which is towed behind a seismic or source vessel; the pulsed signals are predominantly composed of low frequency energy. The signals are propagated deep into the earth where they are reflected when they encounter different geological layers. Reflected signals are recorded and analysed to build up a picture of sub-sea geological structures. The length of time needed for a survey is determined by the area to be surveyed and the efficiency of the vessel data acquisition operation.

Understanding the potential impacts of sounds generated during marine seismic surveys on marine life (and in particular on cetaceans) is a key environmental issue. There are two main concerns: physiological impacts on individuals – particularly on marine mammals – and behavioural impacts. In the former, the concern has been damage to or impairment of hearing and the impact this might have at the population level if a significant number of individuals are affected. In the latter, the consideration ranges from minor changes in behaviour that are not likely to cause any significant impact to marine life to significant events that could lead to death, such as stranding of animals. To date there is no evidence to show that sounds generated by air-gun sources have caused a stranding of animals. In terms of behavioural effects the focus has been on changes that potentially affect 'life functions' such as feeding, breeding and migrating.

This report focuses on potential physiological impacts on marine mammals

There are no experimental studies that provide specific information on the 'levels of sound' that can cause harm to marine mammals (harm is usually expressed in terms of permanent impairment of hearing – Permanent Threshold Shift or PTS). No animal has ever been tested to the point of PTS and experiments have been limited to generating Temporary Threshold Shifts (TTS). There are relatively few experiments that measure TTS as a result of exposure to pulsed sounds. In 2008, however, a group of leading scientific experts in the field of bioacoustics conducted a major review of the available scientific (peer-reviewed) literature and derived a series of Noise Exposure Criteria for marine mammals (often referred to as the "Southall Noise Exposure Criteria[†]"). The criteria, whose derivation contained a number of conservative assumptions, were expressed both in terms of sound pressure level and sound exposure level (a measure of the energy received by an animal). One aim of the work was to provide regulatory authorities with a more scientific basis for establishing permit conditions and mitigation requirements.

Marine seismic operations are generally strictly controlled by national regulatory authorities who will impose restrictions on operations that are designed in the most part at avoiding physical harm to animals. Restrictions include 'safety' or 'exclusion' zones around vessels, the use of Marine Mammal Observers (MMOs) and acoustic methods for detecting (locating and in some cases characterising) marine mammals.

† *Brandon L. Southall, Ann E. Bowles, William T. Ellison, James J. Finneran, Roger L. Gentry, Charles R. Greene Jr., David Kastak, Darlene R. Ketten, James H. Miller, Paul E. Nachtigall, W. John Richardson, Jeanette A. Thomas, & Peter L. Tyack (2007).* ***Marine Mammal Noise Exposure Criteria: Initial Scientific Recommendations****. Aquatic Mammals, Volume 33, Number 4, ISSN 0167-5427*

The *Guidelines for minimising acoustic disturbance to marine mammals from seismic surveys*, first published by the UK Joint Nature Conservation Committee (JNCC) in 1998 and revised in 2004, have become broadly accepted by a range of regulatory agencies across the world to the extent that they are a *de facto* 'mitigation standard' at least in terms of the approach they advocate. The JNCC guidelines were reviewed again in 2008 as part of a wider UK government consultation on 'disturbance' (arising from the EU Habitats Directive and its translation into UK law). The updated 2010 version of the Guidelines maintains the approach based on exclusion zones and Marine Mammal Observers, but made more specific reference to Passive Acoustic Monitoring (PAM).

Establishing safety zones around survey vessels is a common sense measure. Once the designated area around a survey vessel has been cleared, by visual observation and in some cases also using passive acoustic 'listening', the source array is started up over a period of 20 to 30 minutes – a soft-start or ramp-up procedure. First, a single air-gun element in the array is started and subsequently other elements in the array are added, increasing the sound towards the operating level. The idea is that animals are warned of an approaching load sound such that they move away. 'Soft start' has become a standard procedure for many geophysical survey companies as regulatory agencies adopt the approach as part of their required mitigation measures.

Recently, there has been growing concern about whether the inability to see animals at night or in poor visibility (fog or sea state) could lead to significantly greater risk to marine mammals (than soft-start conducted in good visibility) if soft-start is started too close to the animals. Limiting the soft-start procedure to only under 'good visibility' would significantly increase the costs of operations and could also lead to unintended consequences on marine mammals if feeding or migration were disrupted by the presence of survey vessels over extended periods of time.

This modelling study has been conducted to investigate whether soft-start – in a worst case scenario – might result in hearing damage to marine mammals. The initial assumptions included placing animals either directly in the path of an approaching vessel undergoing a 'typical' soft start procedure with source pulses generated every 25 metres, or being placed off to one side of the approaching vessel. It is assumed that a nominal 500 metre exclusion zone had been cleared before start up. Sound pressure levels and sound exposure levels are calculated at different locations relative to the source and compared to the relevant criteria published by Southall *et al*. The study was conducted by JASCO Applied Sciences of Victoria, Canada.

Two modelling approaches were used in this study. Initially a parabolic equation (PE) approach was used to model the sound field directly below and to the side of a source array, moving in a straight line during the initial stages of a soft-start procedure. However, this method was not able to predict sound energy propagating at very steep take off angles between the sound source and animal location, which represented when an animal was located directly under or close to the source array. It was expected the PE prediction would underestimate the exposure directly under the ship using this approach. To test this, an alternative wavenumber integration technique was used to model these high angle cases. With the wavenumber modelling approach, estimated sound levels were actually lower than predicted by the PE method for locations close to the source array. This suggested that the results derived from the PE modelling would be conservative for locations close to the source array. This step was important to validate and improve confidence in the results.

No instances were found in which the threshold levels for hearing injury for cetaceans were reached during the initial stages of the soft-start sequence. This suggests that the animals are not at significantly greater risk of harm when a soft-start is initiated in low visibility conditions. The threshold criterion for pinnipeds was approached in the worst case model. Thus, for example, where seismic surveys operate in the vicinity of a pinniped 'haul-out', additional mitigation might be in order to manage potential risks to animals.

MODEL BASED ASSESSMENT OF UNDERWATER NOISE FROM AN AIRGUN ARRAY SOFT-START OPERATION

By

David Hannay
Roberto Racca
Alex MacGillivray

JASCO Applied Sciences
Suite 2101 – 4464 Markham Street
Victoria, BC V8Z 7X8
Canada
Tel: +1.250.483.3300

for

International Association of Oil and Gas Producers (OGP)
209-215 Blackfriars Road
London, SE1 8NL
United Kingdom

8 October 2010

Contents

Tables

Figures

1 Introduction

This report presents results of an acoustic modelling study that estimates the received sound levels at locations in the water column near a towed seismic airgun array during a typical soft-start procedure in which the number and total volume of the airguns in the source array increase over time. The soft-start approach is a mitigation measure for reducing the risk that marine mammals near an airgun array are exposed to harmful sound levels as the seismic source starts to operate. The underlying assumption is that an animal will take evasive action and establish a safe distance between itself and the source when exposed to lower sound levels during the initial phases of the soft-start sequence. The main issue then becomes whether an animal might be exposed to sound levels that result in auditory injury from the exposure to sound levels from the reduced source. A modelling study was performed to quantify the received sound levels from a representative soft-start sequence, in both a shallow 50 m water depth scenario and a deep 2000 m water depth scenario, and to evaluate those sound levels in the context of current knowledge about injury thresholds.

The modelling studies were performed with JASCO's Airgun Array Source Model (AASM) and two acoustic propagation models: FWRAM and a custom wavenumber integral model. FWRAM is based on a parabolic equation method for fluid propagation media, extended to treat losses from compressional-to-shear wave conversions at bottom layer interfaces. It was recognized that the parabolic equation (PE) method does not accurately predict very steeply propagating sound energy and therefore produces inaccurate results at receiver positions directly under or close to the source airgun array. Close-range sound levels are relatively higher than at greater distances and therefore contribute more significantly to cumulative sound exposure levels. A new acoustic propagation model based on the wavenumber integration approach was used to improve sound pressure estimates for short-range receiver locations. This modelling method is accurate to within a few meters from the individual airgun elements in all directions. It was applied to the same deep water scenario for a subset of receiver locations, and the results are compared to the original PE model results. The shallow water scenario did not require use of the wavenumber integral model because steep angle propagation in that environment is less important; only the sound from one source point at most will propagate at an angle too steep to be treated correctly using the PE approach. Consequently PE modelling was performed for all shallow water scenarios.

2 Model Scenarios

2.1 Source–Receiver Geometry

A planar arrangement of receiver locations relative to the straight line of source points (source line) is considered as shown in Figure 1 below. Receivers are arranged to provide seven profiles spaced along a section of source line where soft-start is performed. Each profile has five co-linear receiver stations at increasing perpendicular distance from the source line: directly on the source line, and at 100, 250, 500, and 1000 m away (in the *y*-direction in Figure 1). Seven primary profiles are spaced 750 m apart along the source line (*x*-direction) to provide sound level predictions at different steps of the soft-start sequence, with the first profile being 175 m from the start of the sequence. Two secondary profiles (1A and 2A in Figure 1) are inserted at the mid-points of the first three primary profiles to increase sampling near the start of the soft-start procedure. These intermediate profiles are only considered for wavenumber integral modeling in the deep environment scenario. The source-point interval is 25 m (in the *x*-direction), so that the 8th source point and every 30th source point thereafter are directly abeam of a primary receiver profile. The gradual increase in the number of active airguns (discussed in Section 2.2) occurs over 12 steps of 15 source points each, or 350 m. The receiver profiles, therefore, are located at the midpoint of Step 1 and every other step thereafter. The full airgun array is activated during the 13th and final step, which includes extra source points beyond the last receiver profile for a total of 230 points along the source line.

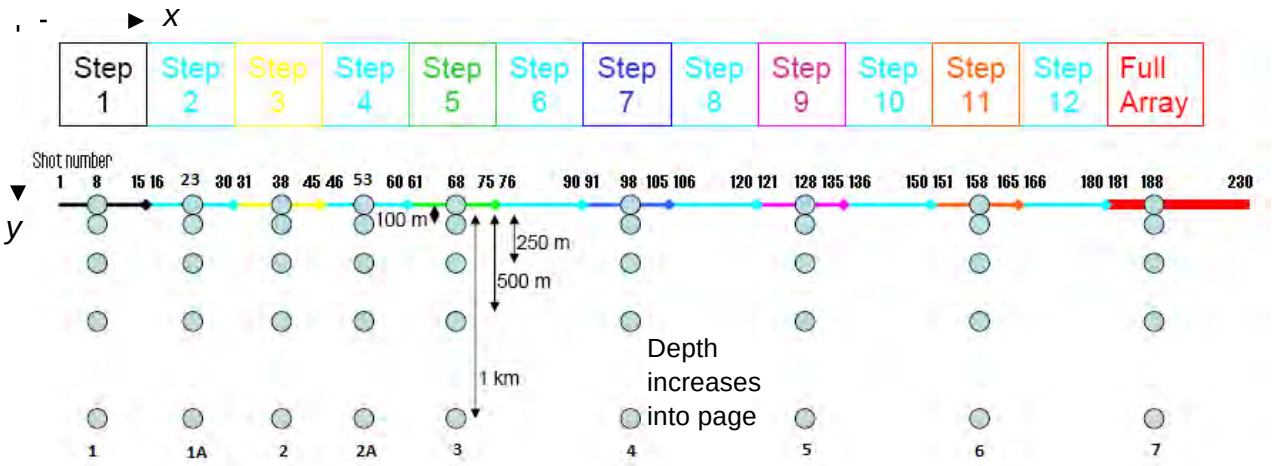

Figure 1: Plan view of receiver locations (grey circles) relative to the line of source points (source line) and the progression of airgun array soft-start steps in the model scenarios. Profiles are numbered at the bottom of the figure. Spacing between source points is 25 m.

The receiver depths for the FWRAM modelling span the water depth since that model calculates acoustic pressure on a dense depth grid. The FWRAM results are evaluated at several specified depths and the maximum value over depth is also output. The wavenumber integral model calculates pressures only at specified depths. The source was located always 6 m below the surface, the assumed operational depth of the array.

2.2 Soft-Start Sequence Progression

An industry standard airgun array configuration of 28 active airgun elements, of varying sizes, totalling approximately 3100 in^3 of volume was modelled. As described in the UK JNCC Guidelines, a soft-start sequence begins with the smallest airgun, with additional airgun elements introduced at each step of the soft-start according to the sequence shown in Table 1. As mentioned previously, each of the twelve steps consists of 15 source points. Since source points are separated by 25 m, each step corresponds with a 350 m segment along the line between the first and last source points.

Table 1: Airgun array soft-start sequence for the modelling study.

Step	Add-in airguns	Total volume (% final)
1	1	0.65
2	1	1.9
3	1	3.2
4	3	7.1
5	3	12.0
6	3	19.7
7	2	26.5
8	2	32.0
9	1	40.1
10	3	49.8
11	3	62.8
12	3	75.7
13	2	100.0

3 Modelling Approach

3.1 Airgun Array Source Levels

The apparent far-field pressure commonly specified for seismic airgun arrays is generally not relevant for estimating potential impacts on marine mammals and fish for the following reasons:

- Peak source levels for seismic survey airgun array sources are usually quoted relative to the vertical direction; however, due to the directional dependence of the radiated sound field, source levels off to the sides of the array are generally lower.
- Far field source levels do not apply in the near field of the array where pressures of the individual airguns do not add coherently; sound levels in the near field are, in fact, lower than would be calculated from far field estimates which assume coherent summation from all array elements.

The acoustic source level of seismic airgun arrays varies considerably in both the horizontal and vertical directions due to complex interactions between the signals from the component airguns. These differences in array output with respect to direction and angle from the vertical are referred to as the array response or directivity. The interactions must be accounted for to correctly predict the sound field generated by an airgun array in a given direction. If the source signatures of the individual airguns are known, then it is possible to estimate the array source level in any direction by summing the contributions of the airgun elements with the appropriate time delays, according to their relative positions.

JASCO has developed the full-waveform airgun array source signature model AASM (MacGillivray 2006) to compute the source level and directivity of airgun arrays. The source model is based on the physics of the oscillation and radiation of airgun bubbles, as described by Ziolkowski (1970). The model solves a set of parallel differential equations describing the airgun bubble oscillations. In addition to the basic bubble physics, AASM also accounts for non-linear pressure interactions between airguns, port throttling, bubble damping, and GI-gun behaviour (Dragoset 1984, Laws *et al*. 1990, Landro 1992). The source model includes four empirical parameters that are tuned so that the model output matches observed airgun behaviour. The model parameters were fitted to a large library of real airgun data using a "simulated annealing" global optimization algorithm. These airgun data were obtained from a previous study (Racca and Scrimger 1986) that measured the signatures of Bolt 600/B guns ranging in volume from 5 to 185 in^3. The optimization was performed in the time domain against measurements including frequencies up to 2 kHz. The model may be less accurate for different airgun source brands or model types.

The AASM requires as inputs the airgun layout, volumes, towing depths, and operating pressures. The output of the source model is a set of "notional" signatures for each of the array elements. The notional signatures are the pressure waveforms of the individual airguns, accounting for the interaction with other airguns in the array, at a standard reference distance of 1 m. Figure 2 shows the airgun signatures for the present study computed with AASM.

Two approaches were used for combining the notional individual airgun pressure signatures: For parabolic equation-based modelling, the resulting notional signatures were summed with the appropriate phase delays based on direction in the horizontal plane to obtain the far-field, angle-dependent, source signature of the array; for wavenumber integral-based modelling, carried out only for the deep-water scenario, the notional signatures were treated separately so appropriate phase and amplitude differences depended on the 3-dimensional receiver location relative to each airgun.

The interaction between the signals from individual airgun elements creates a far-field directivity pattern in the overall acoustic emission from the array. This directivity is particularly prominent at frequencies in the mid-range of several tens to several hundred Hz: at lower frequencies the array appears omni-directional, while at higher frequencies the pattern of lobes becomes too finely spaced to resolve. For an array soft-start as per Table 1, the pattern will evolve from onmi-directional to its final full-array aspect as airguns are brought on-line; at each step of the soft-start the lobes of dominant emission will shift.

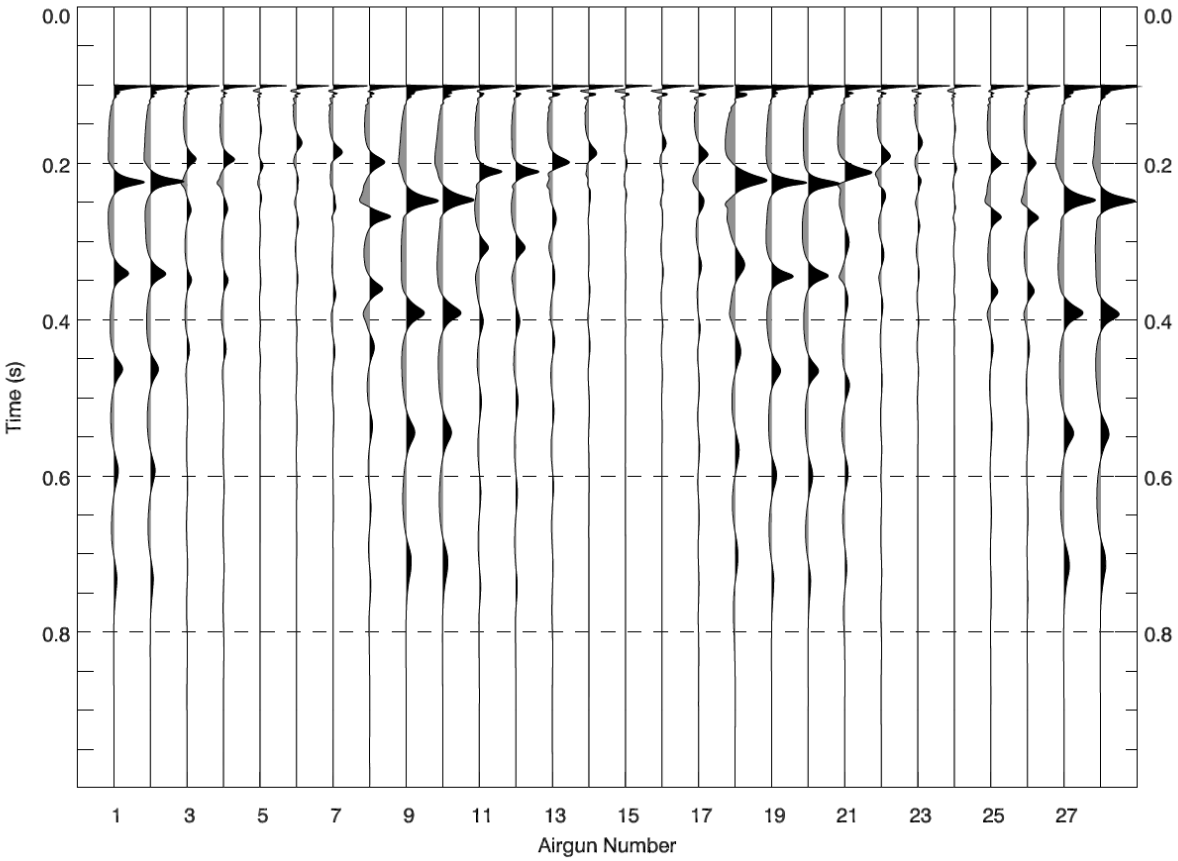

Figure 2: Notional airgun signatures for individual airguns of the 28-airgun 3090 in^3 array.Time periods of positive pressure indicated by black fill, and negative pressure by grey fill. The scale is the same for the pressure signatures from all airguns.

3.2 Sound Propagation

3.2.1 Parabolic Equation Model

The acoustic energy of a source radiates outward and travels through the water as pressure waves. The sound level generally decreases with increasing distance from the source, but the processes that govern sound transmission are complex and depend on the properties of the propagation environment that include the water depth and the acoustic characteristics of the water column and of the geological layers in the sea floor, through which acoustic energy also travels. A number of computational methods are available to predict sound propagation, each of which has different strengths and limitations. JASCO Applied Sciences has developed an advanced modelling package whose algorithmic engine is a modified version of the widely-used Range-dependent Acoustic Model (RAM) (Collins *et al.* 1993, 1996).

RAM is based on the parabolic equation method using the split-step Padé algorithm to efficiently solve range-dependent acoustic problems. The model assumes that outgoing energy dominates over back-scattered energy and computes the solution for the outgoing wave equation. An uncoupled azimuthal approximation is used to provide two-dimensional transmission loss values in range and depth. RAM has been enhanced by JASCO to approximately model shear wave conversion at the sea floor using the equivalent fluid complex density approach of Zhang and Tindle (1995).

Sound propagation models employ acoustic parameters specific to the geographic region of interest, including the water column sound speed profile, bathymetry, and seabed geoacoustic properties to produce site-specific estimates of the noise field as a function of range from the source and depth of the receiver. For this study a particular implementation of the model (FWRAM) was used, which performs full-waveform (Fourier synthesis) acoustic field computations using the enhanced variant of RAM mentioned above. The algorithm is run at finely spaced frequencies (1 Hz in this case) to compute a 1-second impulse-response function for the ocean environment. This response function is combined with the direction-specific far-field signature of the array (at the

appropriate soft-start step) produced by AASM to yield a synthetic time series at the receiver point, from which desired sound level metrics are obtained. Had the study called for computation of the rms SPL metric, which requires precise determination of the received pulse length, FWRAM would have had to be run at a finer frequency resolution to produce a longer synthetic time series and avoid "wrap around" of late arrival components of the signal. In this study only the SEL and peak SPL metrics (see Section 3.3) were required, which are unaffected or negligibly affected by wrap-around.

The parabolic equation modelling method, as implemented in RAM and its variants, has a geometric limitation that must be recognized in order to quantify the results of this initial study. The algorithm does not provide accurate estimates of transmission loss at steep propagation angles relative to the horizontal, i.e. for receiver positions that are laterally close to the source relative to the receiver depth. In such cases the predicted received levels will be lower than the true values. This limitation is more important for high frequencies than low frequencies. An accuracy limit of 45° to the horizontal is considered safe with 8 Padé coefficients, although appropriate selection of computational grid spacings can widen the acceptable angle range. Greater precision at close ranges requires alternative estimation methods. The following section describes the wavenumber integral method implemented to address the steep-angle limitation of the parabolic equation method as discussed above.

3.2.2 Wavenumber Integral Model

A new acoustic propagation model was developed to address the steep angle limitations of the parabolic equation model used for the initial stage of this study. The new model is based on the wavenumber integral method described for example by Jensen *et al.* (1993) and Frisk (1994). Wavenumber integration methods, also referred to as Fast Field Programs (FFPs), often use Fast Fourier Transforms (FFTs) to perform the integrations. Wavenumber integral methods in seismology are often referred to as reflectivity methods or discrete wavenumber methods. While the wavenumber integral approach is accurate at steep propagation angles, it generally is applicable only for range-independent problems in which water layer and bottom layer properties do not vary with distance from the source. The deep water test case used in this study is range-independent so results here are unaffected by this limitation.

The wavenumber integral approach uses a Hankel transform to decompose the spherical pressure field emitted by each airgun into a continuum of outward-propagating plane-cylindrical waves. The general form of the Fourier-decomposed pressure field for one frequency at range r and depth z is

$$g(r,z) = \int_{-0}^{\infty} G(k_r,z) J_0(k_r,r) k_r dk_r$$

where k_r is the horizontal component of the wave vector for each plane-cylindrical wave component and $G(k_r,z)$ is the solution to the depth-separated wave equation for that component at receiver depth z. Function $G(k_r,z)$ depends on the source depth, water column properties and seabed reflectivity. Seabed reflectivity depends on the seabed layer properties: compressional- and shear-wave speeds and attenuation coefficients, and layer densities. The seabed reflectivity method used here is that described by Brekhovskikh (1980). The wavenumber k_r is related to slowness s by $k_r = \omega \cdot s$, where ω is the angular frequency.

We use an integration range of k_r=0, representing straight down propagation, to a truncated upper limit corresponding with slowness $(1200 \text{ m/s})^{-1}$. This slowness represents a horizontal but depth-evanescent cylindrical plane wave in the water. All computations are carried out from 5 to 500 Hz in 0.25-Hz steps to yield 4-s time records at each receiver position. The wavenumber step is frequency dependent and chosen to give 22.5° maximum phase error between wavenumber steps at the maximum source-receiver range. This approach requires finer wavenumber sampling at high frequencies than at low frequencies. The number of wavenumber steps is more than 33,000 at 500 Hz for the receivers on Profile 1. Computation time for all 230 source positions at one receiver location was approximately 9 hours on a Toshiba Vostro 1500 laptop with 2 GHz Intel T7300 Duo Core CPU.

3.3 Sound Metrics

By convention, underwater sound levels are measured in decibels relative to a reference pressure of 1 µPa. To characterize the intensity, or loudness, of impulsive sound for the purpose of estimating biological impact, various sound level metrics are commonly used. The three most commonly employed sound level metrics are peak sound pressure level (peak SPL), root-mean-square sound pressure level (rms SPL) and sound exposure level (SEL). In this study the exposure criteria against which sound levels are assessed are peak SPL and SEL – or more precisely cumulative SEL over all seismic source points. For completeness and comparison, however, the definitions of all three metrics are provided below.

The peak SPL is the maximum instantaneous sound pressure level attained by an impulse, $p(t)$:

$$peak\ SPL = 20\log_{10}\left(\max|p(t)|\right)$$

The rms SPL is the root-mean-square pressure level over a time window, T, containing the impulse:

$$rms\,SPL = 10\log_{10}\left(\frac{1}{T}\int_T p^2(t)\,dt\right)$$

By convention, when computing airgun safety radii, the time interval T is most often taken to be the "90% energy pulse duration" rather than a fixed time window (Malme *et al.* 1986, Greene 1997, McCauley *et al.* 1998). This time window is computed for each seismic pulse signal as the interval containing 90% of the pulse energy, and the resulting metric is commonly referred to as the 90% rms SPL. Because the window length T is used as a divisor, pulses that are more spread out in time have a lower rms level for the same total acoustic energy.

The SEL is the time-integral of the square pressure over a fixed time window long enough to include the entire pulse:

$$SEL = 10\log_{10}\left(\int_T p^2(t)\,dt\right)$$

SEL has units of dB re µPa^{2}s. It is a measure related to sound energy flux density rather than sound pressure. Depending on the application and context SEL for airgun signals may be expressed as a per-pulse metric or as a cumulative metric over multiple pulses. SEL from multiple pulses is computed by summing in linear energy the SEL values for individual pulse:

$$SEL = 10\log_{10}\left\{\sum_{n=1}^{N}\int_0^T p_n^2(t)dt\right\}$$

where N is the number of pulses or exposures.

3.4 Marine Mammal Hearing

Marine mammal hearing sensitivity varies with frequency. Audiograms represent the threshold of hearing as a function of frequency. Audiograms for marine mammals are characterized by relatively lower sensitivity (higher threshold values) at very low and very high frequencies. The frequencies of highest sensitivity and at which sensitivity decreases vary among species. Audiograms have been measured for several species of pinnipeds, and for a limited number of odontocetes. No direct measurements of audiograms for mysticetes have been made to date.

The potential for sound from seismic sources to affect marine mammals depends on how well the species can hear the sounds produced (Ireland *et al.* 2007a). Sounds are less likely to disturb animals if they are at frequencies that the animal cannot hear well. An exception to this may be when the sound pressure is so high as to cause non-auditory physical injury, whether temporary or permanent. For non-injurious sound levels, frequency weighting curves based on audiograms may be applied to account for sound levels at particular frequencies in a manner reflective of the receiver's sensitivity to those frequencies (Nedwell *et al.* 1998).

An NMFS-sponsored Noise Criteria Committee proposed standard frequency-weighting curves — referred to as M-weighting filters — for use with marine mammal species (Gentry *et al.* 2004). M-weighting filters are band-pass filter networks designed to reduce the sound level of inaudible or less-audible frequencies for five broad classes of marine mammals:

1. Low frequency cetaceans (LFC),
2. Mid-frequency cetaceans (MFC),
3. High-frequency cetaceans (HFC),
4. Pinnipeds in water (PINN), and
5. Pinnipeds in air.

The amount of discount applied by M-weighting filters for less-audible frequencies is not as great as would be indicated by the corresponding audiograms for these groups of species. The rationale for applying a smaller discount than would be suggested by the audiogram is due in part to a characteristic of human hearing: perceived equal loudness curves increasingly have less rapid roll-off outside the most sensitive hearing frequency range as sound levels increase. This is the reason that C-weighting curves for humans, used for assessing loud sounds such as blasts, are flatter than A-weighting curves used for quiet to mid-level sounds. Additionally, out-of-band frequencies, though less audible, can still cause physical injury (either temporary or permanent) if pressure levels are very high. The M-weighting filters, therefore, are designed primarily for high sound level impacts such as temporary or permanent hearing threshold shifts. The use of M-weighting should therefore be considered conservative (in the sense of overestimating the potential for impact) when applied to lower level impacts such as onset of behavioural change impacts. Figure 3 shows the decibel frequency response of the four standard underwater M-weighting filters.

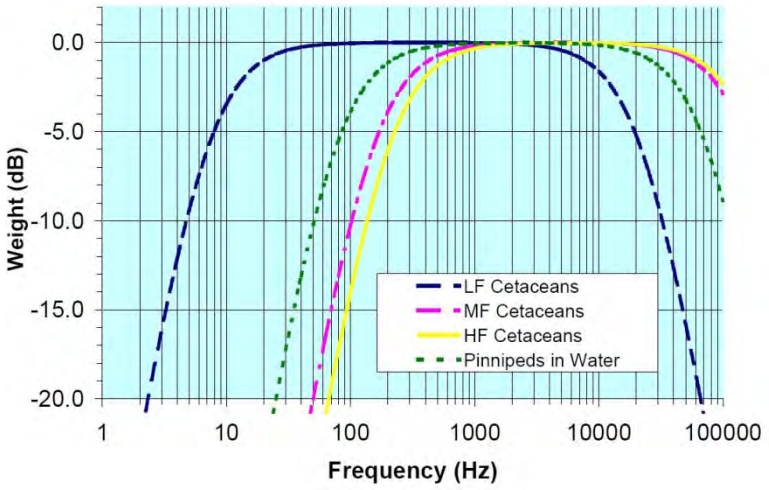

Figure 3. M-weighting filter curves for four species groups.

These filters have unity gain (0 dB) through the pass band and high- and low-frequency roll-off at approximately -12 dB per octave. The amplitude response of the M-weighting filters is defined in the frequency domain by the following function:

$$G(f) = -20\log_{10}\left[\left(1+\frac{f_{lo}^2}{f^2}\right)\left(1+\frac{f^2}{f_{hi}^2}\right)\right]$$

The roll off and pass band of these filters are controlled by the two parameters f_{lo} and f_{hi}; the parameter values that are used for the four different standard M-weighing curves are given in Table 2.

Table 2. Low- and high-frequency cutoff parameters for standard marine mammal M-weighting curves.

M-weighting filter	f_{lo} *(Hz)*	f_{hi} *(Hz)*
Low frequency cetaceans (LFC)	*7*	*22000*

Mid-frequency cetaceans (MFC)	*150*	*160000*
High-frequency cetaceans (HFC)	*200*	*180000*
Pinnipeds underwater (PINN)	*75*	*75000*

4 Modelling Environment

4.1 Bathymetry

We assumed constant water depth for both the 2000 m deep water scenario and the 50 m shallow water scenario, The deep scenario is representative, for example, of seabeds beyond the edge of the continental shelf. The shallow scenario is representative of shallow seas or locations on the continental shelf. The constant bottom depth provided a range-independent environment for parabolic equation modelling, which allowed the impulse-response function for the ocean environment to be computed only once for a given source-receiver range and then used for all seismic source points with the appropriate airgun array soft-start configuration and source-receiver directionality. The wavenumber integral modelling approach implemented here accounted for the relative geometry of individual airguns relative to each receiver location instead of using the simpler but approximate directivity function method.

4.2 Geoacoustic Properties of the Seafloor

For location-specific modelling, the seabed geoacoustic properties (sound speed and attenuation for both compressional and shear waves) are generally inferred from information about the geology within the study area. This is obtained from a variety of studies which may include exploratory drilling and surficial sediment sampling. For the present modelling study we used a set of geoacoustic properties taken from a previous JASCO modelling study in the Beaufort Sea (Table 3 below).

Table 3: Geoacoustic parameters used for parabolic-equation modelling of the deep-water scenario. Depth is in metres below seafloor.

Depth (mbsf)	***Density (g/cm^3)***	***P-wave velocity (m/s)***	***P-Attenuation (dB/λ)***	***S-wave velocity (m/s)***	***S-Attenuation (dB/λ)***
0–100	1.6 – 2.0	1500 – 1800	0.1 – 0.5	150	4.0
>100	2.0	1800	0.5	150	4.0

Table 4: Geoacoustic parameters used for parabolic-equation modelling of the shallow-water scenario. Depth is in metres below seafloor.

Depth (mbsf)	***Density (g/cm^3)***	***P-wave velocity (m/s)***	***P-Attenuation (dB/λ)***	***S-wave velocity (m/s)***	***S-Attenuation (dB/λ)***
0	1.50	1510	0.15	130	1.0
13	1.53	1530	0.10	130	1.0
27	1.56	1555	0.10	130	1.0
42	1.60	1600	0.10	130	1.0
57	1.63	1615	0.10	130	1.0
72	1.65	1630	0.10	130	1.0
87	1.80	1750	0.05	130	1.0
252	1.90	1814	0.05	130	1.0

The wavenumber integral model approach, unlike the parabolic equation model approach, required that bottom layer properties be specified in discrete layers. A set of 8 bottom layers were defined to approximate the gradients in the parameters in Table 2 by staircase steps of those parameters over depth. The parameter variation is depicted in Figure 4.

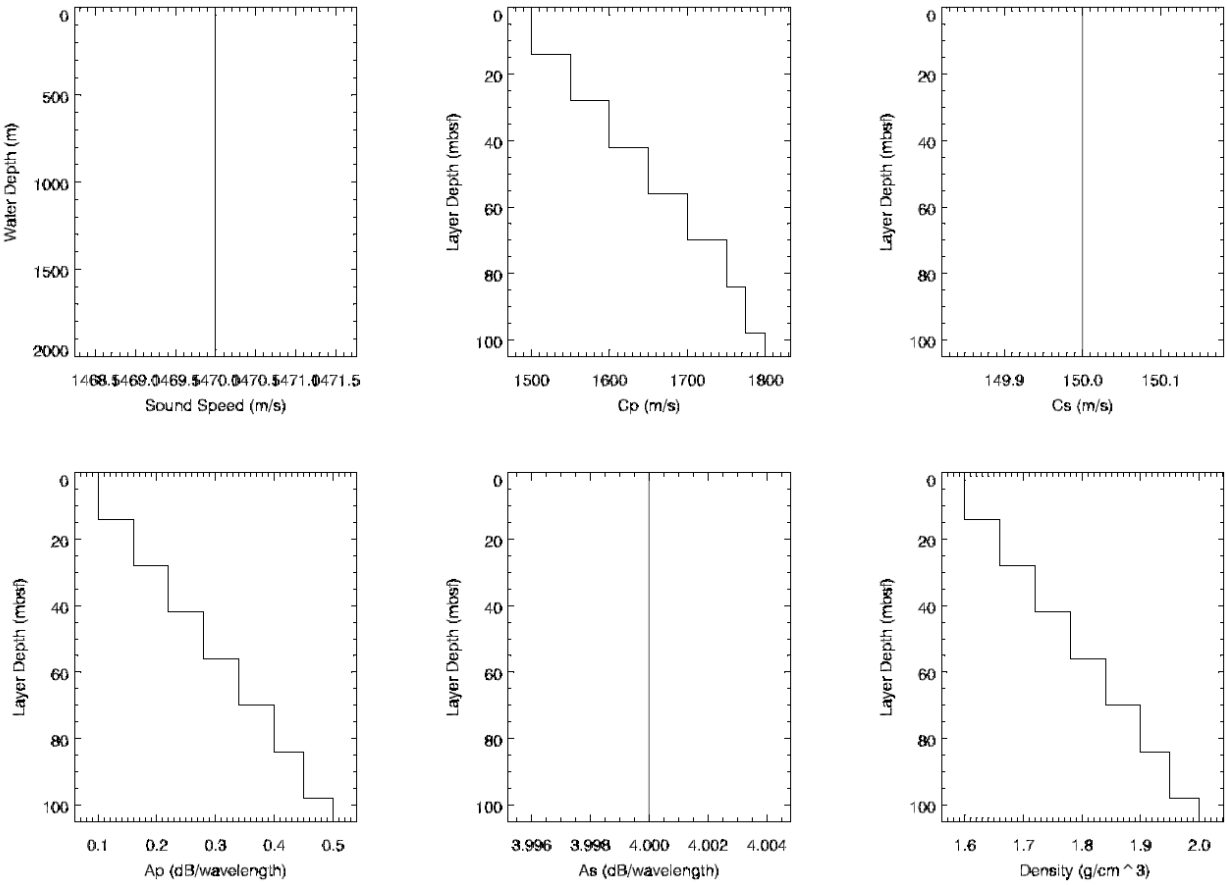

Figure 4: Geoacoustic parameter profiles of the 8-layer seabed used for wavenumber integral modelling for the deep-water scenario: Cp and Cs are compressional and shear wave velocity, respectively; and Ap and As are compressional and shear wave attenuation, respectively.

4.3 Water Sound Speed Profile

For location-specific modelling, representative sound speed profiles particular to an area and season are available from sources such as the U.S. Naval Oceanographic Office's Generalized Digital Environmental Model (GDEM) database (Teague *et al*. 1990). For the present explorative analysis a GDEM-sourced sound speed profile for deep Arctic waters in summer, used in the same Beaufort Sea modelling mentioned above, was taken as starting point. The original sound velocity curve exhibited a near-surface layer (about 50 m thick) with downward refracting properties followed by a typical upward-refracting deep water profile. To avoid a possibly non-representative reduction of received levels at shallower depths due to the downward refracting layer, the top 50 m of the sound velocity profile were made essentially constant for this study. The resulting profile is shown in Figure 5. While the smooth profile was used directly for parabolic equation modelling, a linear profile at 1470 m/s was specified for the wavenumber integral model runs. Future wavenumber integral runs will use a sequence of gradient layers to approximate the smooth variation. The sound speed profile used for modelling the shallow-water scenario was based on CTD measurements taken by JASCO in 50 m water depth off the Mackenzie Delta in August. This profile is listed in Table 4 above.

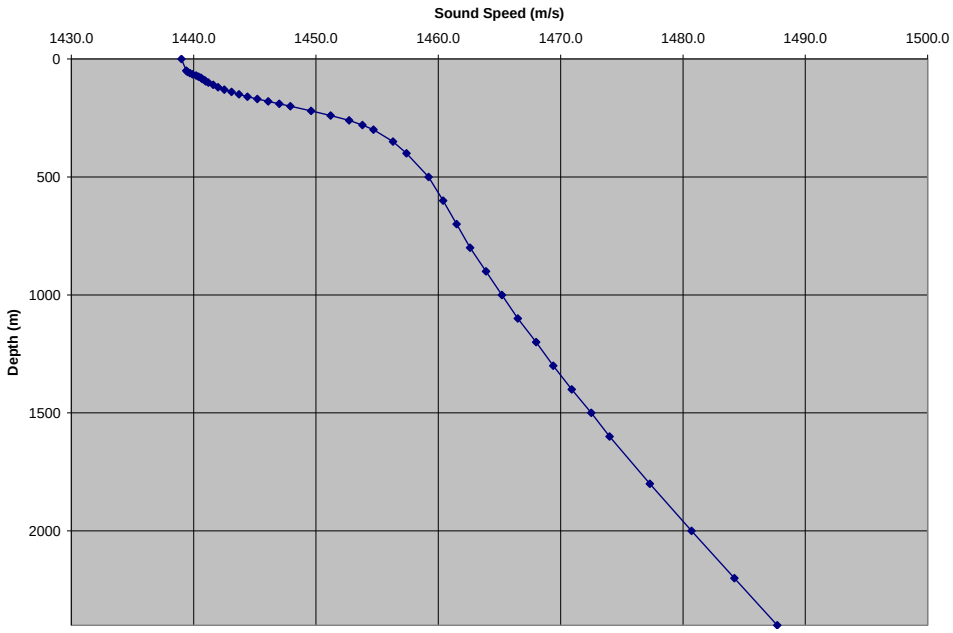

Figure 5: Water sound speed profile used in parabolic equation modelling for the deep-water scenario.

Table 5: Water sound speed profile used for parabolic equation modelling for the shallow-water scenario. Depth is in m below sea floor.

Depth (mbsf)	***P-wave velocity (m/s)***
0	1452.9
10	1451.3
20	1444.5
30	1441.1
40	1440.4
50	1440.1

4.4 Frequencies

Full waveform modelling was carried out in 1-Hz increments between 2 and 2000 Hz for the parabolic equation runs and from 5 to 500 Hz for the wavenumber integral model runs. Frequencies below about 20 Hz are attenuated strongly by destructive interference of surface reflections (ghosts). For environmental impact assessment of seismic surveys this range is fully adequate even though marine mammals can hear to higher frequencies, because most of the energy emitted from an airgun array is concentrated in a spectral range well below the upper modelling limits.

5 Marine Mammal Safety Criteria

Following a review of available literature on marine mammal hearing and physiological and behavioural responses to anthropogenic sound, Southall *et al*. (2007) proposed a set of threshold criteria for injury and behavioural disturbance in marine mammals based on the SEL and peak SPL metrics (discussed in Section 3.3). For a multi-pulse source, such as a seismic airgun array, the following injury criteria are presented:

- SEL: 198 dB re 1 μPa^2-s (M-weighted) for cetaceans and 186 dB re 1 μPa^2-s (M-weighted) for pinnipeds.
- Peak SPL: 230 dB re 1 µPa (flat-weighted) for cetaceans and 218 dB re 1 µPa (flat-weighted) for pinnipeds.

For a given situation the more conservative of these two would be applied. The SEL criterion is M-weighted (Miller *et al.* 2005), meaning that it is adjusted to account for spectral variations of hearing sensitivity of a particular species or group of species, whereas the peak SPL criterion is flat-weighted, meaning that all frequencies are treated equally. In the present modelling only the flat-weighted SEL is computed for the shallow water site results. Flat and M-weighted results were computed from the deep water model results. M-weighting reduces the metric value.

Because the airgun array source is activated repeatedly, the SEL criterion was used to account for the cumulative effect of multiple exposures. Southall *et al.* (2007) assumed no recovery of hearing between exposures, so that the multi-pulse metric for the purpose of assessment against the criterion is defined by simple addition of energy as shown in Section 3.3.

6 Results: Parabolic Equation Model

6.1 Sound Exposure Level (SEL)

The SEL metric results from the PE modelling of both deep- and shallow-water scenarios are presented as graphs of acoustic level, both per-pulse and cumulative, plotted against the distance between the source and the CPA (closest point of approach) to the receivers. Figures 6 through 19 for the deep (2000 m depth) site and Figures 20 through 33 for the shallow (50 m depth) site show the levels at each of the seven primary receiver location profiles; the upper figure on each page shows maximum received levels over all depths, the lower figure levels at a fixed receiver depth of 100 m for deep site results and at a fixed receiver depth of 39 m for the shallow site results. For convenience the first 13 distance labels (in the *x*-direction in Figure 1) on the abscissa of the graphs correspond to the starting source points of the soft-start steps.

The stepwise effect on the received sound levels caused by the number of airguns increasing during the soft-start sequence is clearly visible in the Per-pulse SEL and is most prominent in the early stages of the soft start. This is due to a combination of the significantly greater relative change in overall source array size as the first few airguns are added to the soft-start sequence and the fact that the array directivity properties likely vary more drastically in the initial steps of soft-start.

The limitations of the modelling algorithm at steep propagation angles are evident in traits of the per-pulse SEL curves for receivers at short range from the source. The peaks in the estimated received levels near CPA are seen to be truncated as the algorithm fails to fully account for the steep angle propagation. It can also be expected that as the range to a receiver decreases the selection of the maximum level over all depths may underestimate values as the level estimates at greater depths are more affected by the steeper propagation slant. As mentioned in Section 3.2, a wavenumber integral modelling approach was implemented to examine the near-field pressure signatures. Those results are presented in Section 0.

With due note of the fact that the parabolic equation model underestimates the few seismic source points close to CPA and will have a reducing effect on all cumulative SEL values from that point onward, the modelling results for this metric can be examined in terms of how much acoustic energy a marine mammal would be exposed to within close range of the seismic source at the beginning of the soft-start sequence. The wavenumber integral model results, computed for the deep site only, do not suffer this limitation.

Figure 6 shows that for an animal located 100 m horizontally away from the source line at the midpoint of Step 1 of the soft-start, in 2000 m water depth, the cumulative SEL over the full soft start operation will not exceed 177 dB re 1 μPa^2s. The cumulative SEL will be less than 175 dB re 1 μPa^2s if the animal is 250 m off the side of the source line. These sound levels, would apply only to an animal remaining at the same geographic location relative to the source line for the full duration of the soft-start and moving vertically in the water column tracking the depth at which sound intensity is maximal at any given time. Figure 7 shows that the corresponding sound levels for an animal remaining stationary at 100 m depth would be 175 and 168 dB re 1 μPa^2s. Figure 9 shows that an animal at 100 m depth directly under the source line at the midpoint of Step 3 of the soft-start (not having been deterred at all by the previous 37 source points at increasing levels) would be exposed to a cumulative SEL over the entire soft-start sequence of 183 dB re 1 μPa^2s, or 178 dB if located 100 m to one side of the source. If the animal was following the depth of maximum sound intensity at all times and 100 m horizontally from the source line, the results of Figure 8 indicate it would receive maximum cumulative SEL of 181 dB re 1 μPa^2-s..

The shallow water results (Figure 20 to Figure 33) indicate generally higher SEL levels than at corresponding relative locations from the deep site. This affect is commonly observed in field measurements of airgun array sounds and is due to the contribution of sound energy reflected from the seabed. The shallow water results also suggest that longer-distance sounds contribute a larger fraction of the overall cumulative SEL than from the deepwater environment examined here. As a result, the cumulative SEL value results at shallow site decay much more slowly with distance away from the source line. This feature suggests that the PE modelling method can be assumed to produce accurate results for the shallow environment; its inability to fully account for very steep propagating energy

does not affect the longer-range contributions that are responsible for most of the cumulative SEL. The difference in cumulative SEL's between the 100 m offline and 1 km offline receivers in profile 1 at 100 m depth for the deep site is approximately 9 dB (Figure 7). The corresponding difference for these receivers at 39 m depth at the shallow site is only about 2 dB (Figure 21). Furthermore there is little difference between the maximum-over-depth results and the results at fixed receiver depths of 39 m (just 11 m above the seafloor). Generally the maximum-over depth results are 1-2 dB higher than at the 39 m fixed depth.

Shallow site cumulative SEL levels for receivers at 39 m depth on profile 1, perpendicular to the centre of step 3 of the soft-start procedure, are 181 dB re 1 μPa^2-s directly on the source line, and 179 dB re 1 μPa^2-s at 1 km off the source line (Figure 21). As discussed above, the reason for little difference between these values is that longer-distance pulses contribute a relatively large fraction of the received SEL in shallow water. Similar behaviour, albeit with increasing sound levels, is observed at profiles adjacent to later steps in the soft-start. For example, at profile 5, adjacent to step 9 of the soft-start procedure, the on-line cumulative SEL at 39 m depth is 191 dB re 1 μPa^2-s and at 1 km off the source line it is 183 dB re 1 μPa^2-s (Figure 29). The highest levels occur as expected at the last profile number 7. Here the on-line cumulative SEL at 39 m depth reaches 193 dB re 1 μPa^2-s and at 1 km off the line it is 184 dB re 1 μPa^2-s (Figure 33).

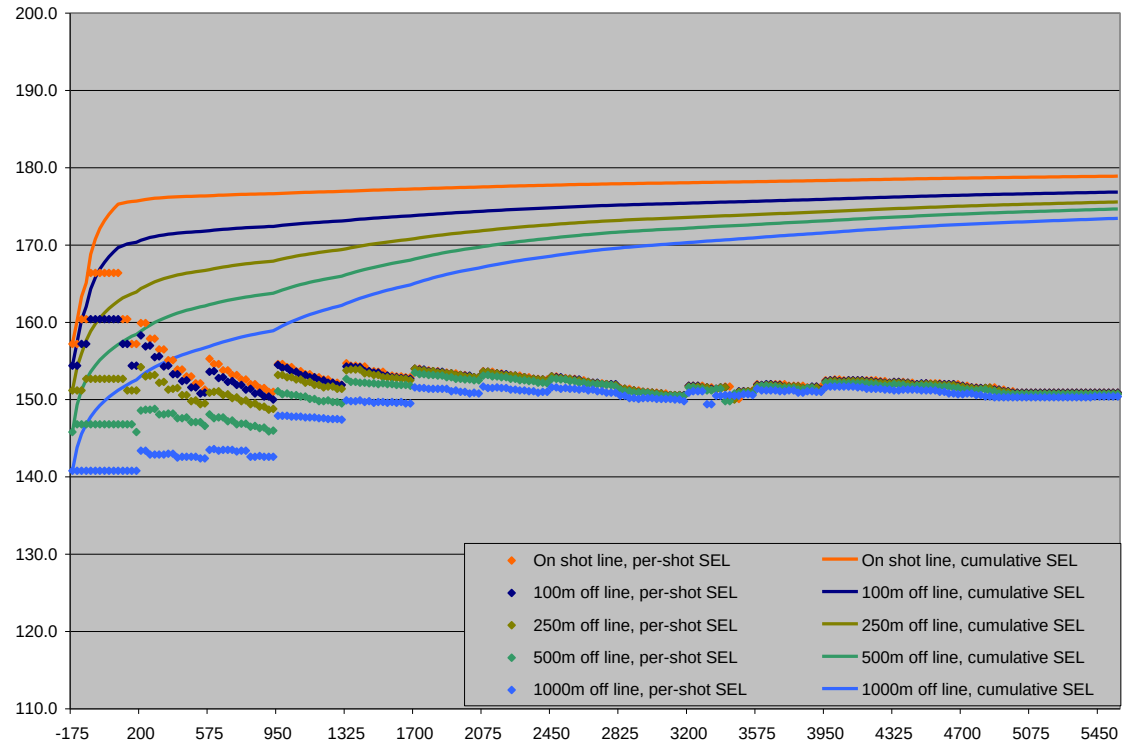

Figure 6: Per-pulse and cumulative SEL for the deep-water scenario for receivers on Profile 1, maximized over all depths.

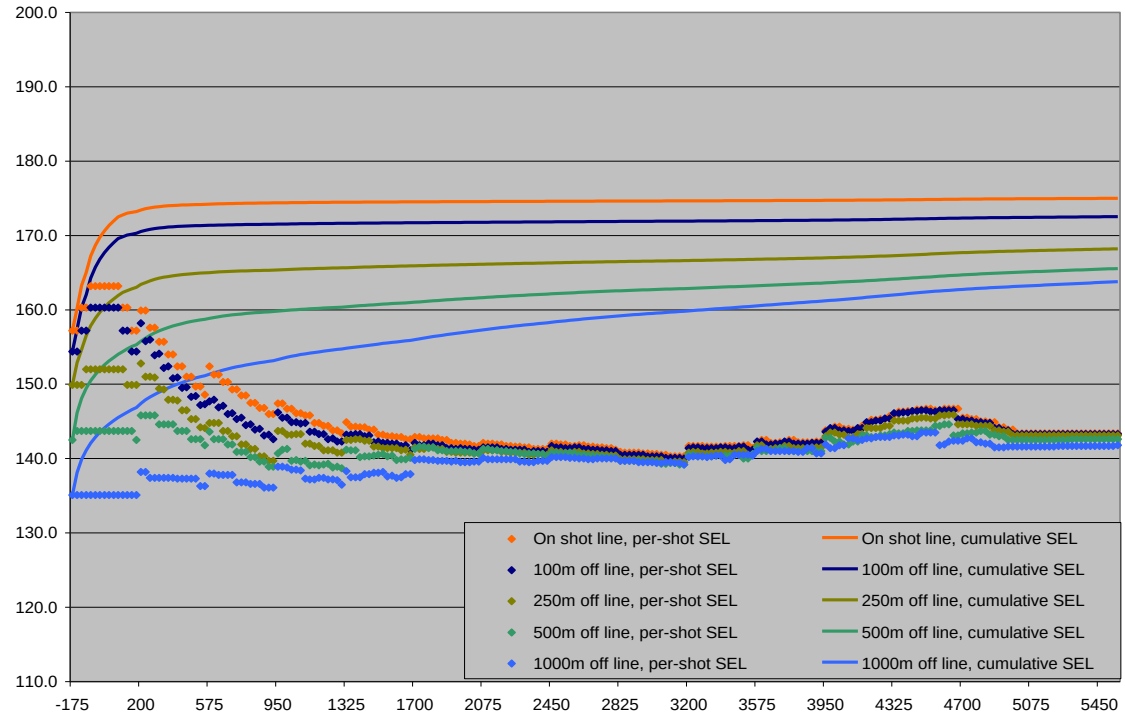

Figure 7: Per-pulse and cumulative SEL for the deep-water scenario for receivers on Profile 1 at 100 m depth.

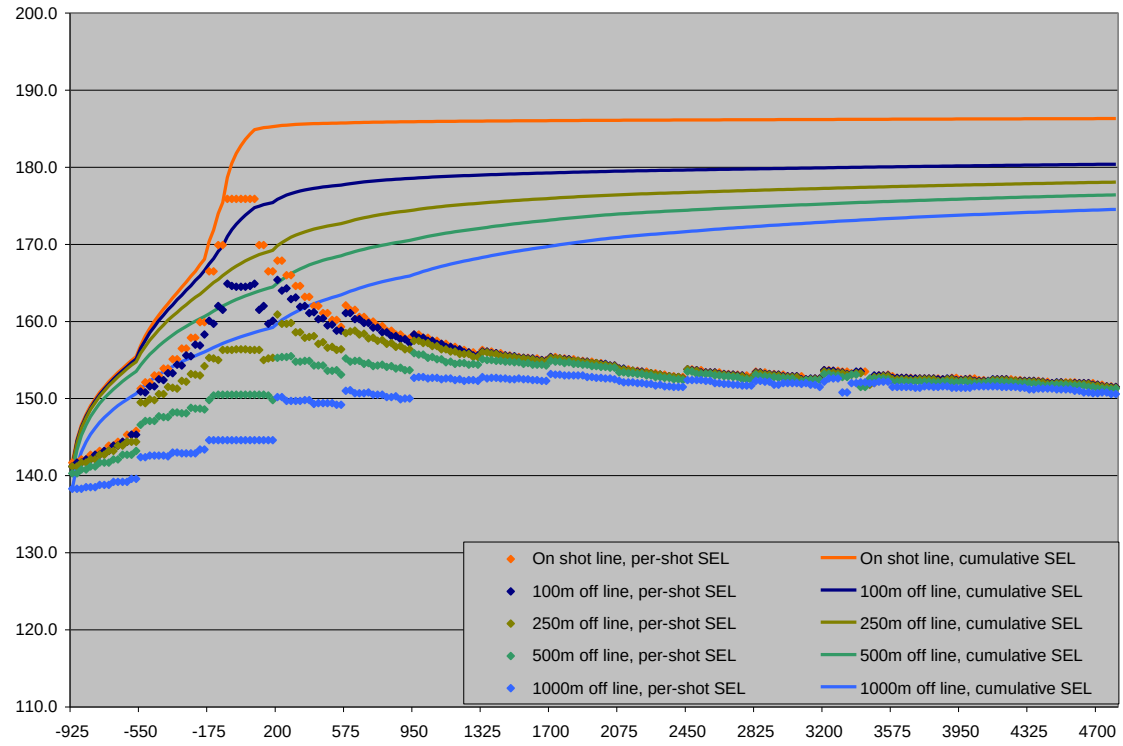

Figure 8: Per-pulse and cumulative SEL for the deep-water scenario for receivers on Profile 2, maximized over all depths.

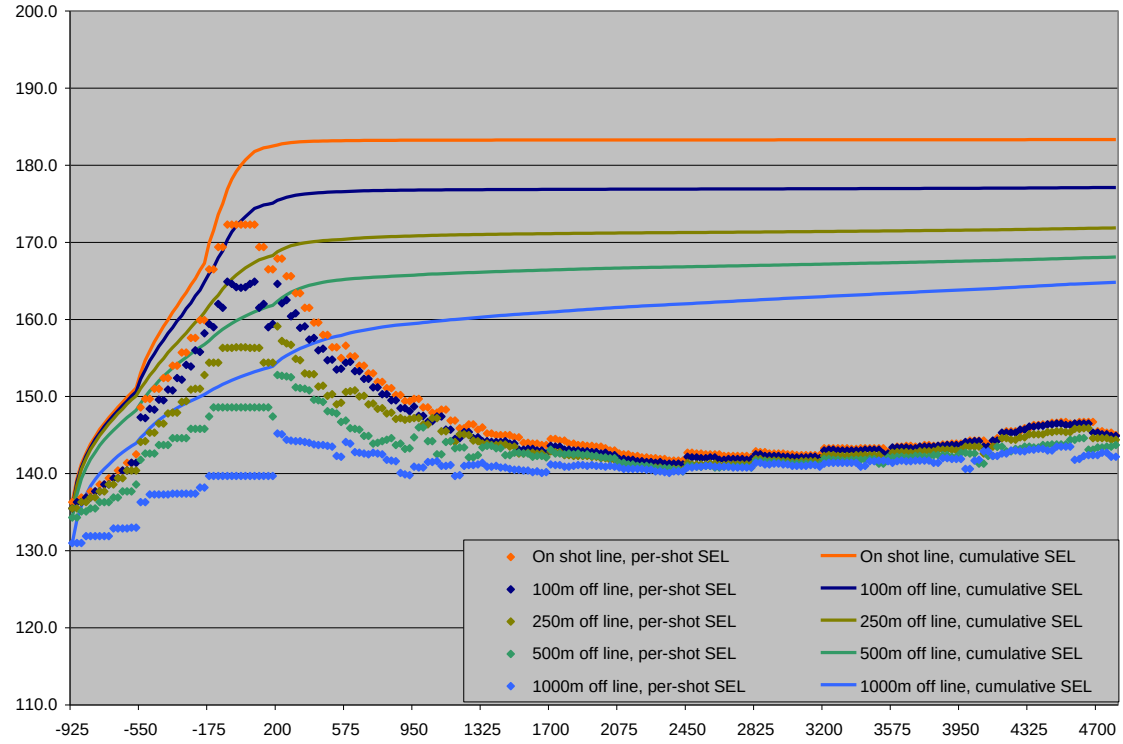

Figure 9: Per-pulse and cumulative SEL for the deep-water scenario for receivers on Profile 2 at 100 m depth.

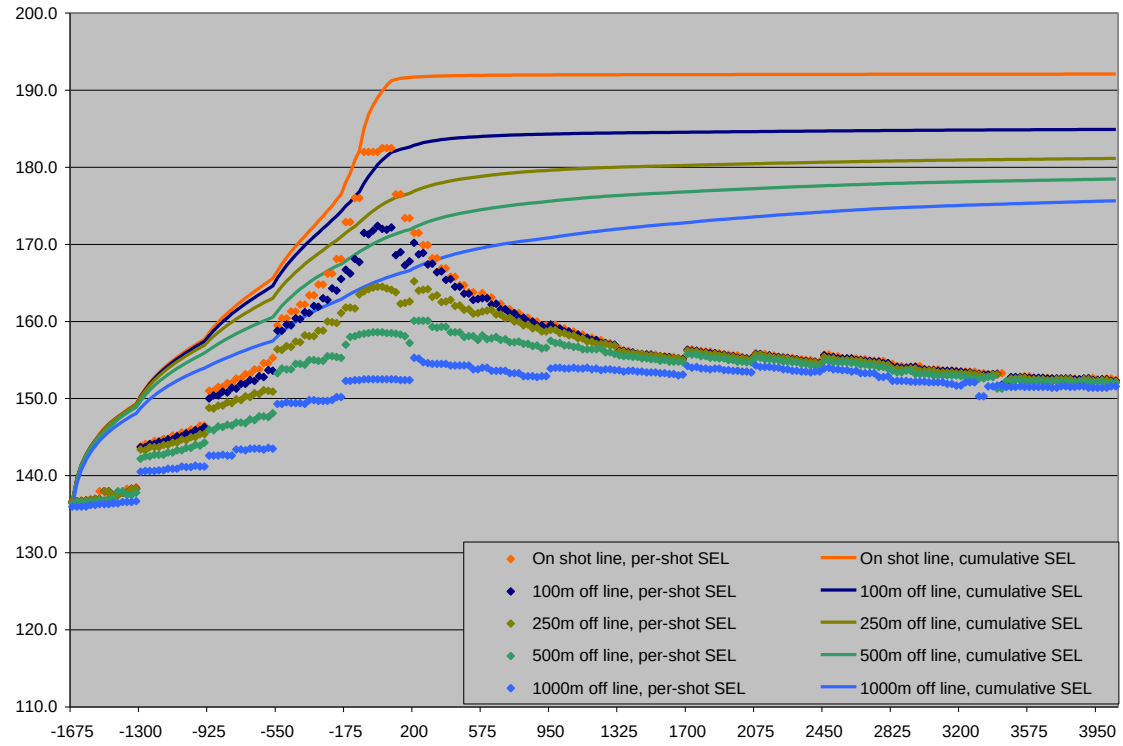

Figure 10: Per-pulse and cumulative SEL for the deep-water scenario for receivers on Profile 3, maximized over all depths.

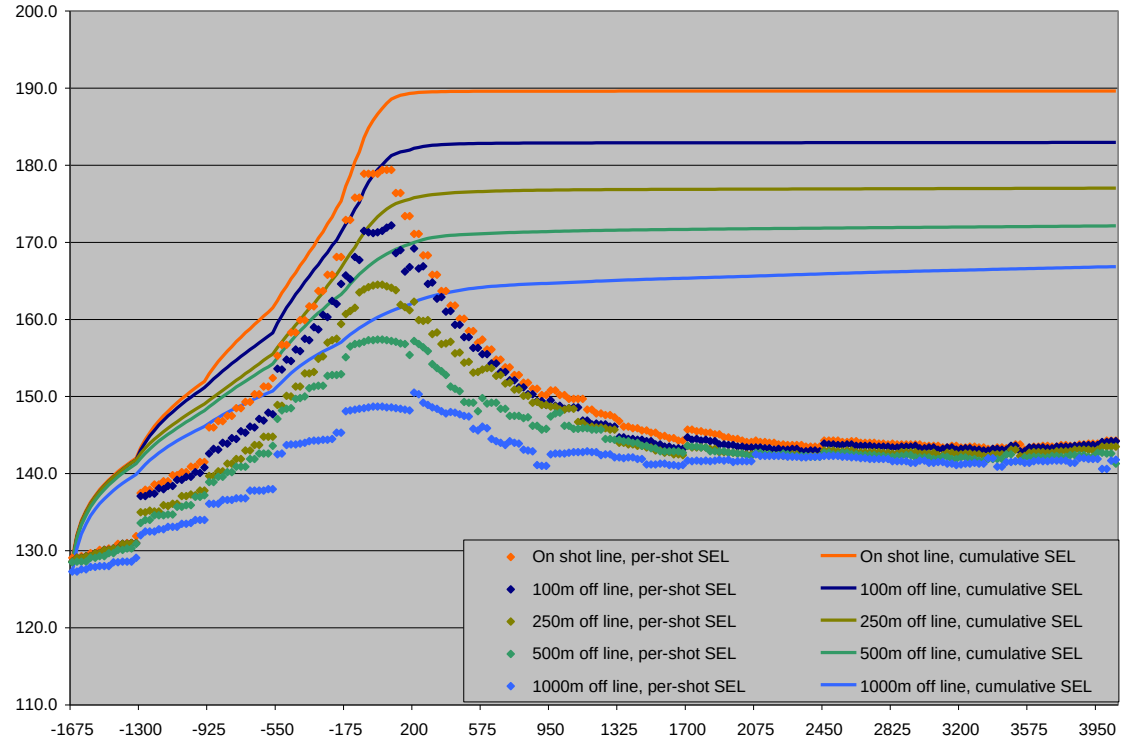

Figure 11: Per-pulse and cumulative SEL for the deep-water scenario for receivers on Profile 3 at 100 m depth.

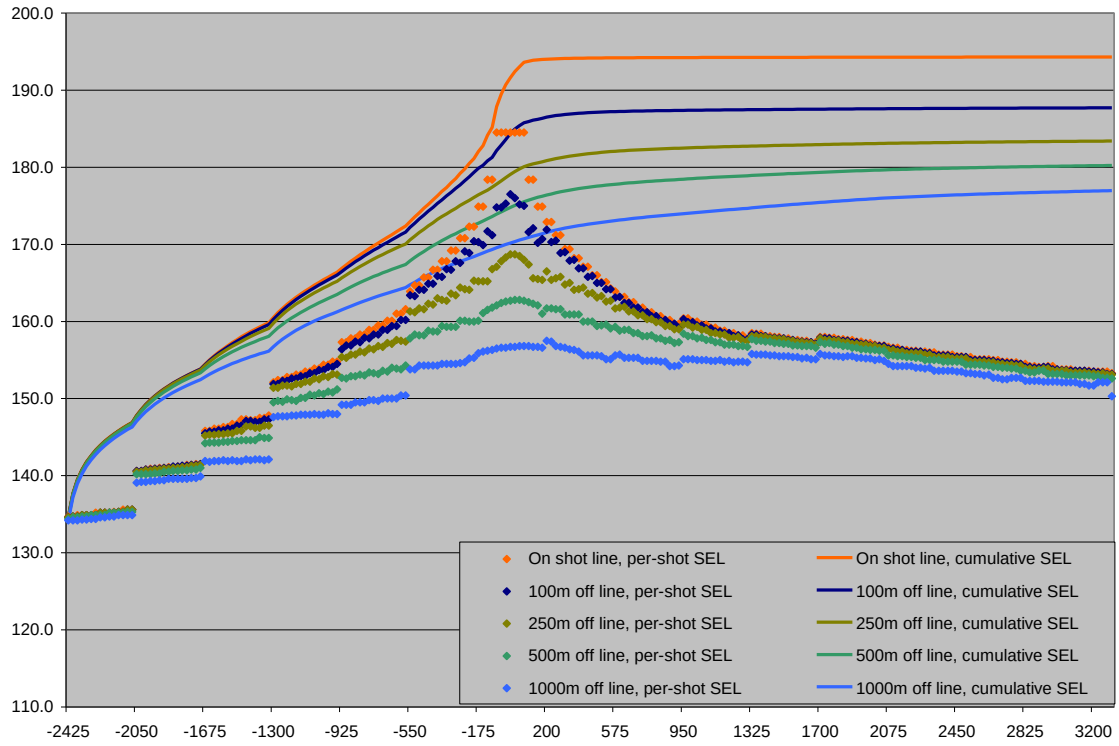

Figure 12: Per-pulse and cumulative SEL for the deep-water scenario for receivers on Profile 4, maximized over all depths.

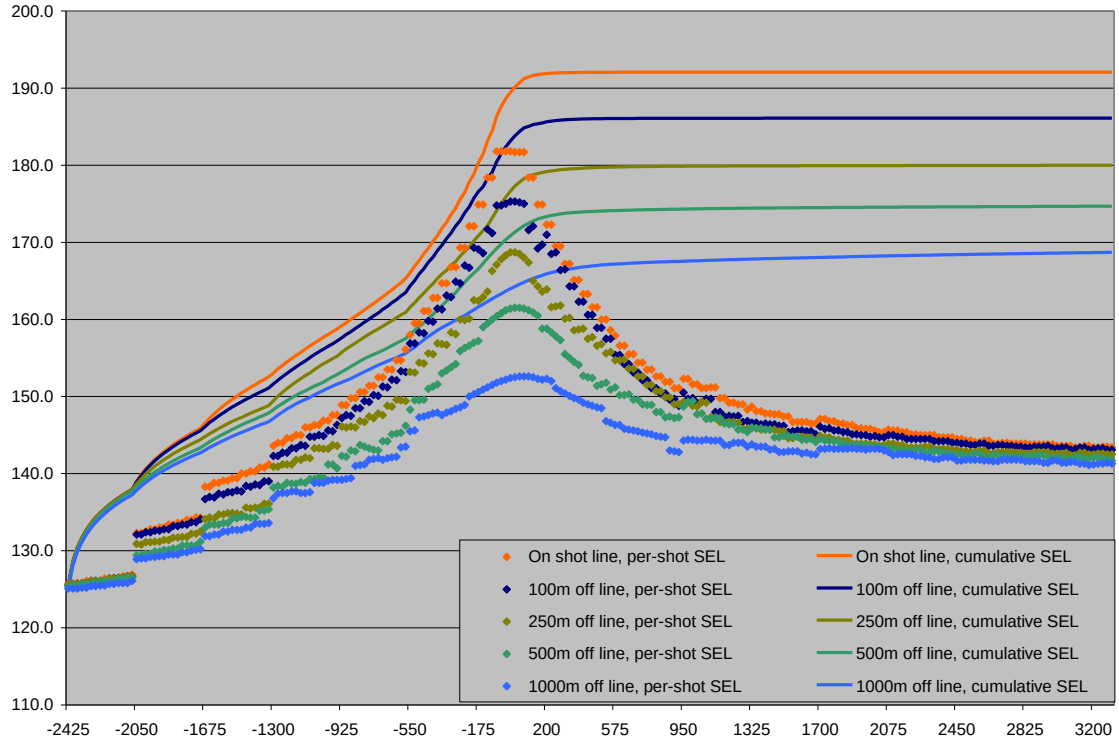

Figure 13: Per-pulse and cumulative SEL for the deep-water scenario for receivers on Profile 4 at 100 m depth.

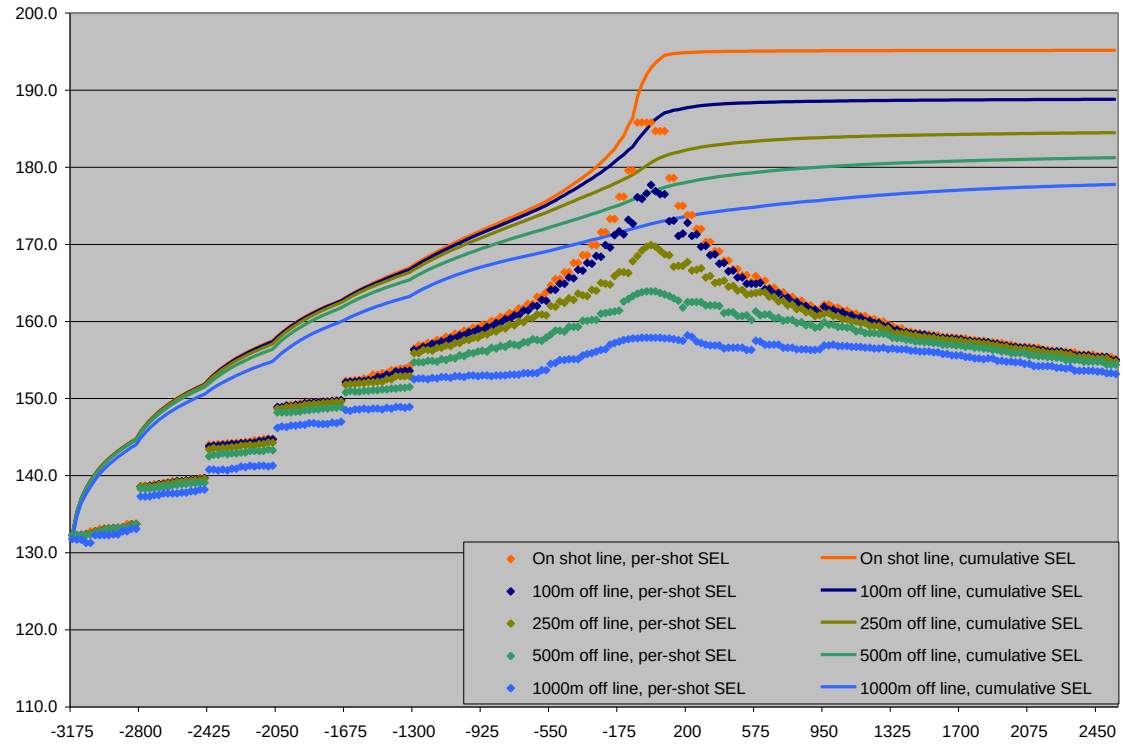

Figure 14: Per-pulse and cumulative SEL for the deep-water scenario for receivers on Profile 5, maximized over all depths.

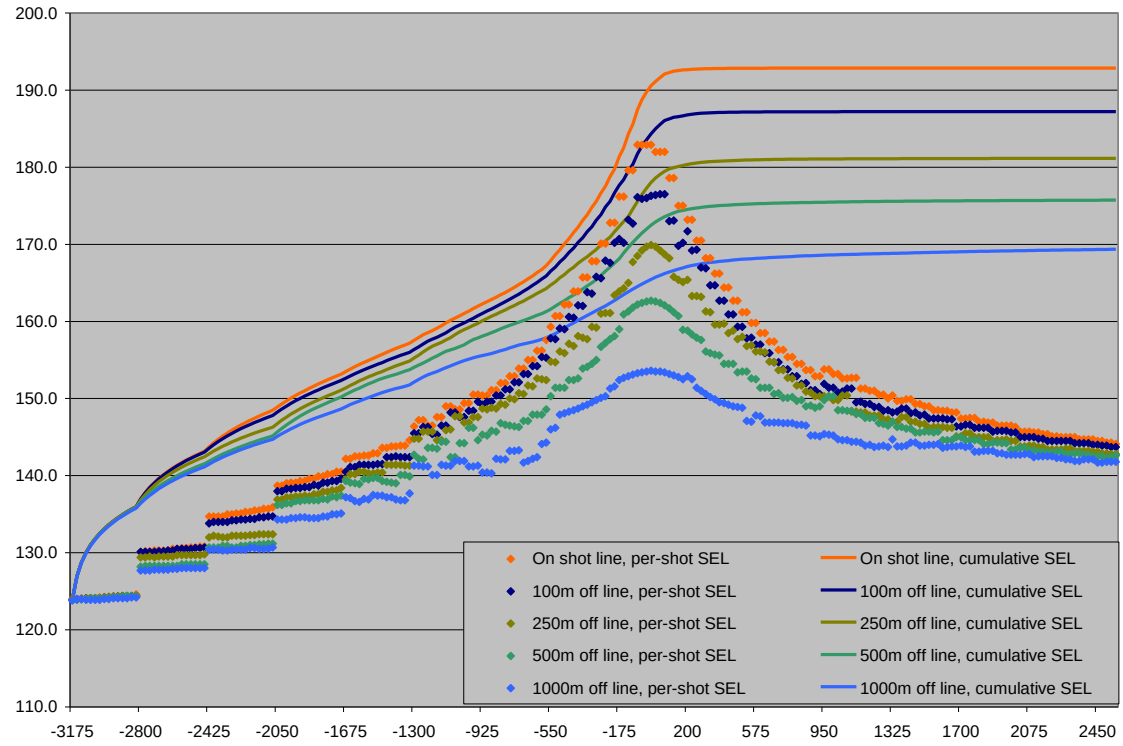

Figure 15: Per-pulse and cumulative SEL for the deep-water scenario for receivers on Profile 5 at 100 m depth.

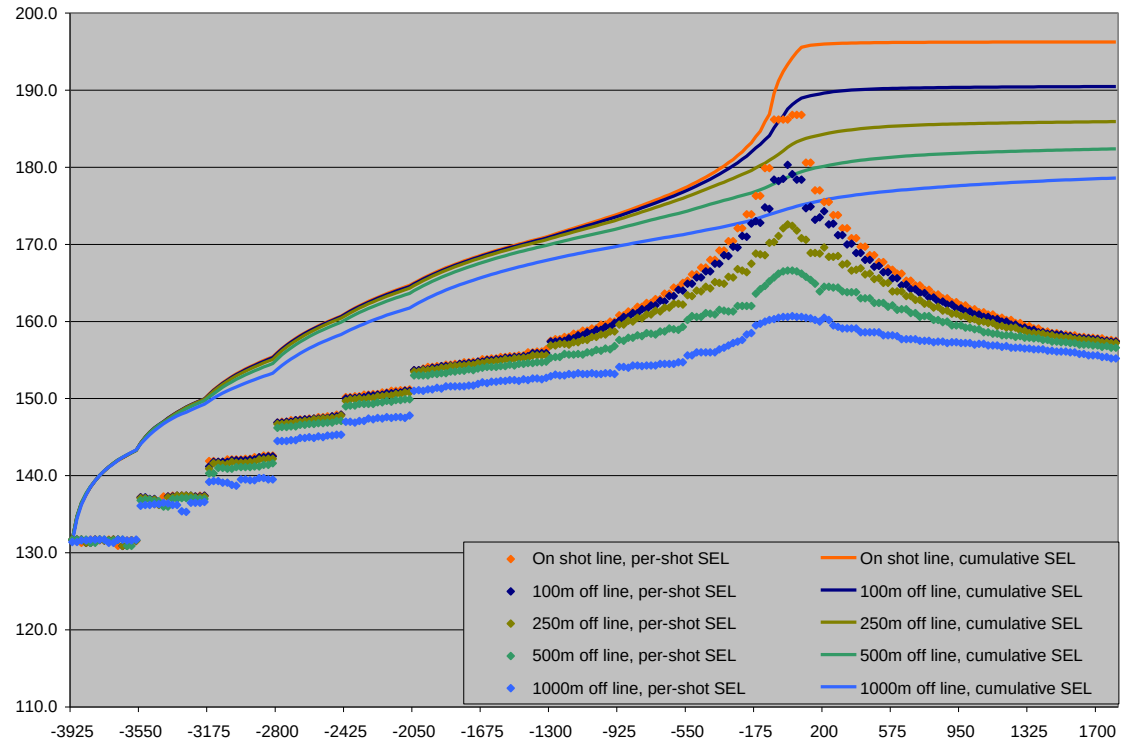

Figure 16: Per-pulse and cumulative SEL for the deep-water scenario for receivers on Profile 6, maximized over all depths.

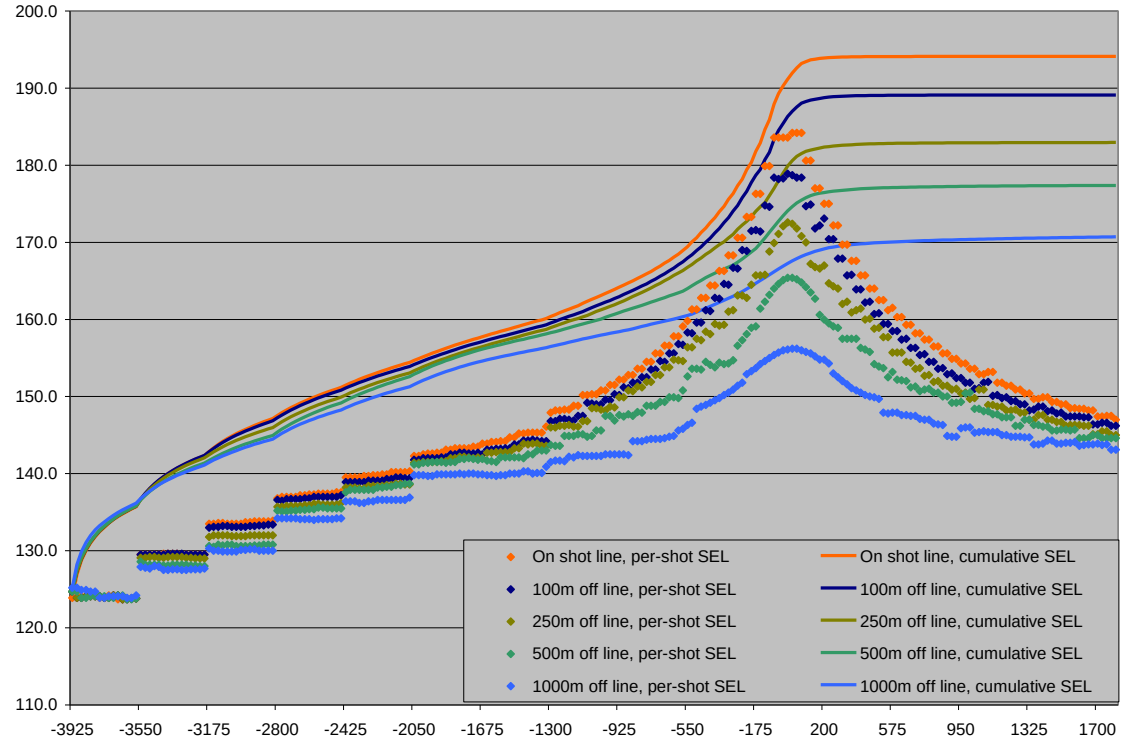

Figure 17: Per-pulse and cumulative SEL for the deep-water scenario for receivers on Profile 6 at 100 m depth.

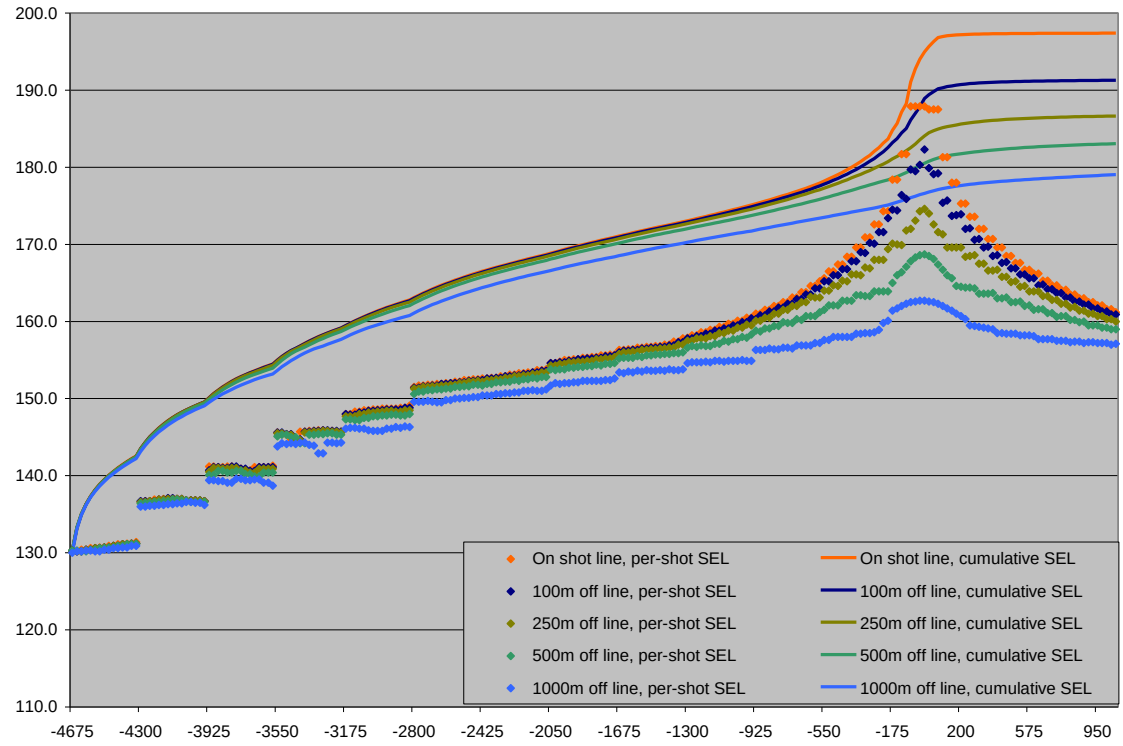

Figure 18: Per-pulse and cumulative SEL for the deep-water scenario for receivers on Profile 7, maximized over all depths.

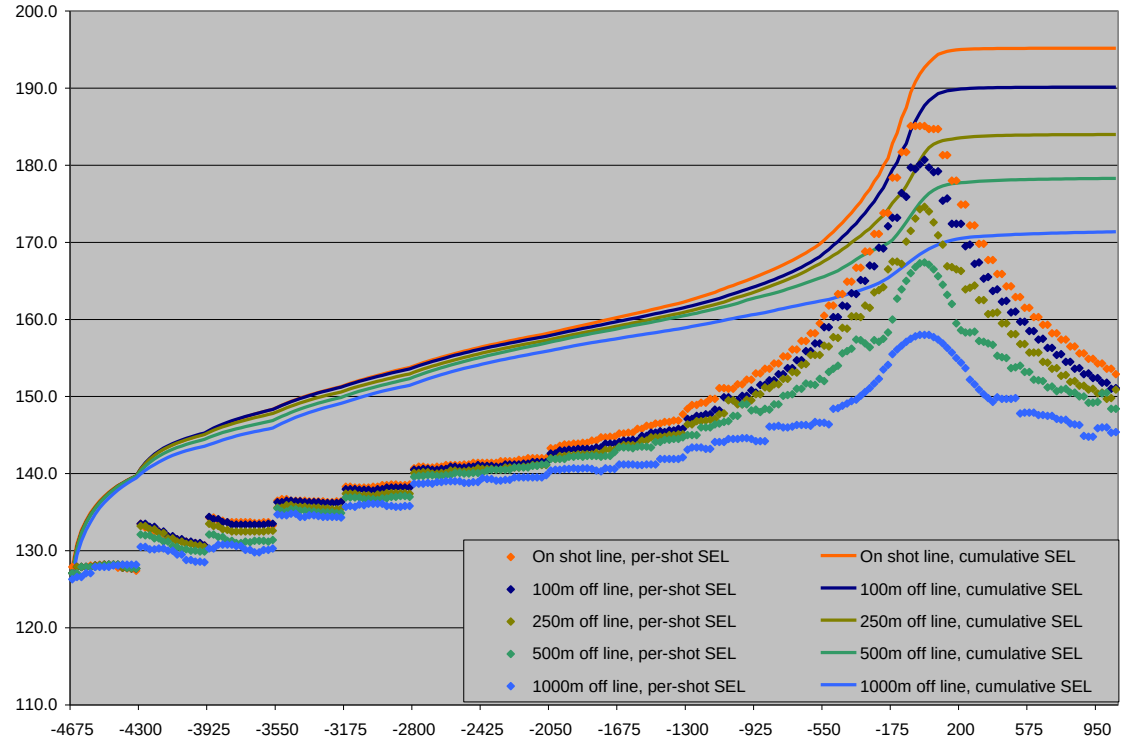

Figure 19: Per-pulse and cumulative SEL for the deep-water scenario for receivers on Profile 7 at 100 m depth.

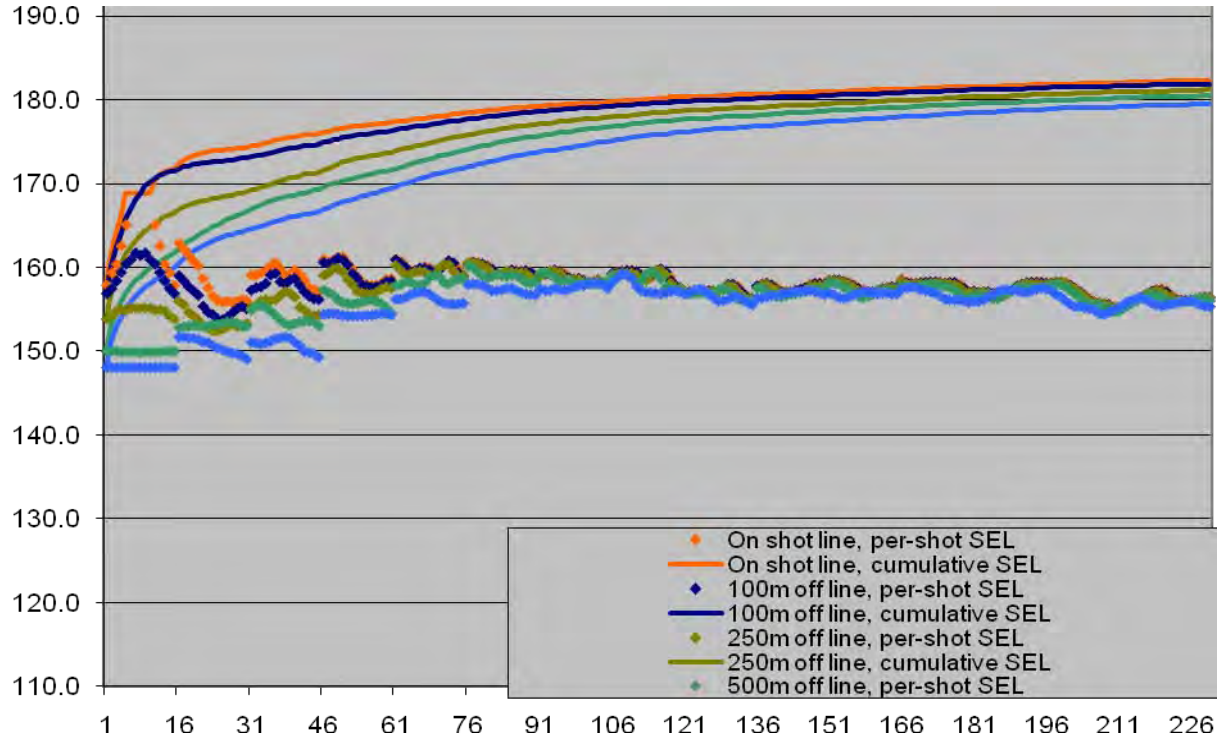

Figure 20: Per-pulse and cumulative SEL versus source point number for the shallow-water scenario for receivers on Profile 1, maximized over all depths.

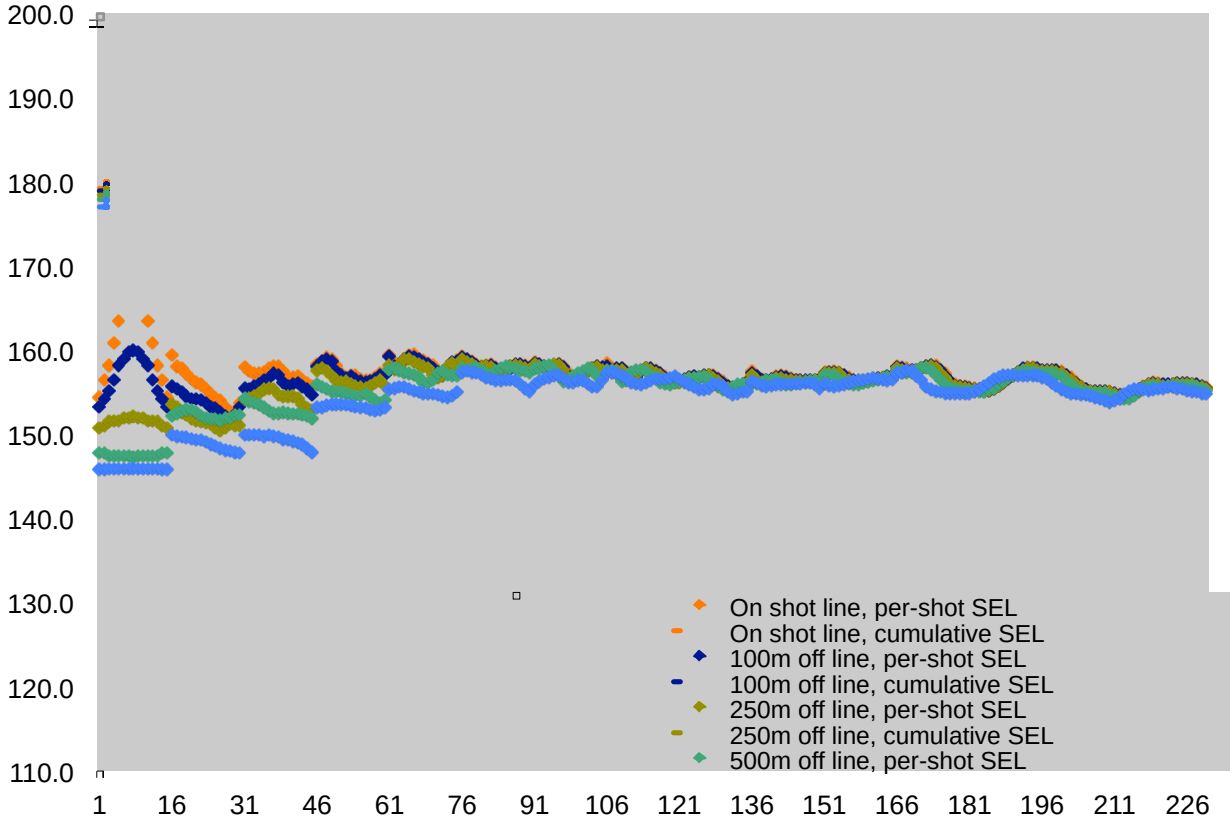

Figure 21: Per-pulse and cumulative SEL versus source point number for the shallow-water scenario for receivers on Profile 1, at 39 m depth.

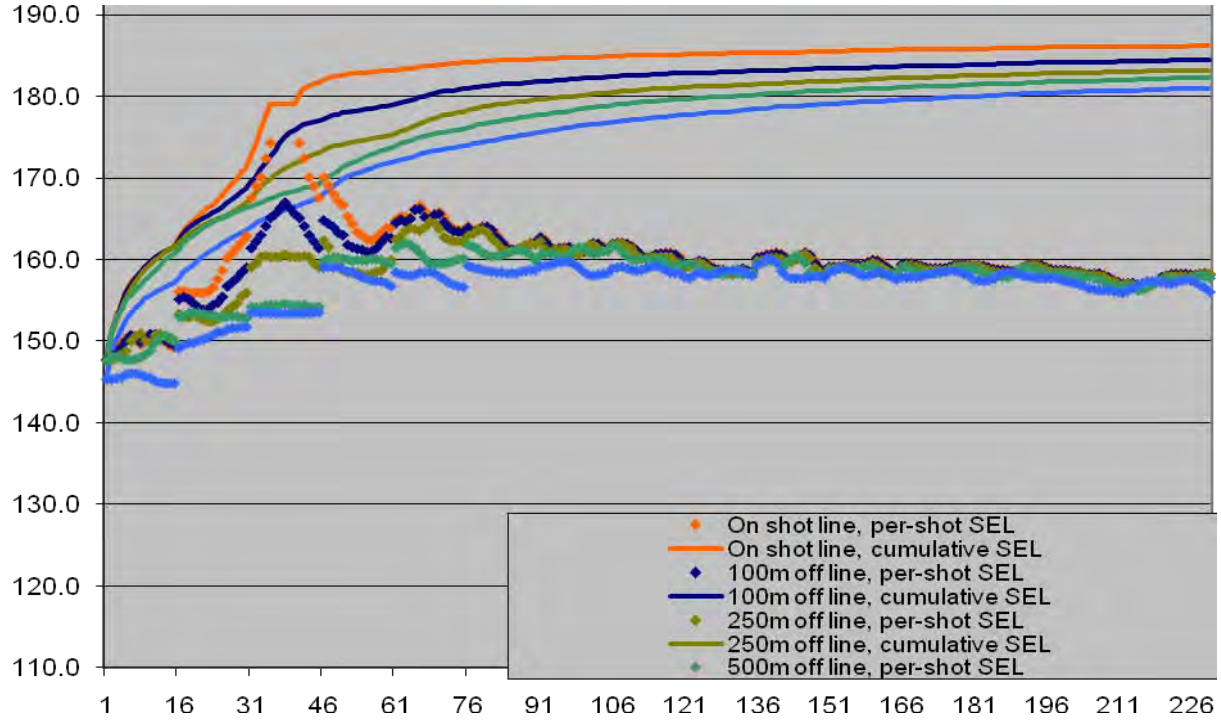

Figure 22: Per-pulse and cumulative SEL versus source point number for the shallow-water scenario for receivers on Profile 2, maximized over all depths.

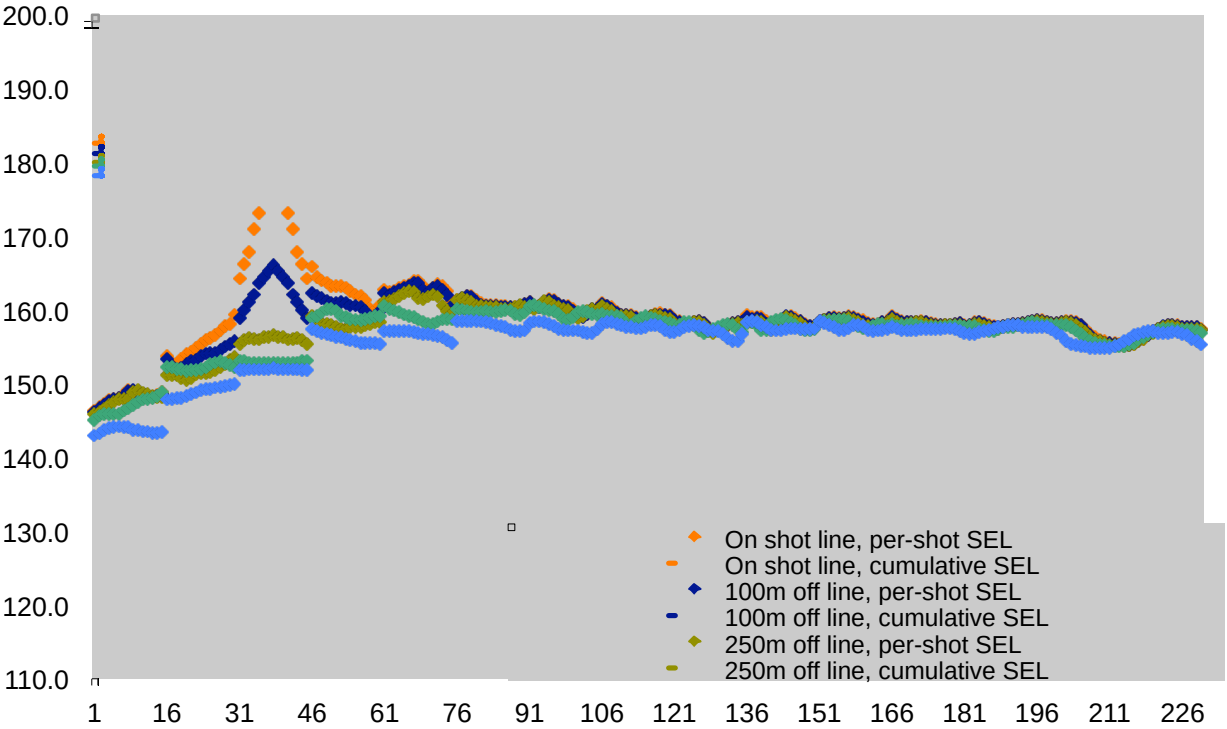

Figure 23: Per-pulse and cumulative SEL versus source point number for the shallow-water scenario for receivers on Profile 2, at 39 m depth.

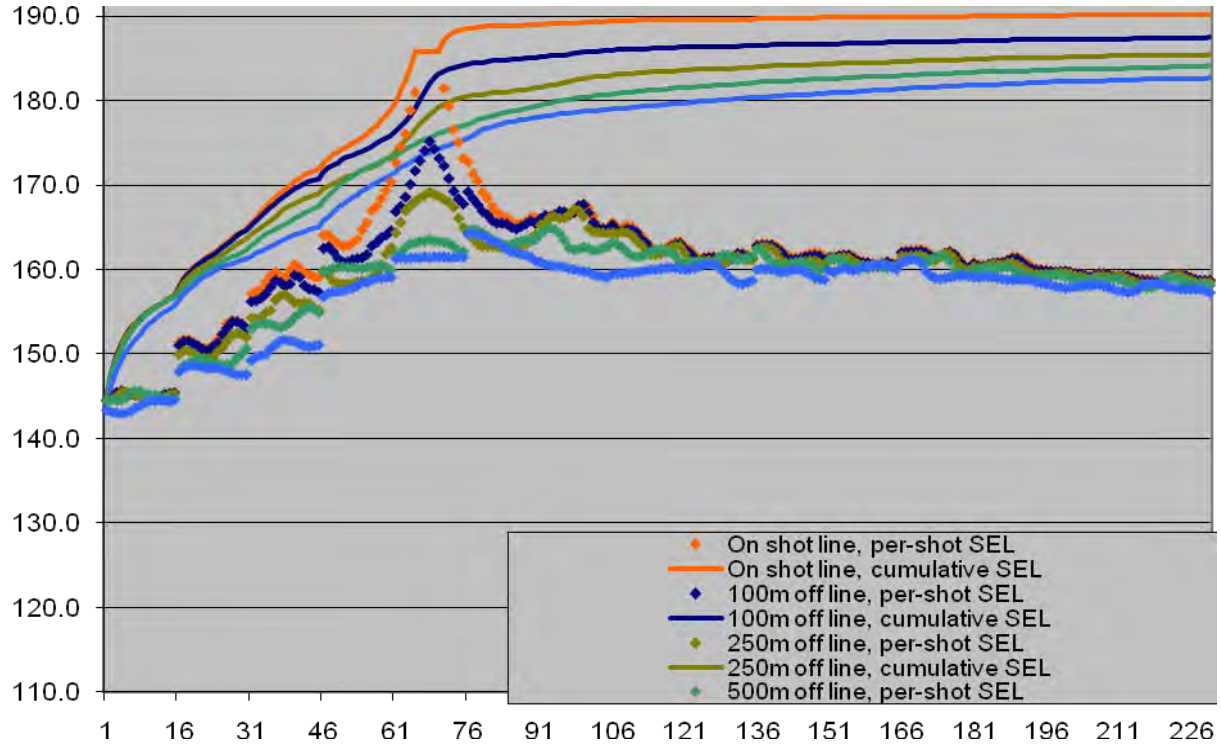

Figure 24: Per-pulse and cumulative SEL versus source point number for the shallow-water scenario for receivers on Profile 3, maximized over all depths.

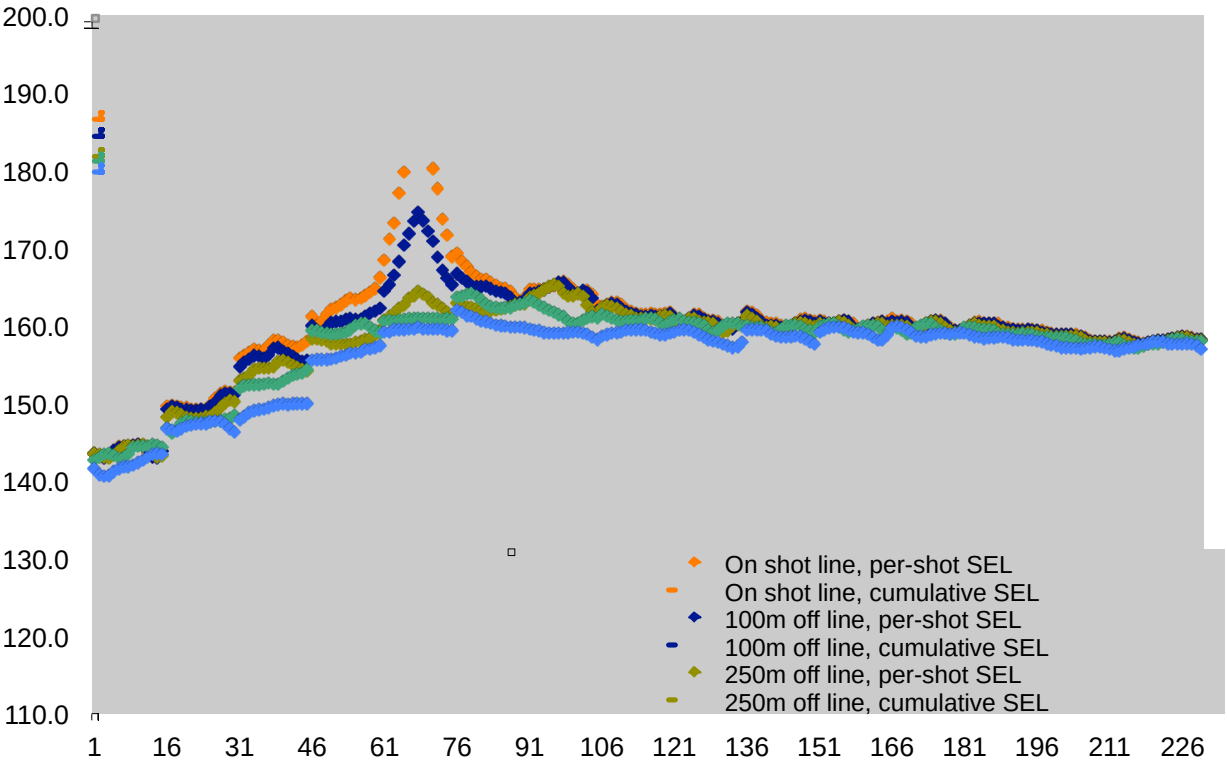

Figure 25: Per-pulse and cumulative SEL versus source point number for the shallow-water scenario for receivers on Profile 3, at 39 m depth.

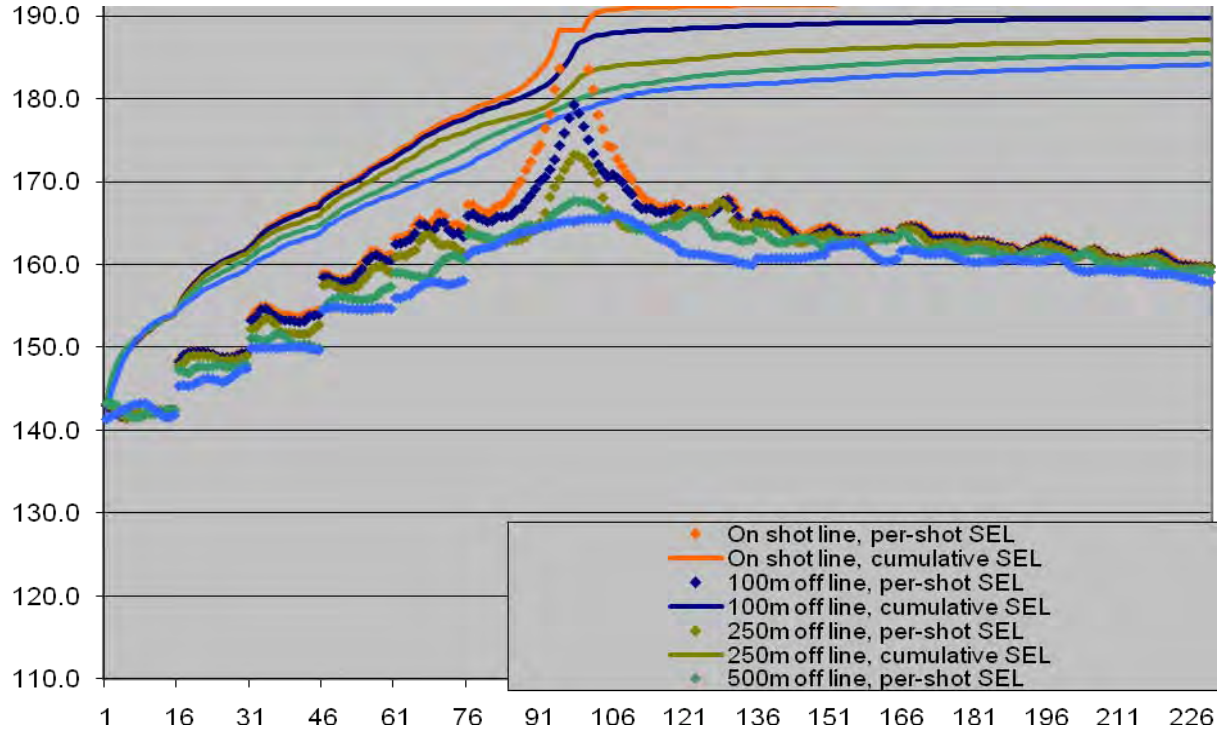

Figure 26: Per-pulse and cumulative SEL versus source point number for the shallow-water scenario for receivers on Profile 4, maximized over all depths.

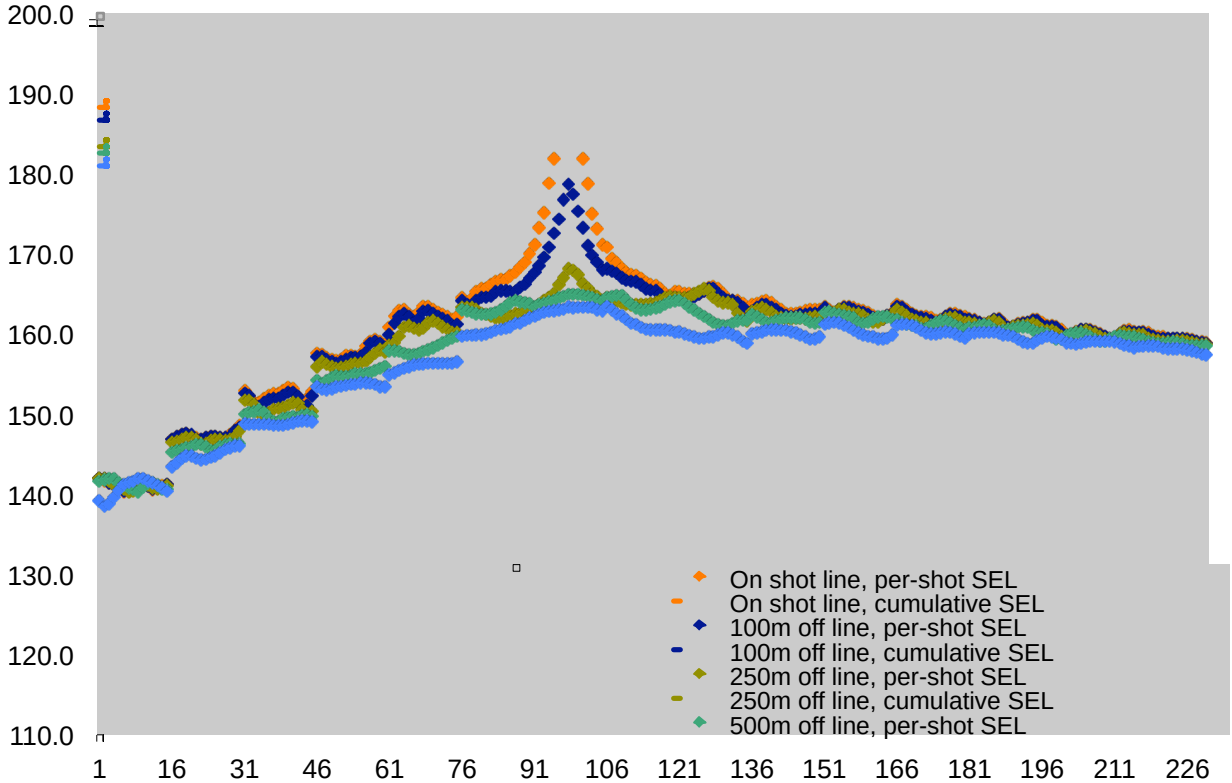

Figure 27: Per-pulse and cumulative SEL versus source point number for the shallow-water scenario for receivers on Profile 4, at 39 m depth.

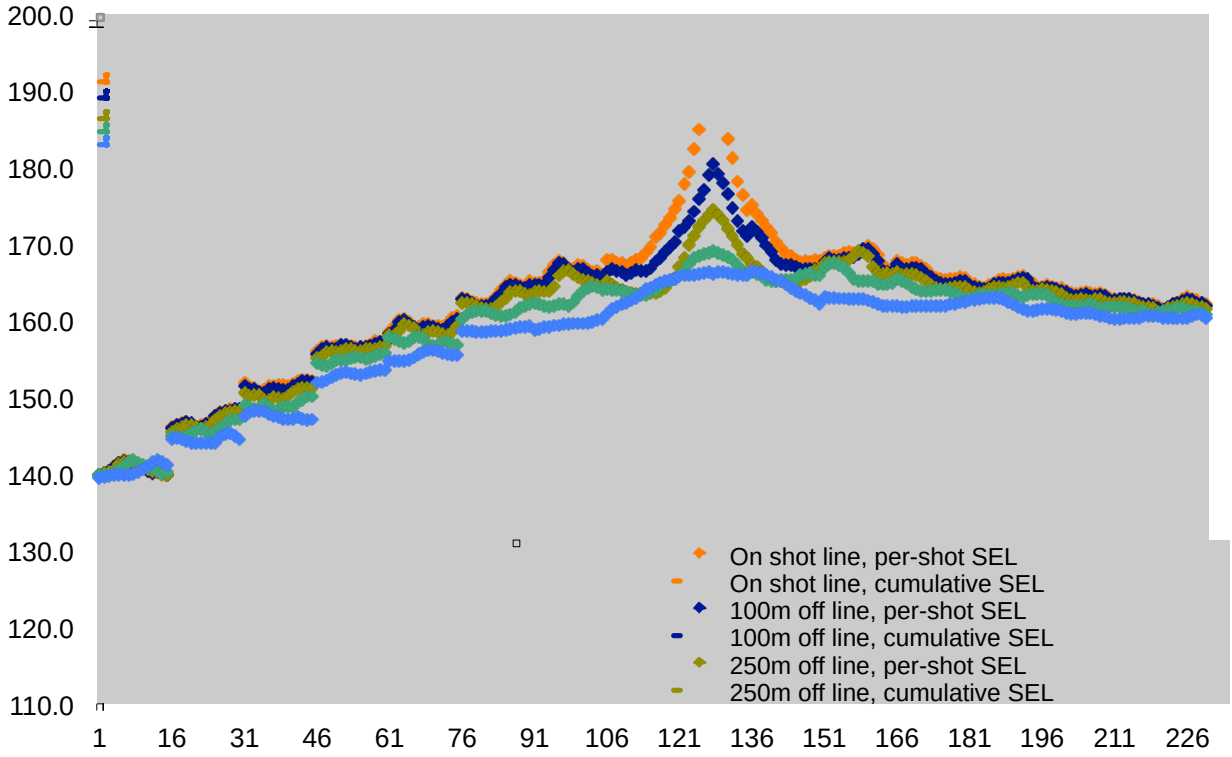

Figure 28: Per-pulse and cumulative SEL versus source point number for the shallow-water scenario for receivers on Profile 5, maximized over all depths.

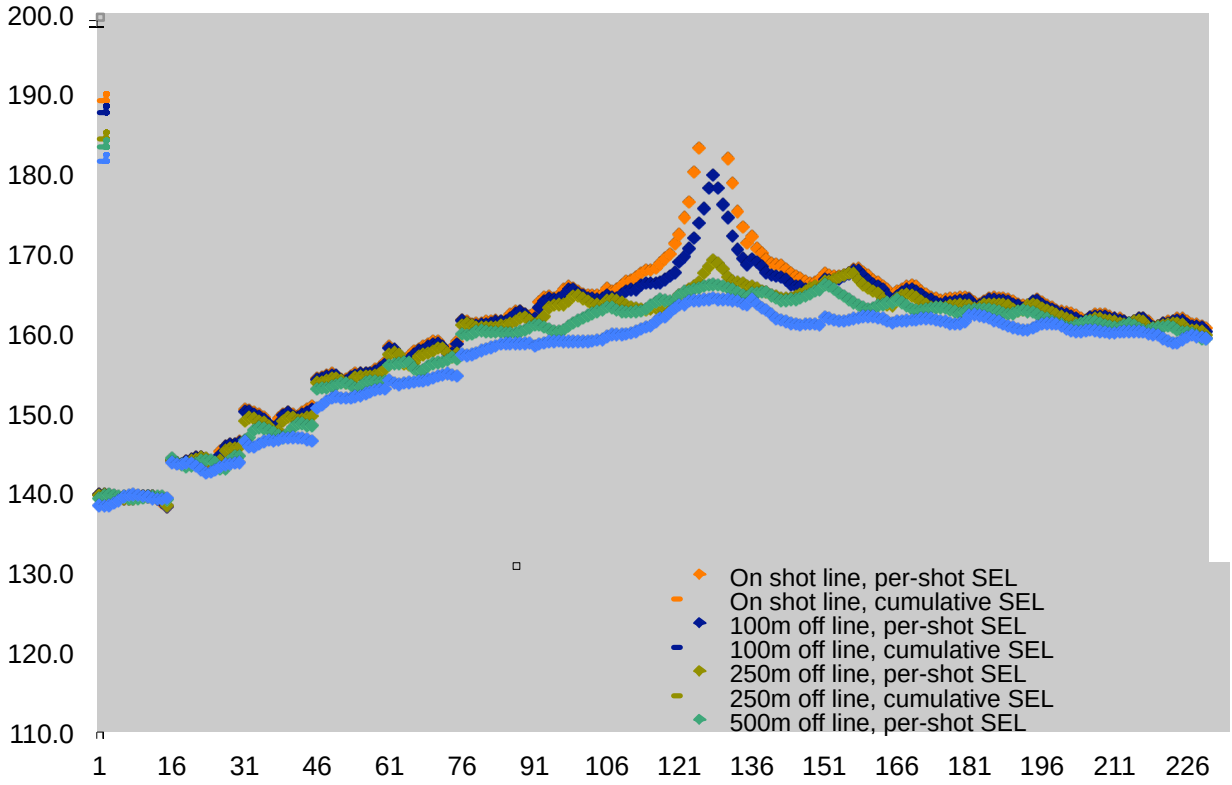

Figure 29: Per-pulse and cumulative SEL versus source point number for the shallow-water scenario for receivers on Profile 5, at 39 m depth.

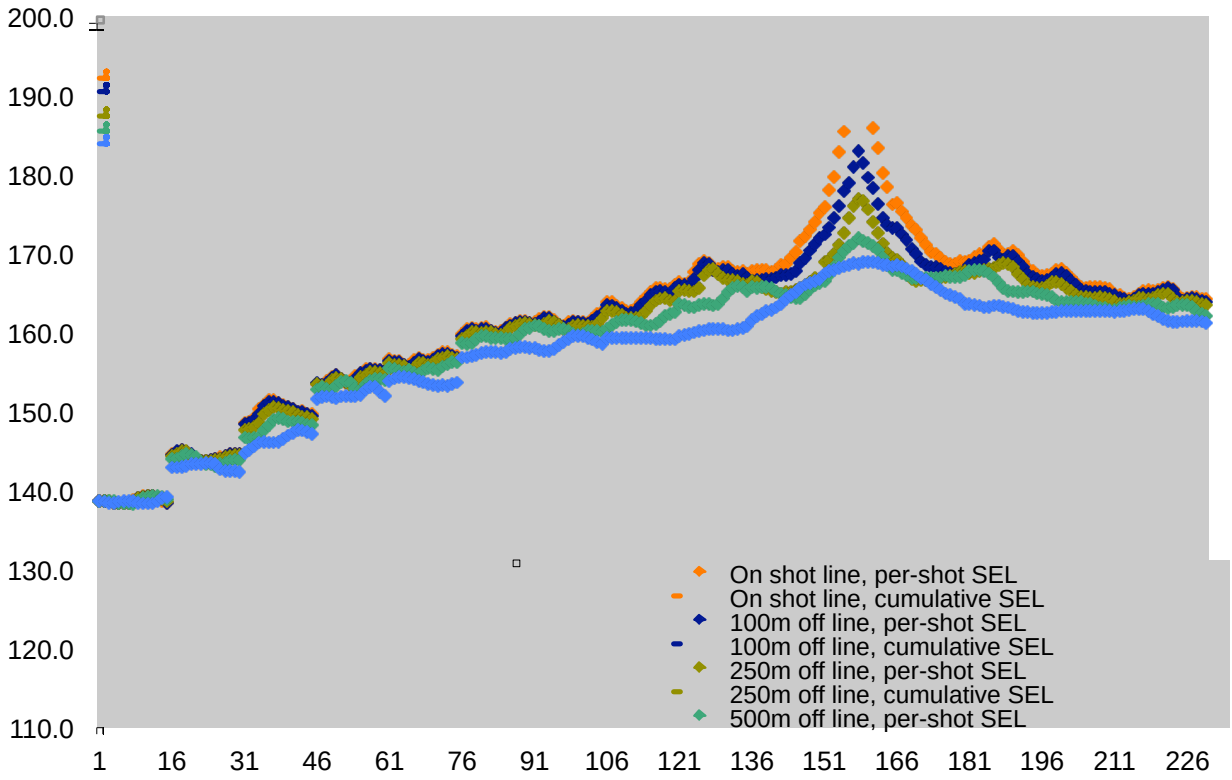

Figure 30: Per-pulse and cumulative SEL versus source point number for the shallow-water scenario for receivers on Profile 6, maximized over all depths.

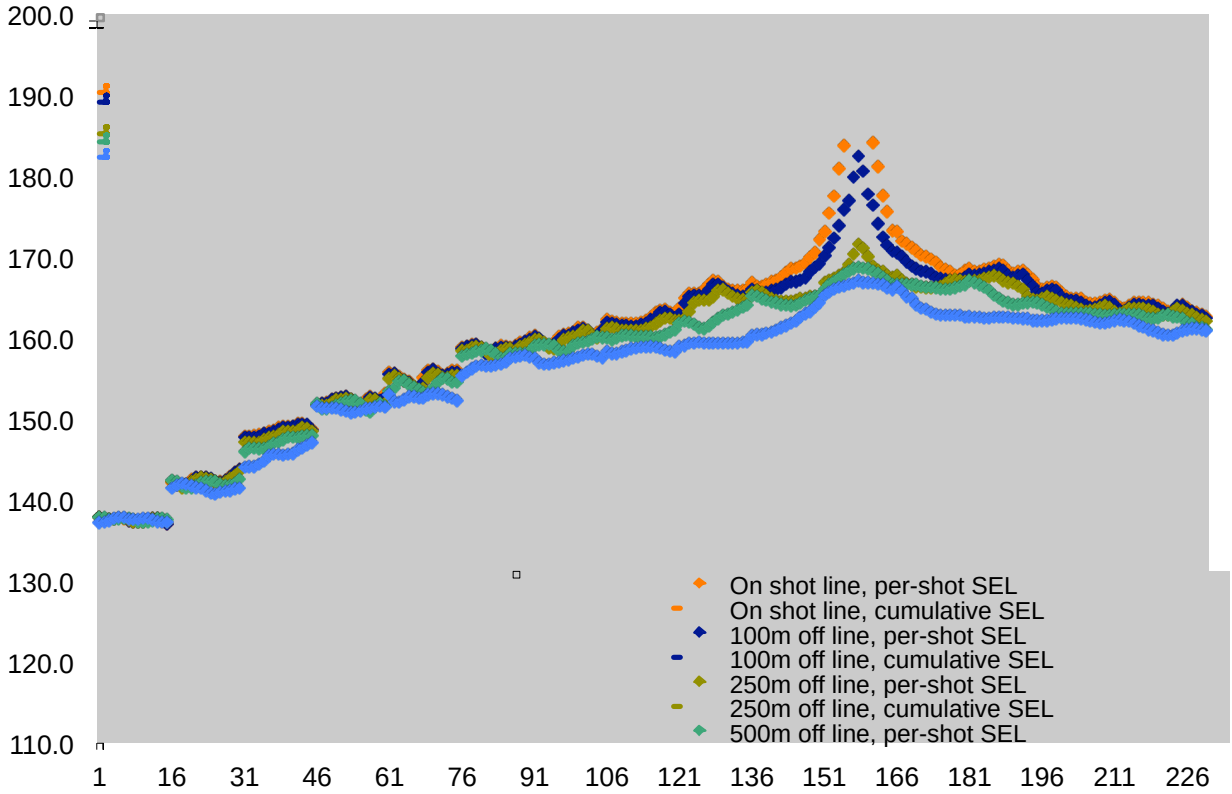

Figure 31: Per-pulse and cumulative SEL versus source point number for the shallow-water scenario for receivers on Profile 6, at 39 m depth.

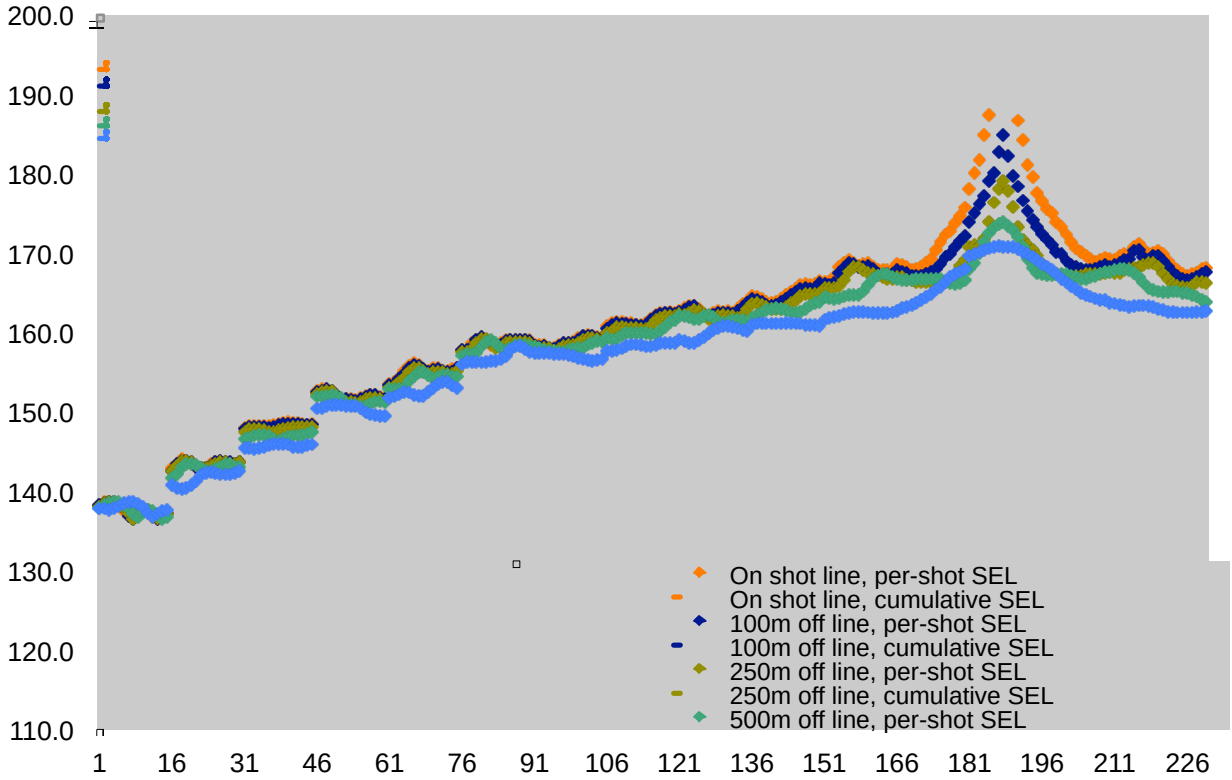

Figure 32: Per-pulse and cumulative SEL versus source point number for the shallow-water scenario for receivers on Profile 7, maximized over all depths.

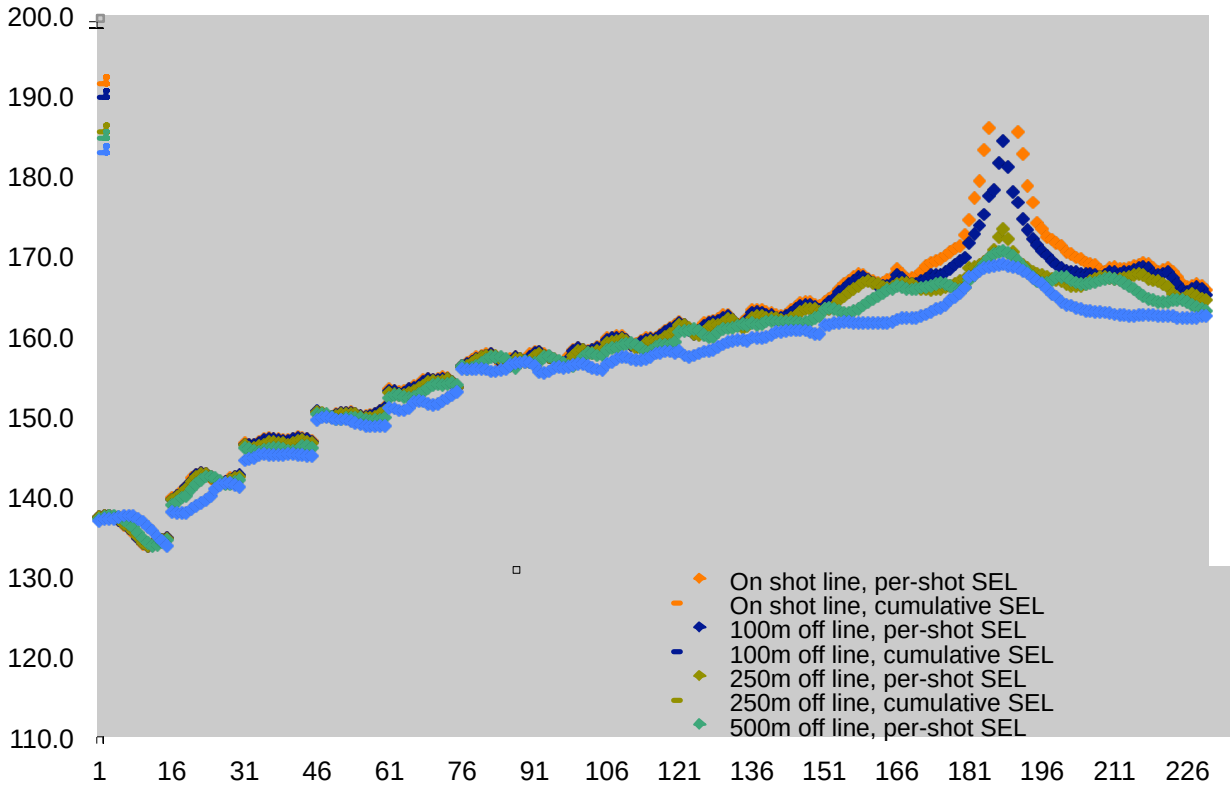

Figure 33: Per-pulse and cumulative SEL versus source point number for the shallow-water scenario for receivers on Profile 7, at 39 m depth.

6.2 Peak Sound Pressure Level (SPL) for Deep Site from PE Model

The peak SPL metric results from the parabolic equation model for the deep site are presented as graphs of acoustic level plotted against the distance between the source and the CPA (closest point

of approach) to the receivers. Figures 34 through 47 on the following pages present the levels at receivers on Profiles 1 through 7; the upper figure on each page shows maximum received levels over all depths, and the lower figure shows levels at a fixed receiver depth of 100 m. As in the previous set of figures, the first 13 distance labels (in the *x*-direction in Figure 1) on the abscissa of the graphs correspond to the starting source point number of the soft-start steps.

As was the case for the per-pulse SEL metric, the effect on the received peak SPL caused by the changes in airgun array configuration during the soft-start is clearly visible and again is most prominent in the early stages of the soft start. Peak level curves are intrinsically more jittery because of the sensitivity of the synthesized waveform amplitude to variations in propagation geometry.

The limitations in the modelling algorithm at steep angles of depression are again evident in the peak SPL curves, resulting in flattened or even slightly depressed maxima near CPA as the algorithm fails to fully account for the propagation. The same considerations expressed for the SEL metric estimation in the previous subsection apply here as well. However, for the peak SPL metric, there is no additive effect of point-wise error as in the case of the cumulative SEL.

Figures 34 and 36 show that for an animal located 100 m off the source line at the midpoint of Steps 1 and 3 of the soft-start, the model estimated values for maximum peak SPL at any depth are about 185 and 187 dB re 1 µPa, respectively. These values are underestimates because of the aforementioned algorithmic limitations, and could in reality reach maxima several decibels higher.

6.3 Peak Sound Pressure Level (SPL) for Shallow Site from PE Model

The peak SPL metric results from parabolic equation modeling for the shallow site are presented in Figure 48 to Figure 61. Again the results are presented as pairs of figures, with the maximum levels over depth given in the upper figure and the level at a fixed depth of 40 m given in the lower figure on the following pages. The horizontal axis labels here represent pulse number from the start of the line.

The shallow site scenario peak pressure results for maximum level over depth exceed the 40 m fixed depth results at the same receiver locations by 1-2 dB. This is expected since the receiver depth difference can be at most 40 m. Peak levels at 100 m off the source line were at most 188 dB re 1 µPa and were 186 dB re 1 µPa at 40 m depth. The corresponding levels on Profile 1 at 1 km distance off-line were 178 dB re 1 µPa and 176 dB re 1 µPa. Interestingly the highest peak levels at 1 km occur for pulses well past the closest-point of approach. This behaviour is attributed to higher pressures from more airgun elements firing later in the soft-start sequence. The higher source pressure dominates the greater acoustic transmission loss incurred by longer propagation distance. The maximum peak pressure received 100 m and 1 km off-line at Profile 3 are 195 dB re 1 µPa and 177 dB re 1 µPa respectively.

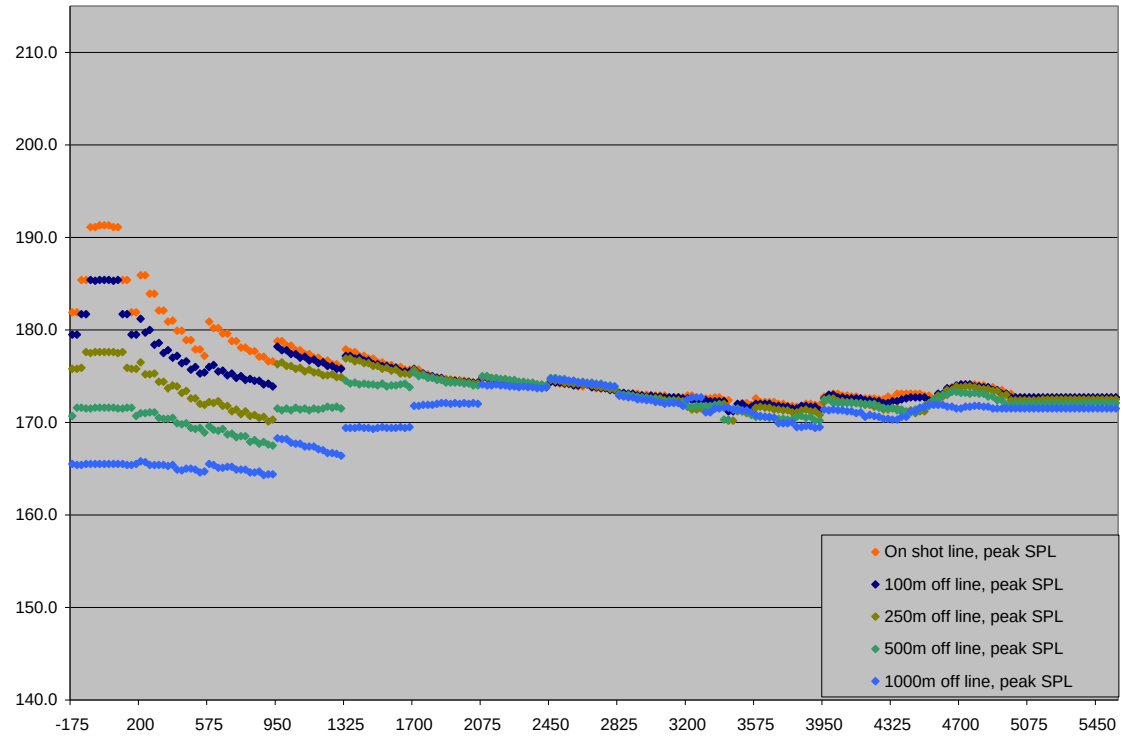

Figure 34: Peak SPL for receivers on Profile 1 of the deep-water scenario, maximized over all depths.

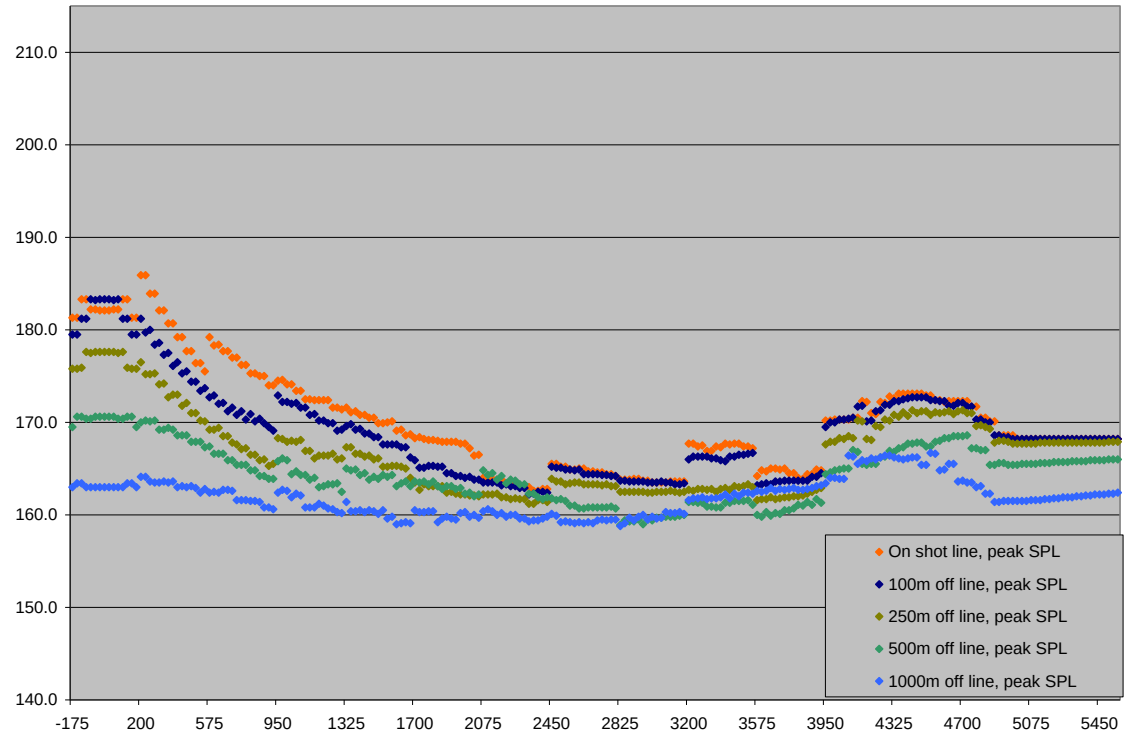

Figure 35: Peak SPL for receivers on Profile 1 of the deep-water scenario at 100 m depth.

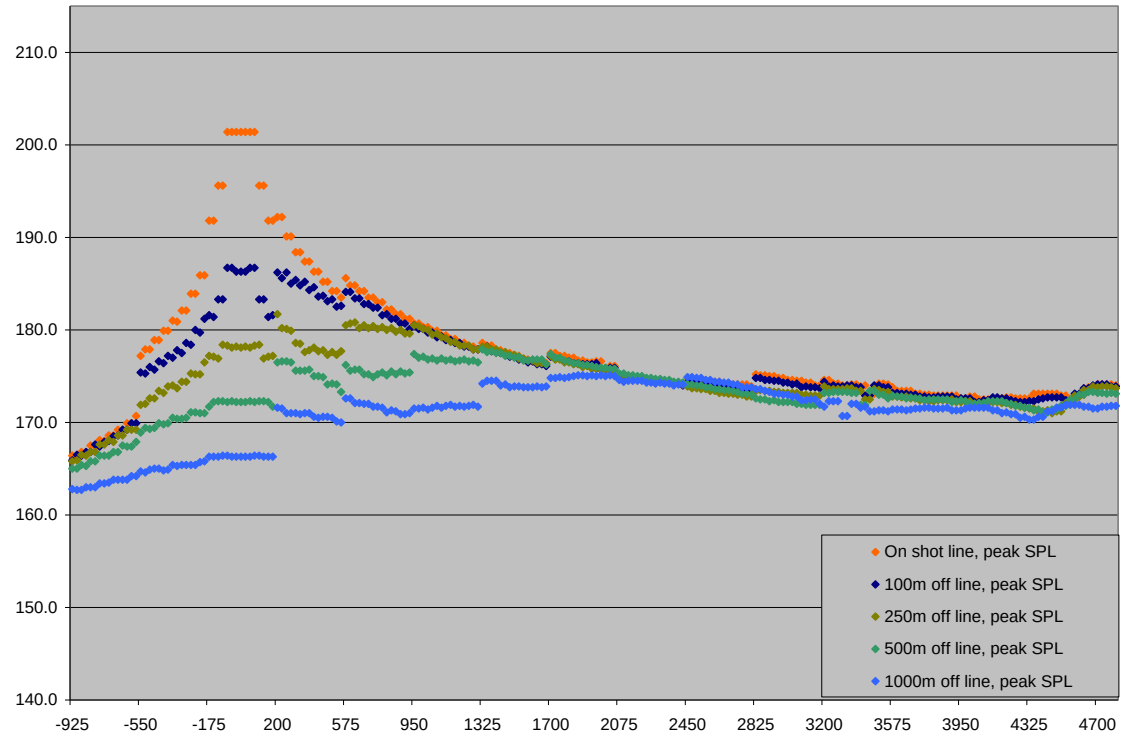

Figure 36: Peak SPL for receivers on Profile 2 of the deep-water scenario, maximized over all depths.

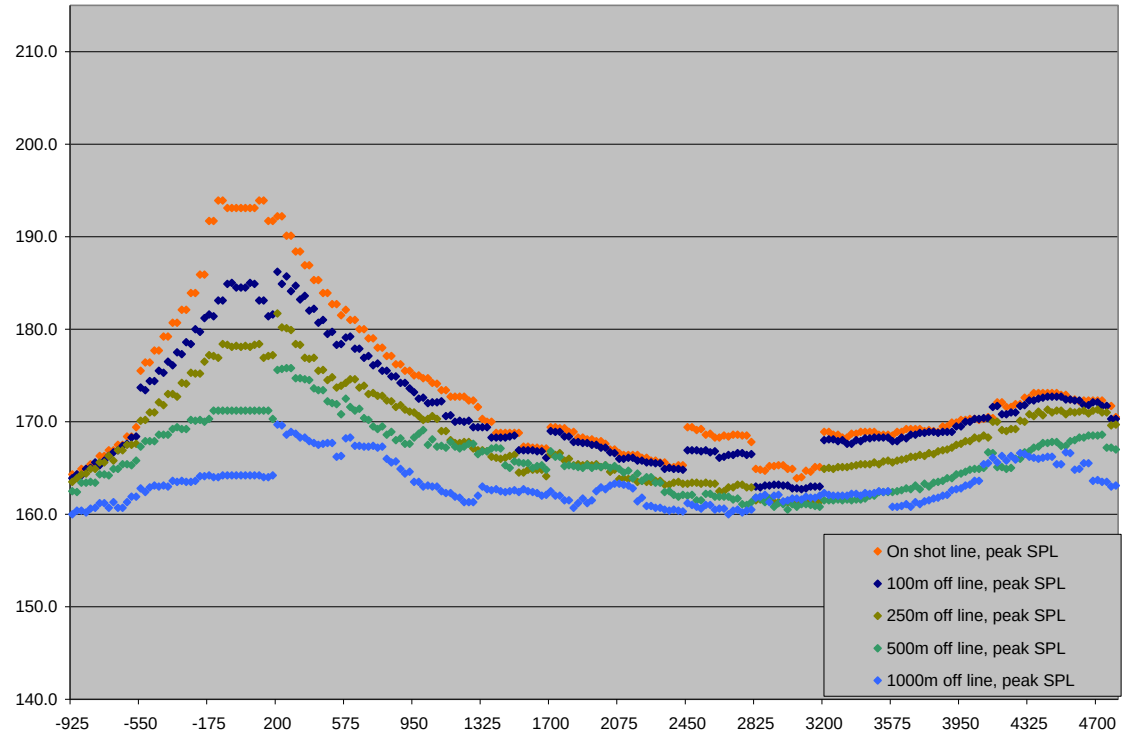

Figure 37: Peak SPL for receivers on Profile 2 of the deep-water scenario at 100 m depth.

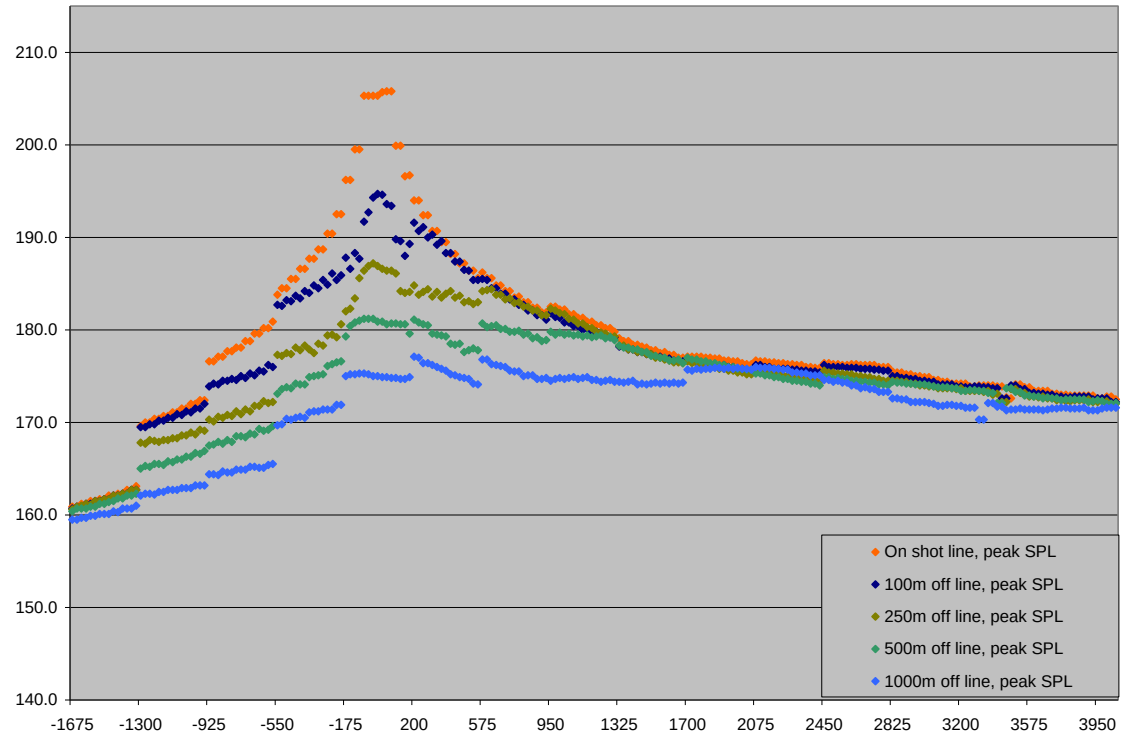

Figure 38: Peak SPL for receivers on Profile 3 of the deep-water scenario, maximized over all depths.

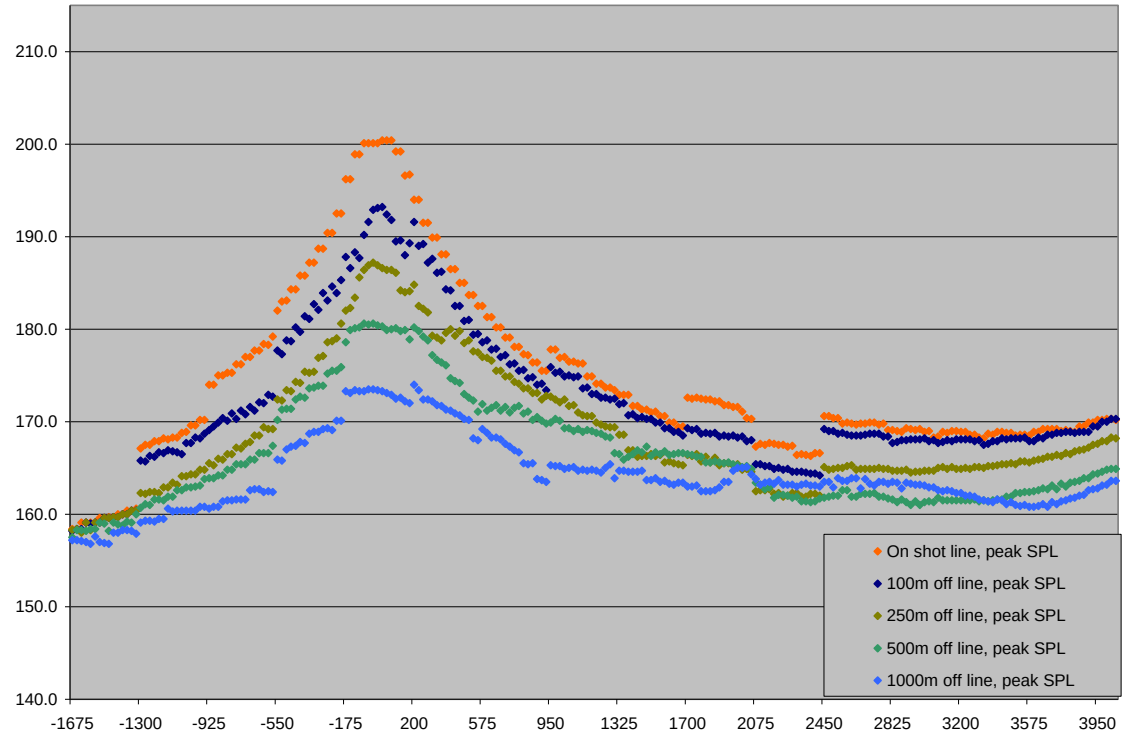

Figure 39: Peak SPL for receivers on Profile 3 of the deep-water scenario at 100 m depth.

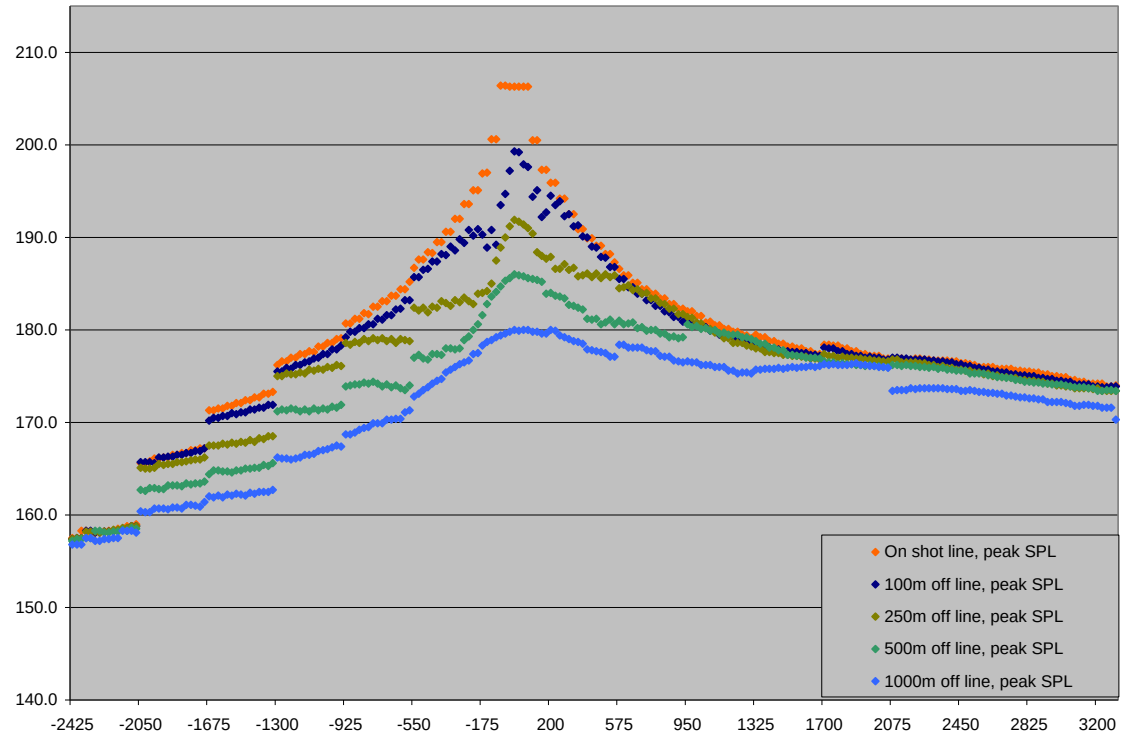

Figure 40: Peak SPL for receivers on Profile 4 of the deep-water scenario, maximized over all depths.

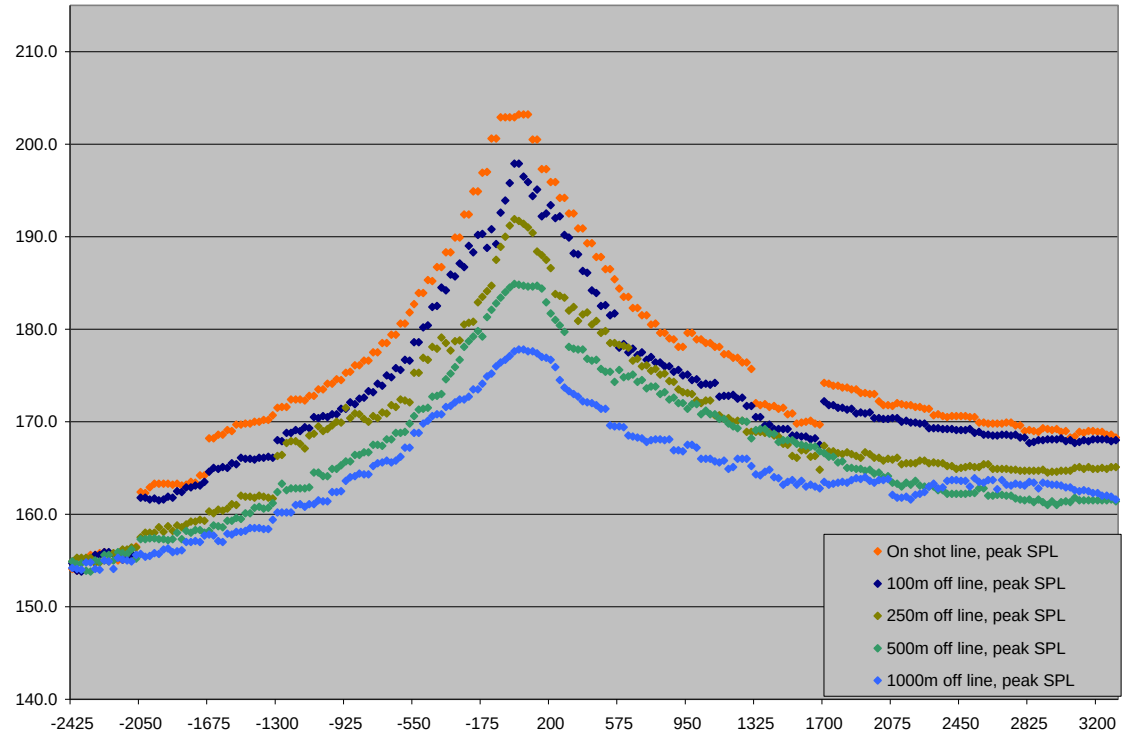

Figure 41: Peak SPL for receivers on Profile 4 of the deep-water scenario at 100 m depth.

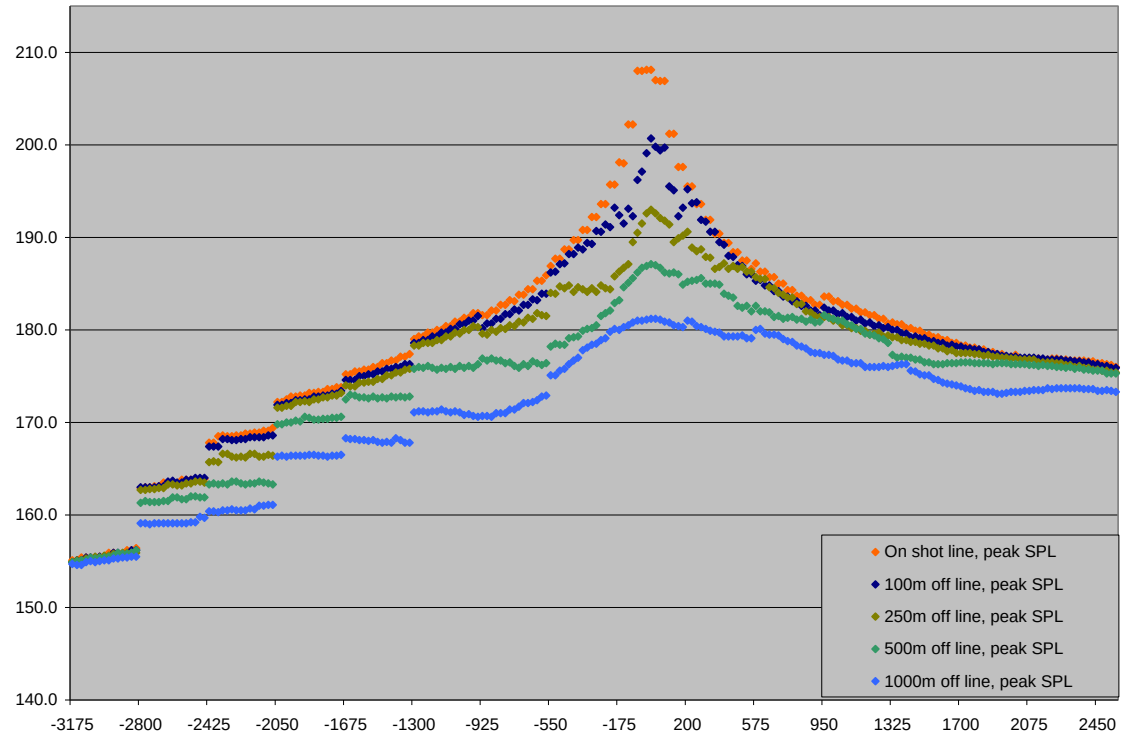

Figure 42: Peak SPL for receivers on Profile 5 of the deep-water scenario, maximized over all depths.

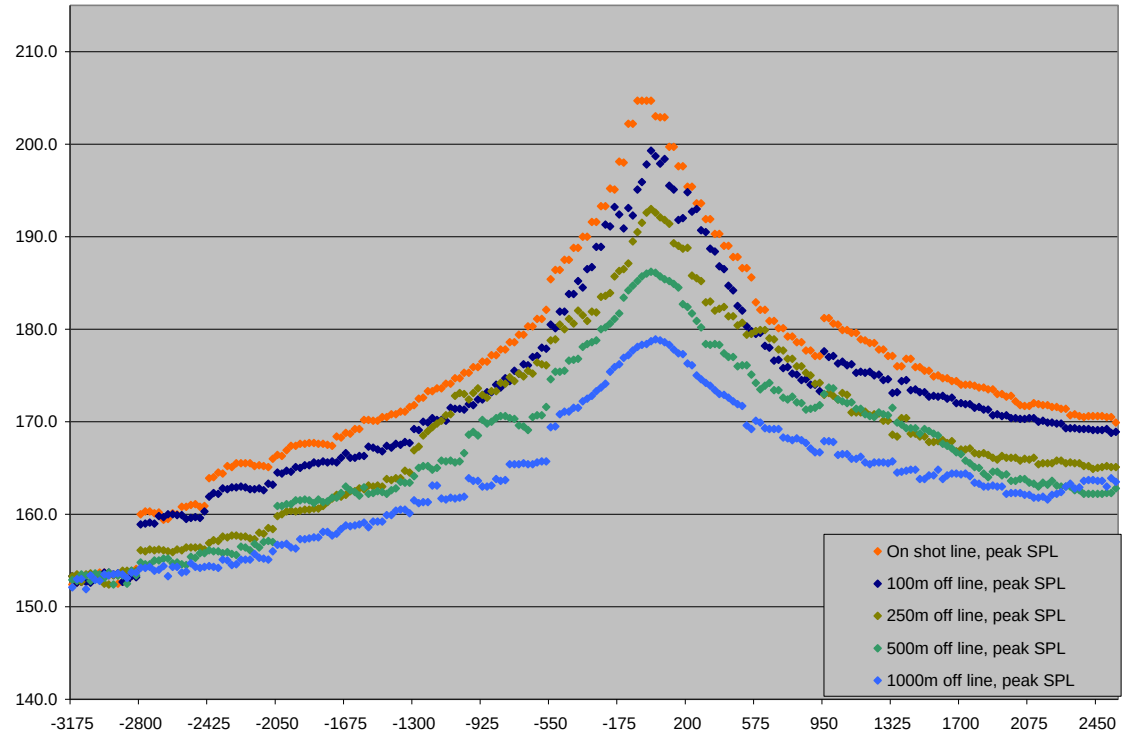

Figure 43: Peak SPL for receivers on Profile 5 of the deep-water scenario at 100 m depth.

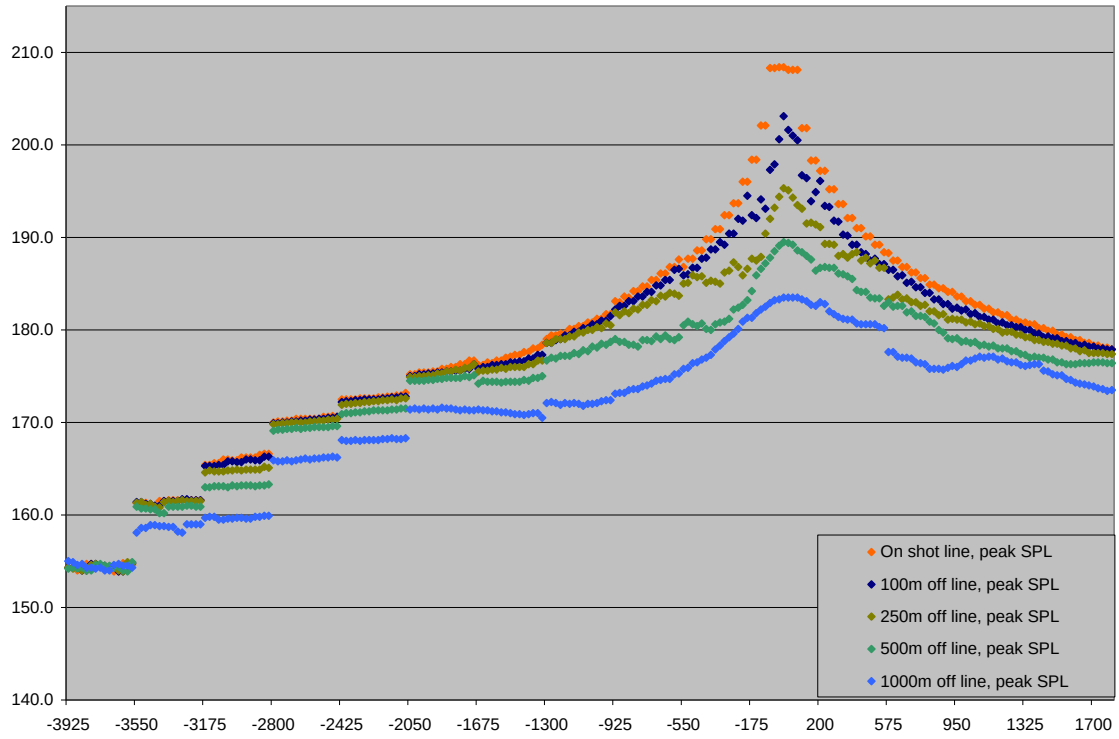

Figure 44: Peak SPL for receivers on Profile 6 of the deep-water scenario, maximized over all depths.

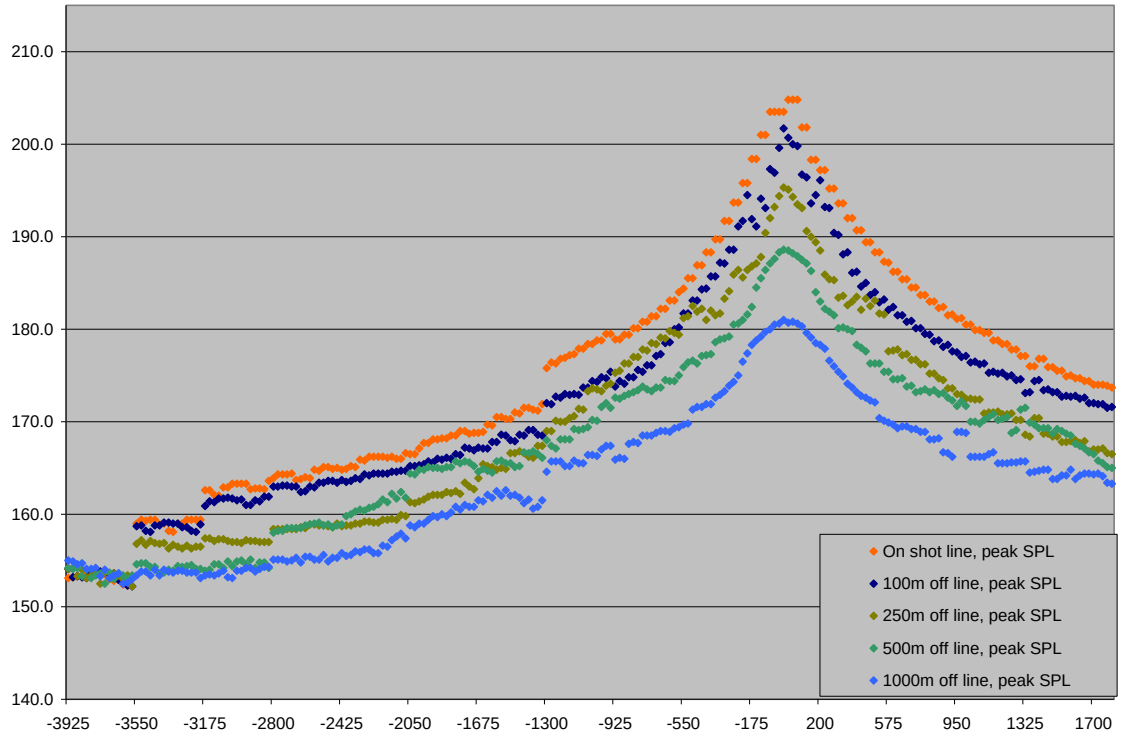

Figure 45: Peak SPL for receivers on Profile 6 of the deep-water scenario at 100 m depth.

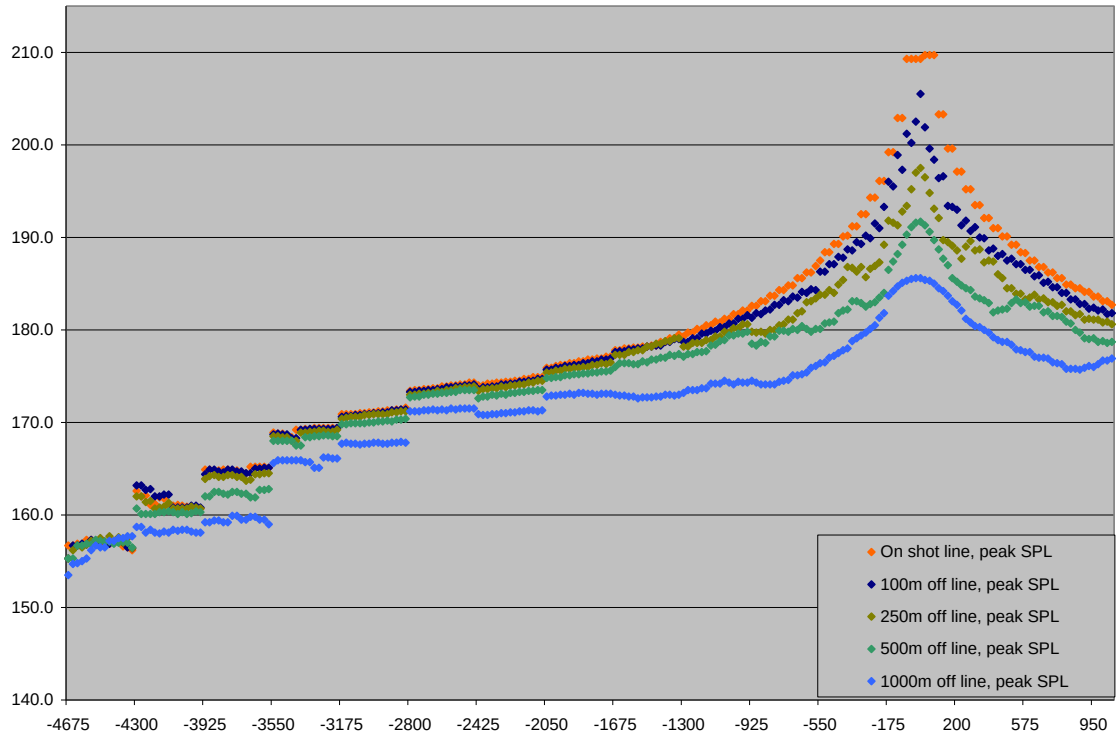

Figure 46: Peak SPL for receivers on Profile 7 of the deep-water scenario, maximized over all depths.

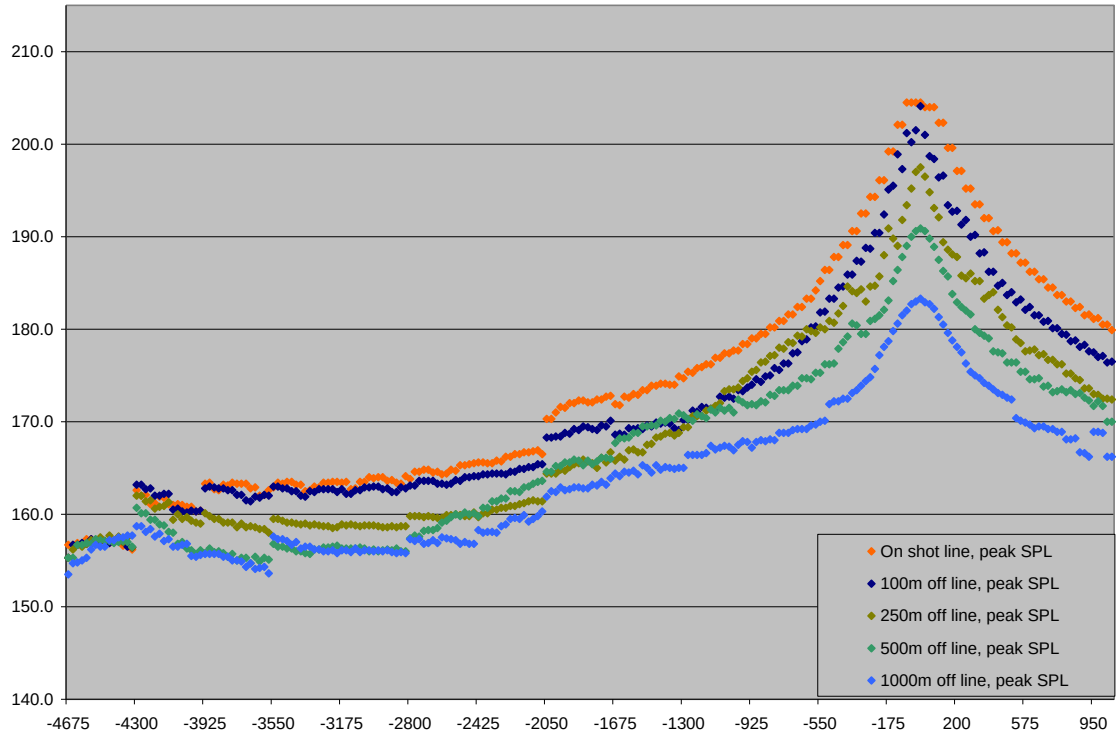

Figure 47: Peak SPL for receivers on Profile 7 of the deep-water scenario at 100 m depth.

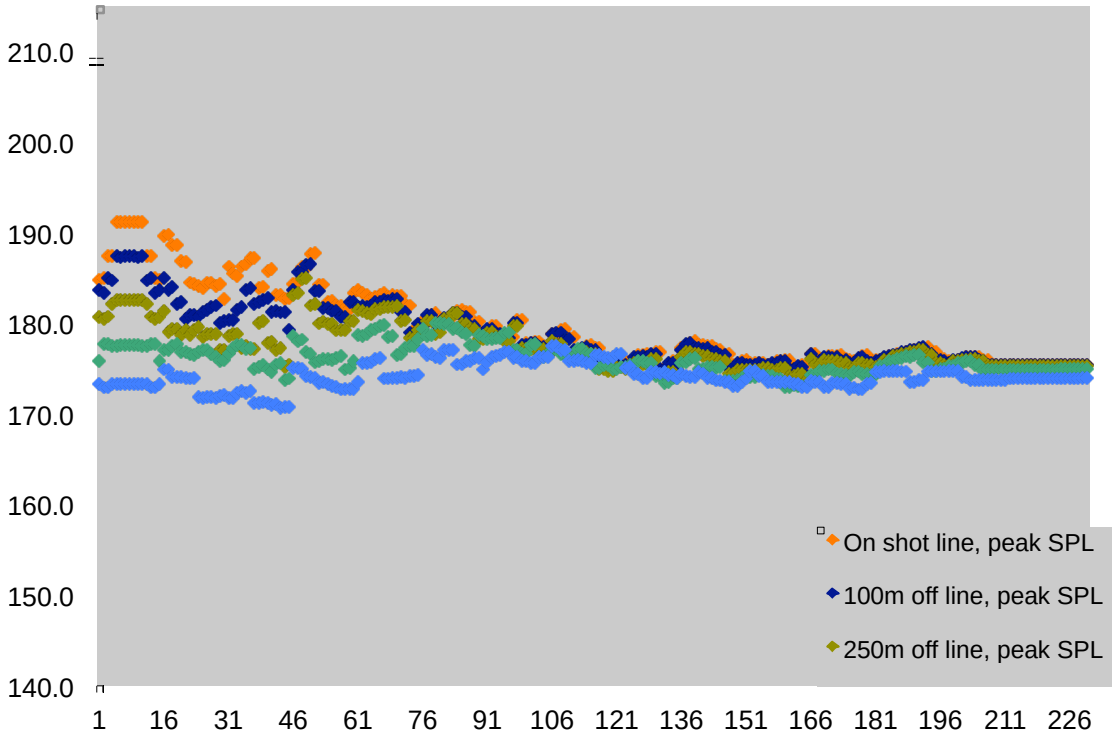

Figure 48: Peak SPL for receivers on Profile 1 of the shallow water scenario, maximized over all depths.

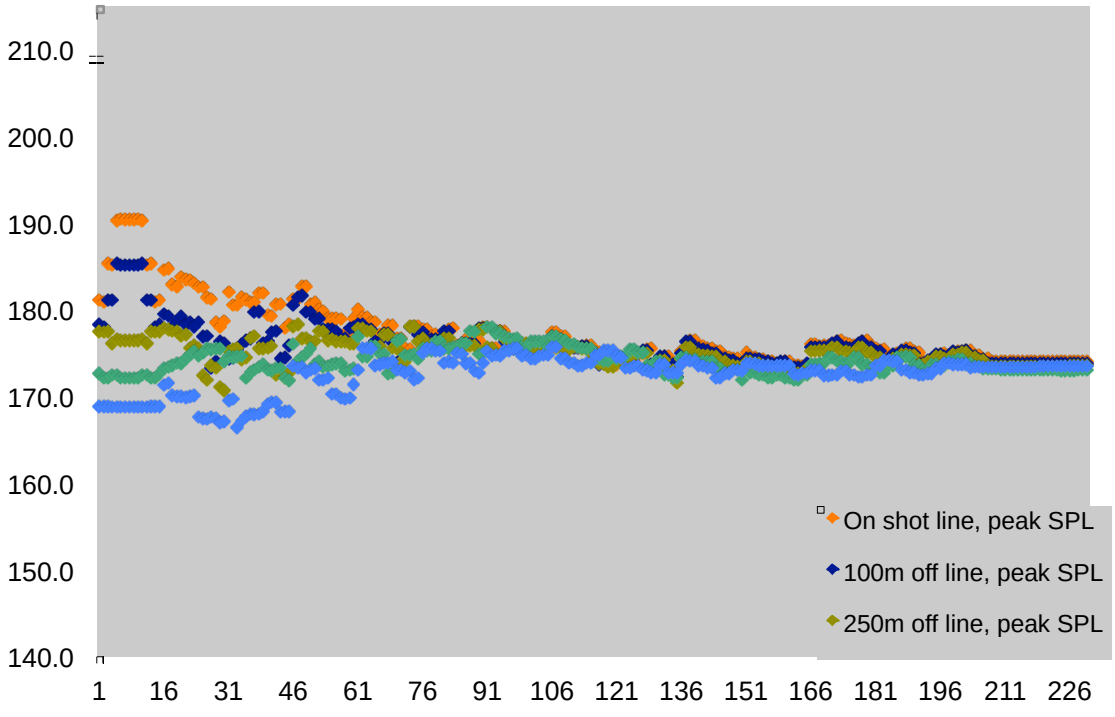

Figure 49: Peak SPL for receivers on Profile 1 of the shallow water scenario at 40 m depth.

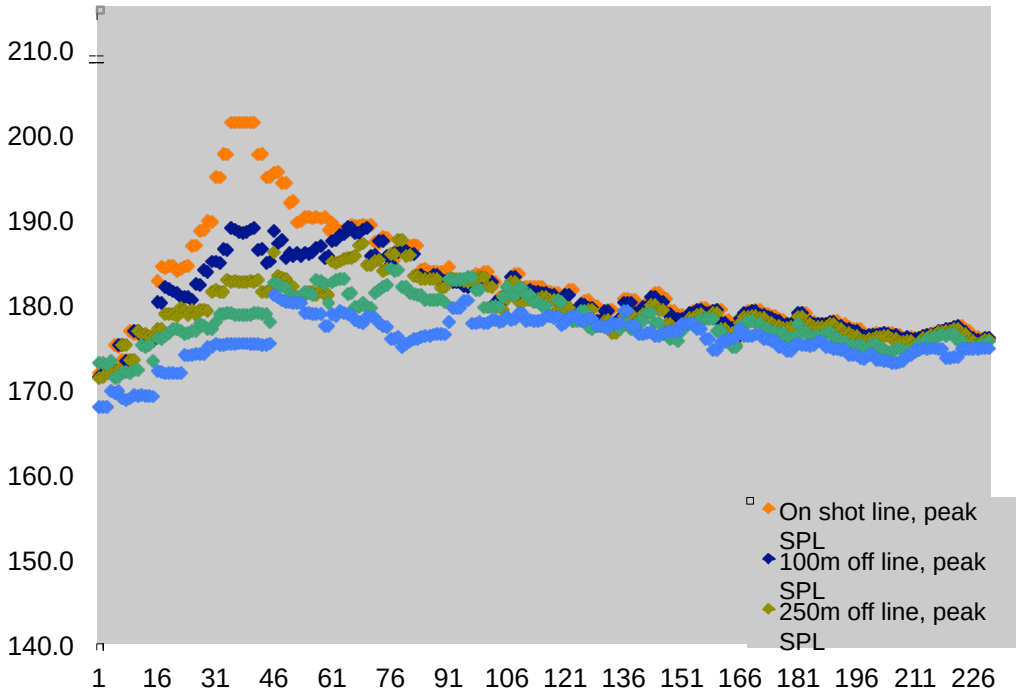

Figure 50: Peak SPL for receivers on Profile 2 of the shallow water scenario, maximized over all depths.

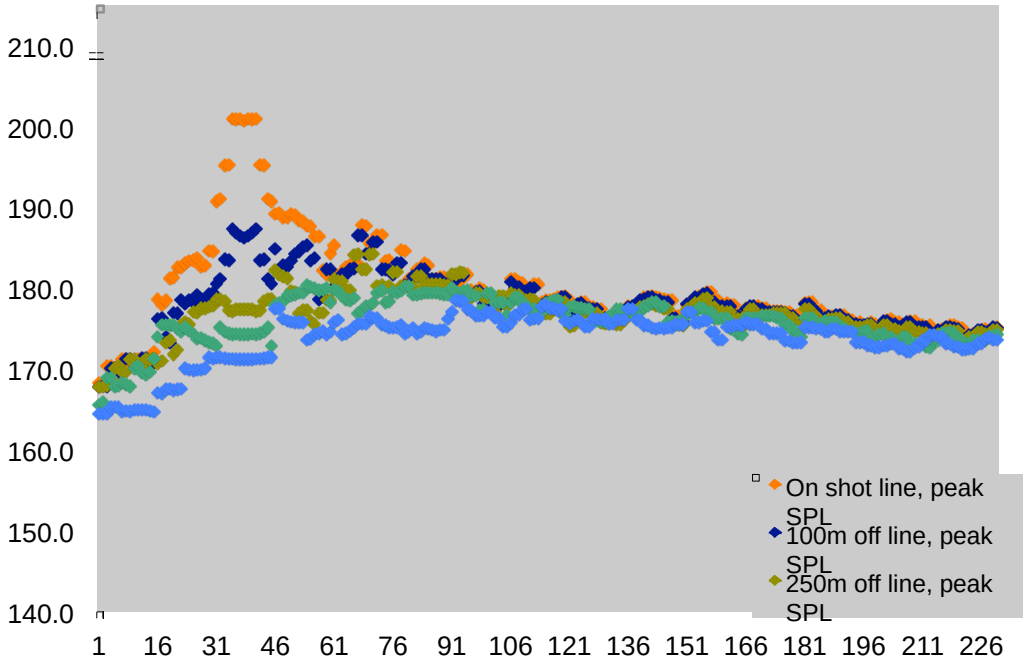

Figure 51: Peak SPL for receivers on Profile 2 of the shallow water scenario at 40 m depth.

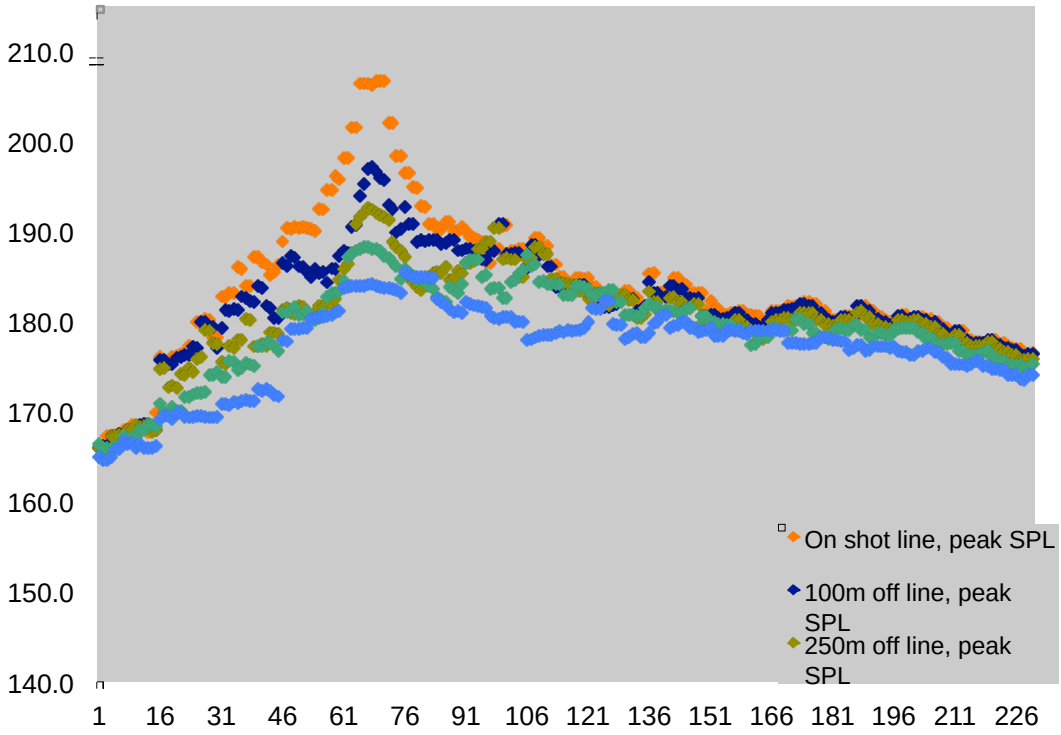

Figure 52: Peak SPL for receivers on Profile 3 of the shallow water scenario, maximized over all depths.

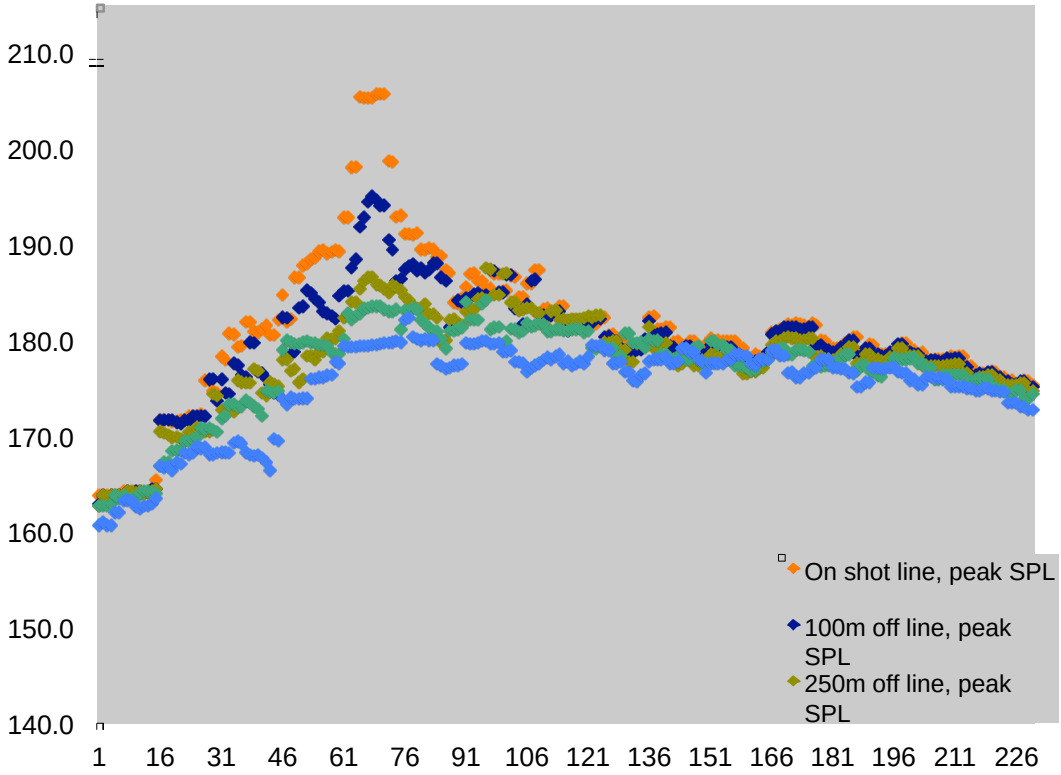

Figure 53: Peak SPL for receivers on Profile 3 of the shallow water scenario at 40 m depth.

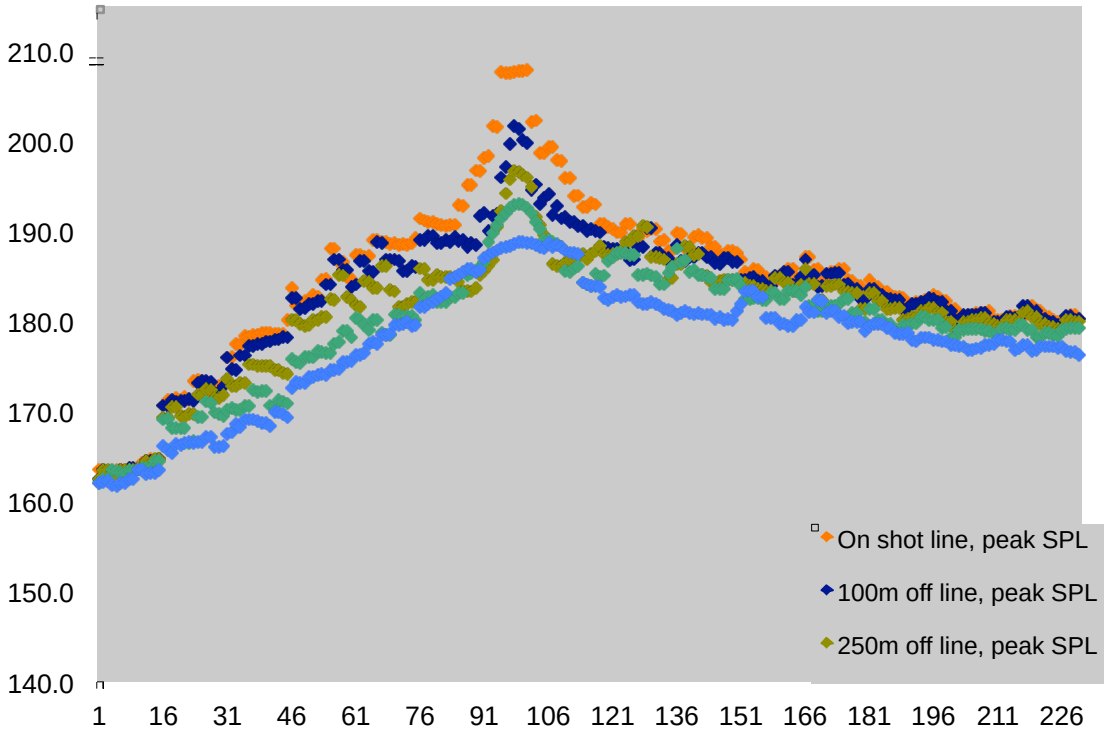

Figure 54: Peak SPL for receivers on Profile 4 of the shallow water scenario, maximized over all depths.

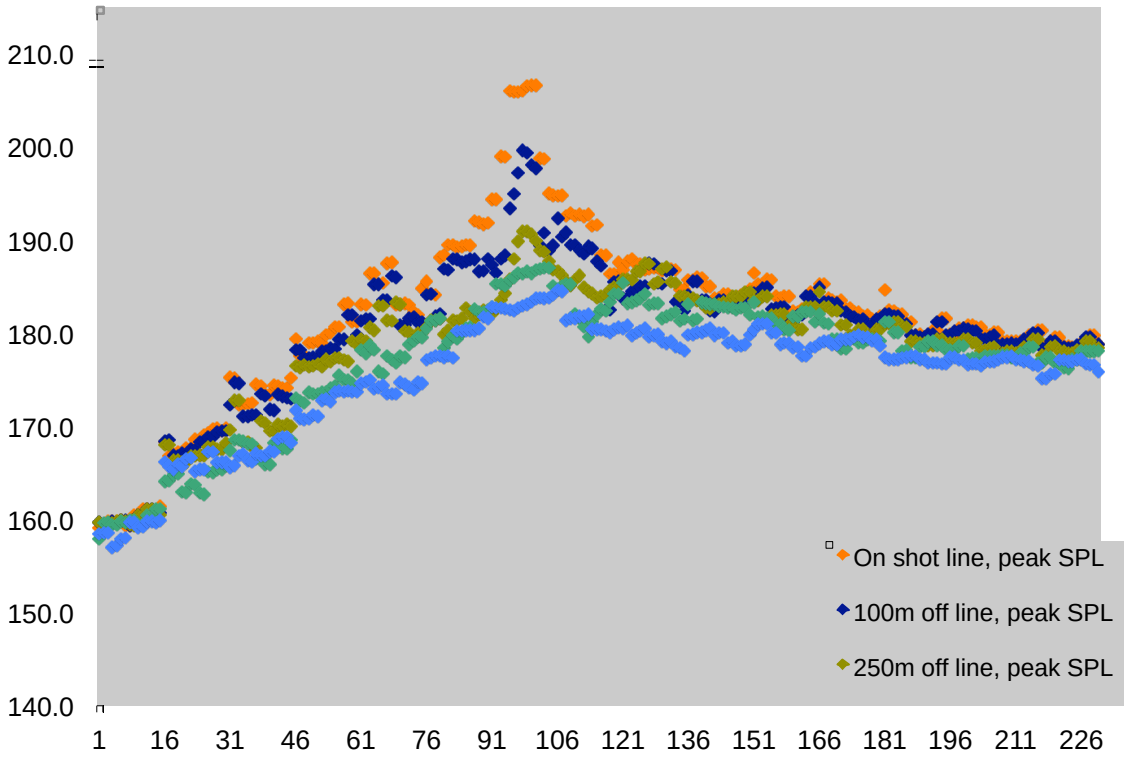

Figure 55: Peak SPL for receivers on Profile 4 of the shallow water scenario at 40 m depth.

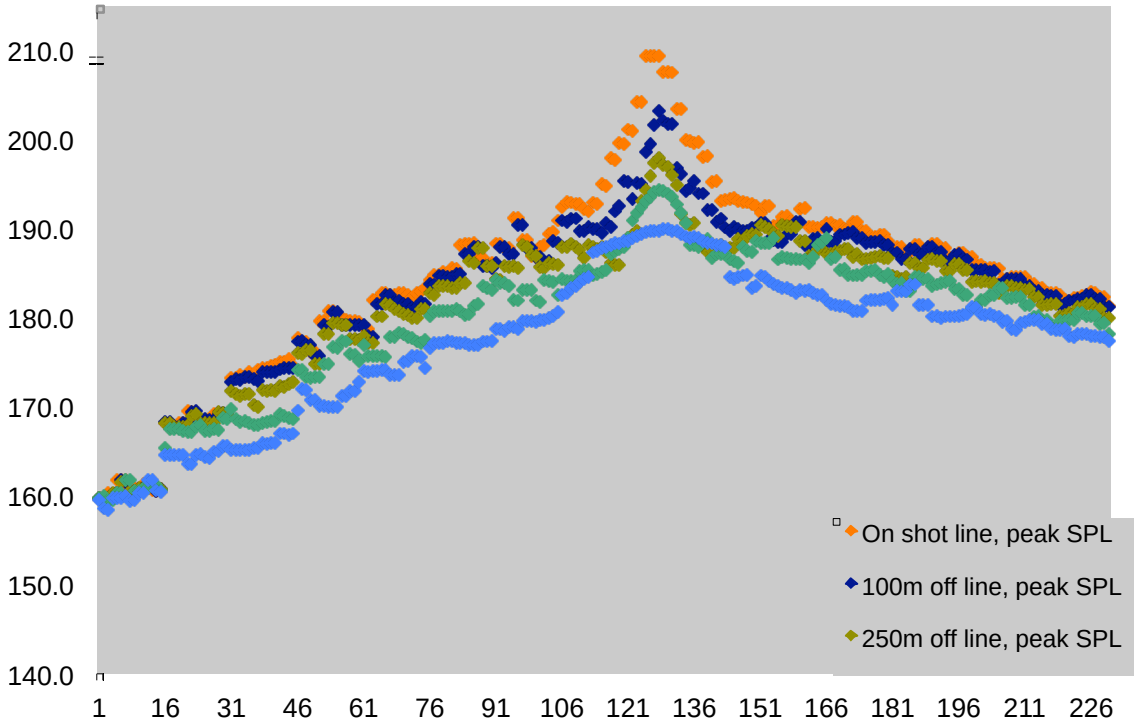

Figure 56: Peak SPL for receivers on Profile 5 of the shallow water scenario, maximized over all depths.

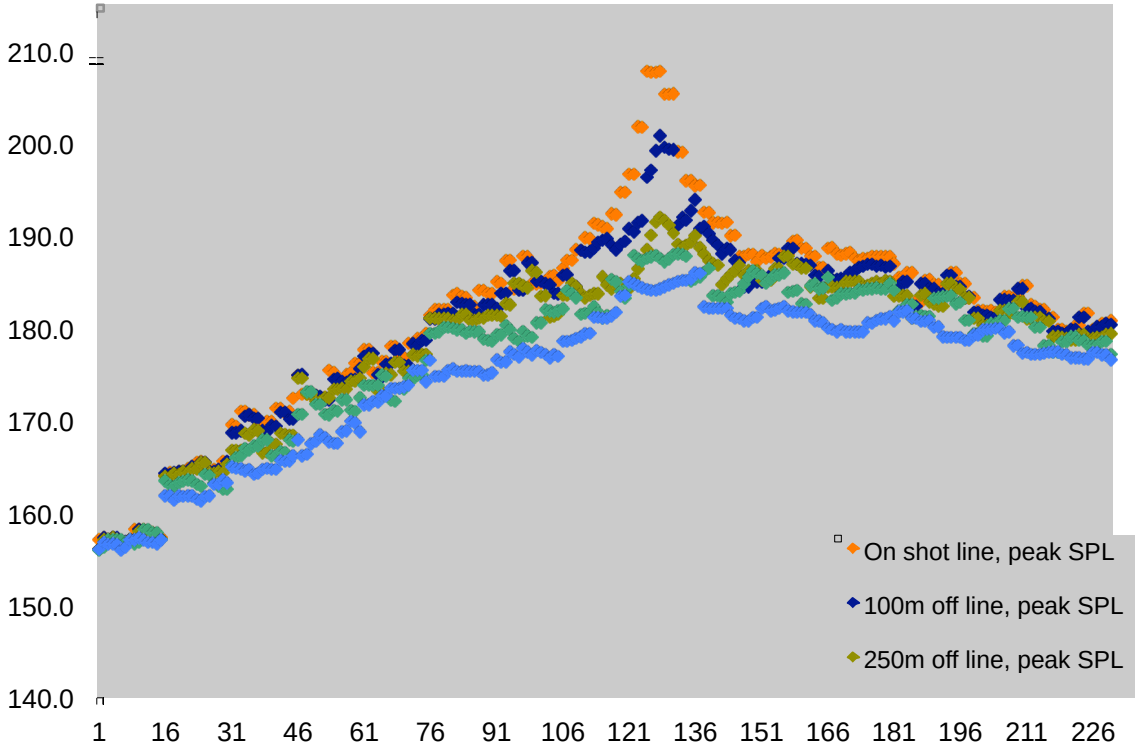

Figure 57: Peak SPL for receivers on Profile 5 of the shallow water scenario at 40 m depth.

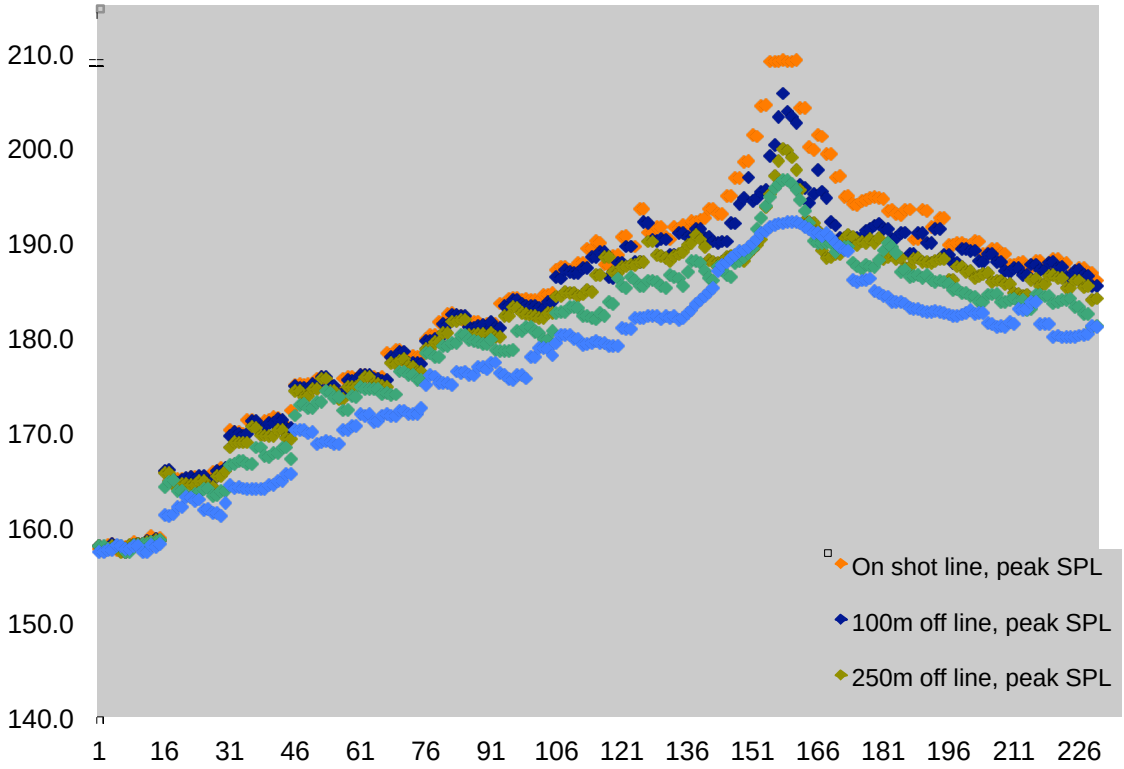

Figure 58: Peak SPL for receivers on Profile 6 of the shallow water scenario, maximized over all depths.

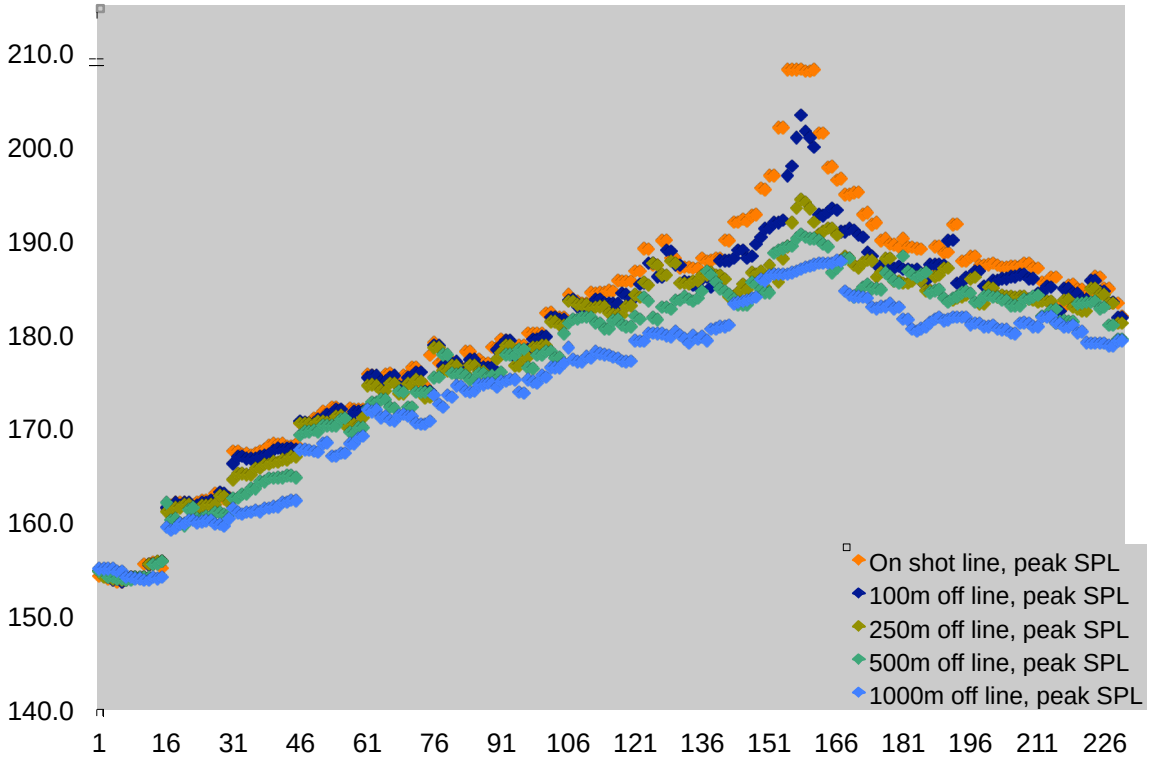

Figure 59: Peak SPL for receivers on Profile 6 of the shallow water scenario at 40 m depth.

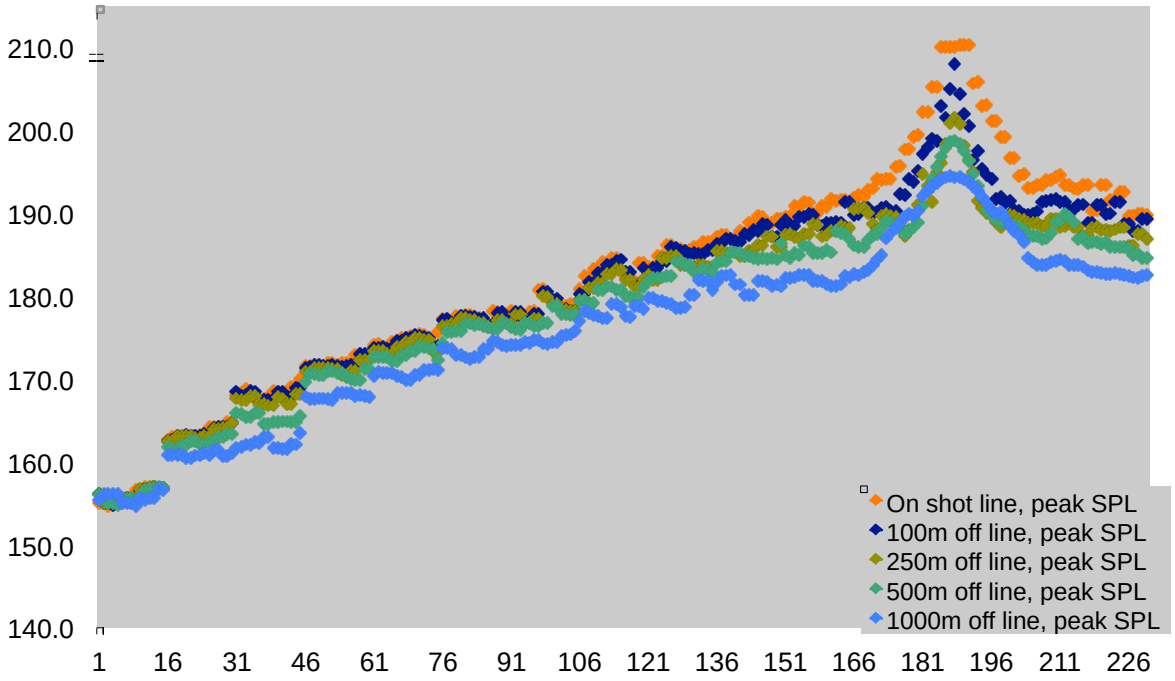

Figure 60: Peak SPL for receivers on Profile 7 of the shallow water scenario, maximized over all depths.

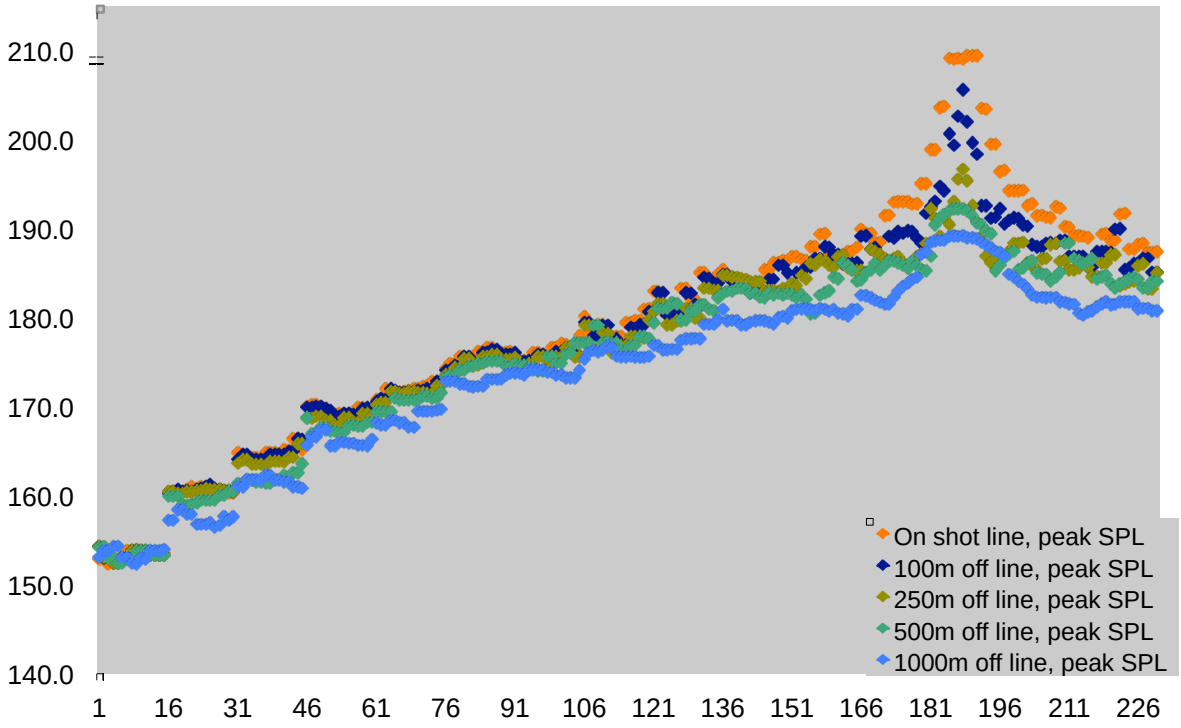

Figure 61: Peak SPL for receivers on Profile 7 of the shallow water scenario at 40 m depth.

7 Results: Wavenumber Integral Model of Deep-Water Scenario

7.1 Pressure Synthetics

While the parabolic equation method provides output simultaneously on a grid of range and depth points, the wavenumber integral results are computed only at specified receiver positions. For this study we ran the wavenumber integral model only for the deep-water scenario (2000 m water depth) for receiver depths of 100, 1000 and 1900 m to provide sampling of the near-surface, mid-depth and near-bottom pressure fields. The model was run for receiver Profiles 1, 1A, 2, 2A, and 3 for the on-line, and 100, 250 and 500-m off-line receivers in each profile to provide more detailed information of sound levels during the initial stages of soft-start. A total of 60 modelling runs were performed (5 profiles × 4 off-line distances × 3 depths).

Each run produced synthetic pressure data sampled at 1024 Hz containing sound pressure in the 5–500 Hz frequency band. These results are presented below in Figures 62 to 71 in pressure versus time format for all source points. Each plot contains the synthetic (modelled) pressures for all 230 source points of the 12 step soft-start sequence. Each step contains 15 source points of a constant airgun configuration as defined in Table 1. Profile 1 occurs at source point number 8 so is centred in Step 1 of the soft-start sequence. Profile 1A occurs at source point 23, centred in Step 2, Profile 2 centred at source point 38 in Step 3, Profile 2A at source point 53 centred in Step 4, and Profile 3 occurs at source point 68 centred in Step 5 (see Figure 1). Some of the 4-s traces are wrapped in time as a result of their calculation through Fourier decomposition even though the depth-dependent function was restricted to the direct path and single order bottom reflected paths: D, B, SB, BS, SBS. In most cases the wrapping is easily recognized. The wrapping does not affect SEL calculations.

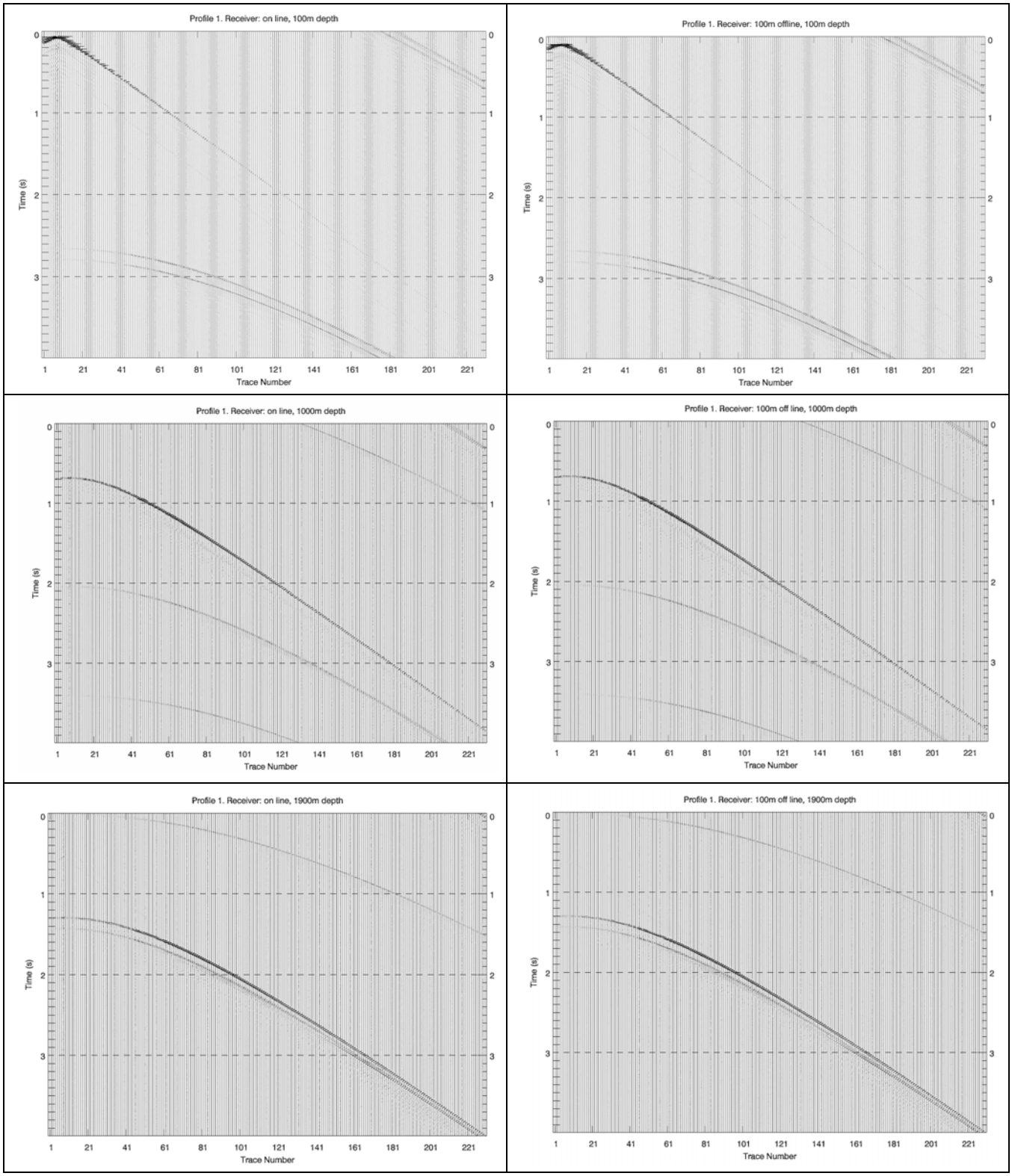

Figure 62: Synthetic pressures for on-line and 100 m off-line receivers of Profile 1.

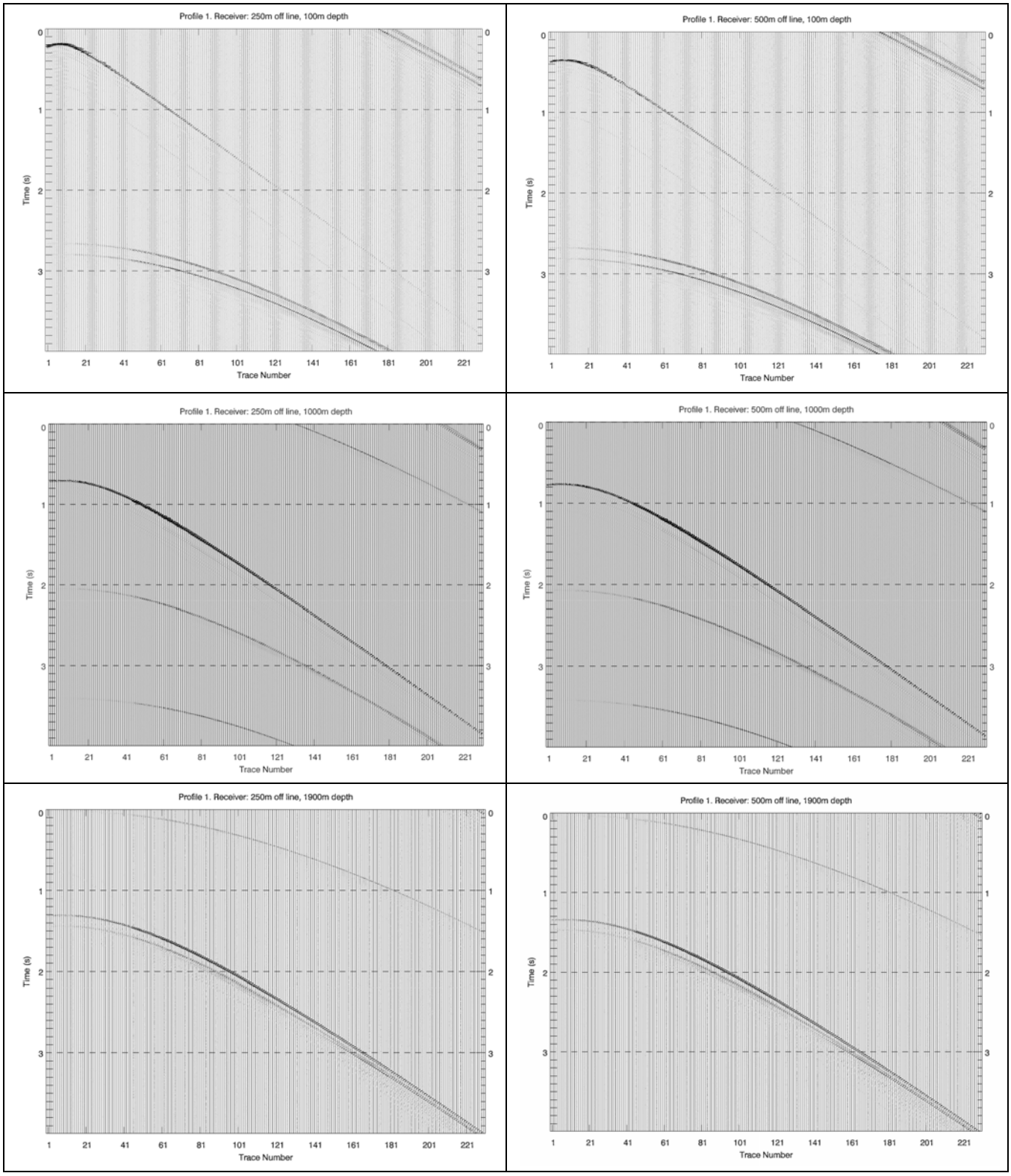

Figure 63: Synthetic pressures for 250 and 500 m off-line receivers of Profile 1.

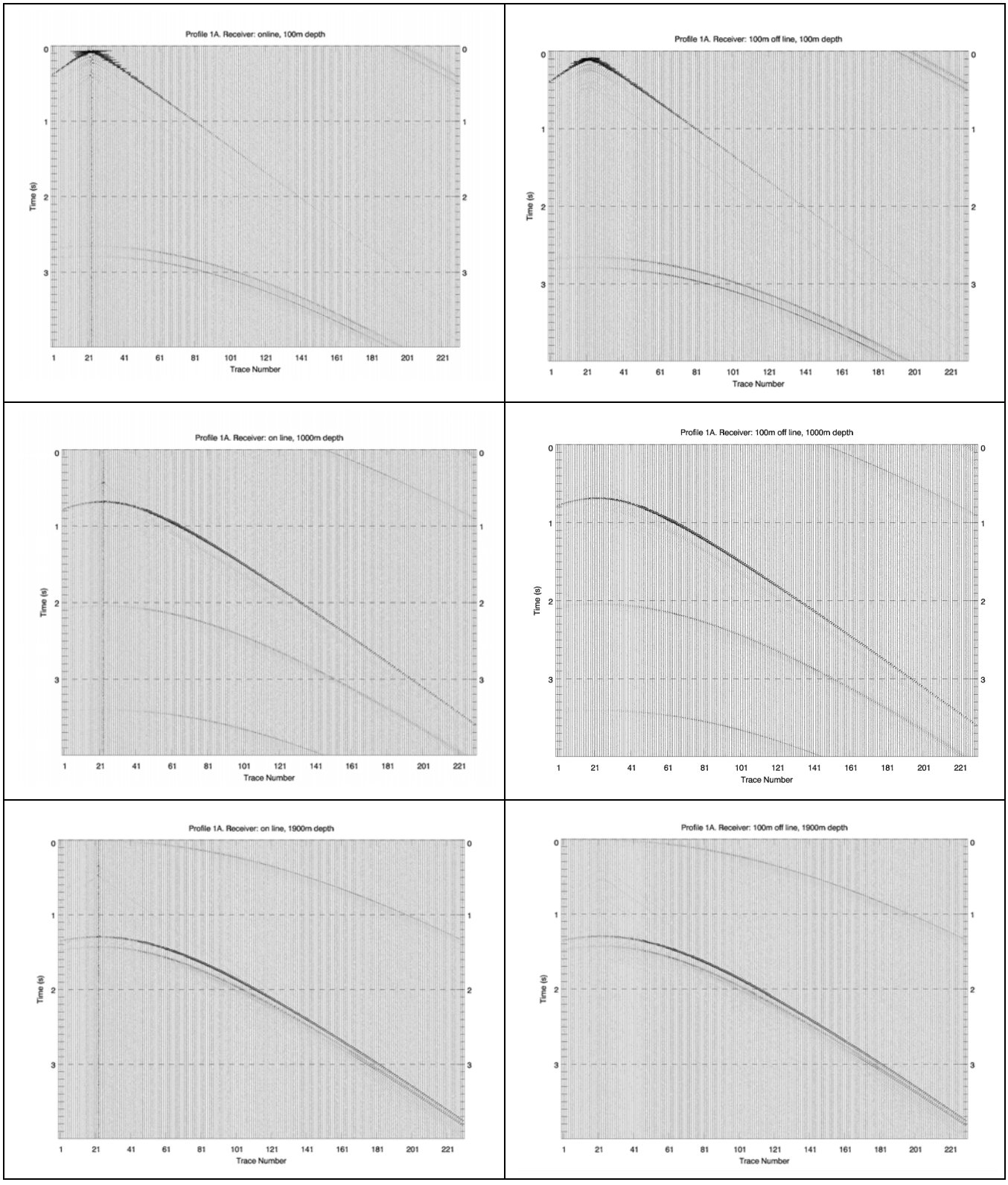

Figure 64: Synthetic pressures for on-line and 100 m off-line receivers of Profile 1A.

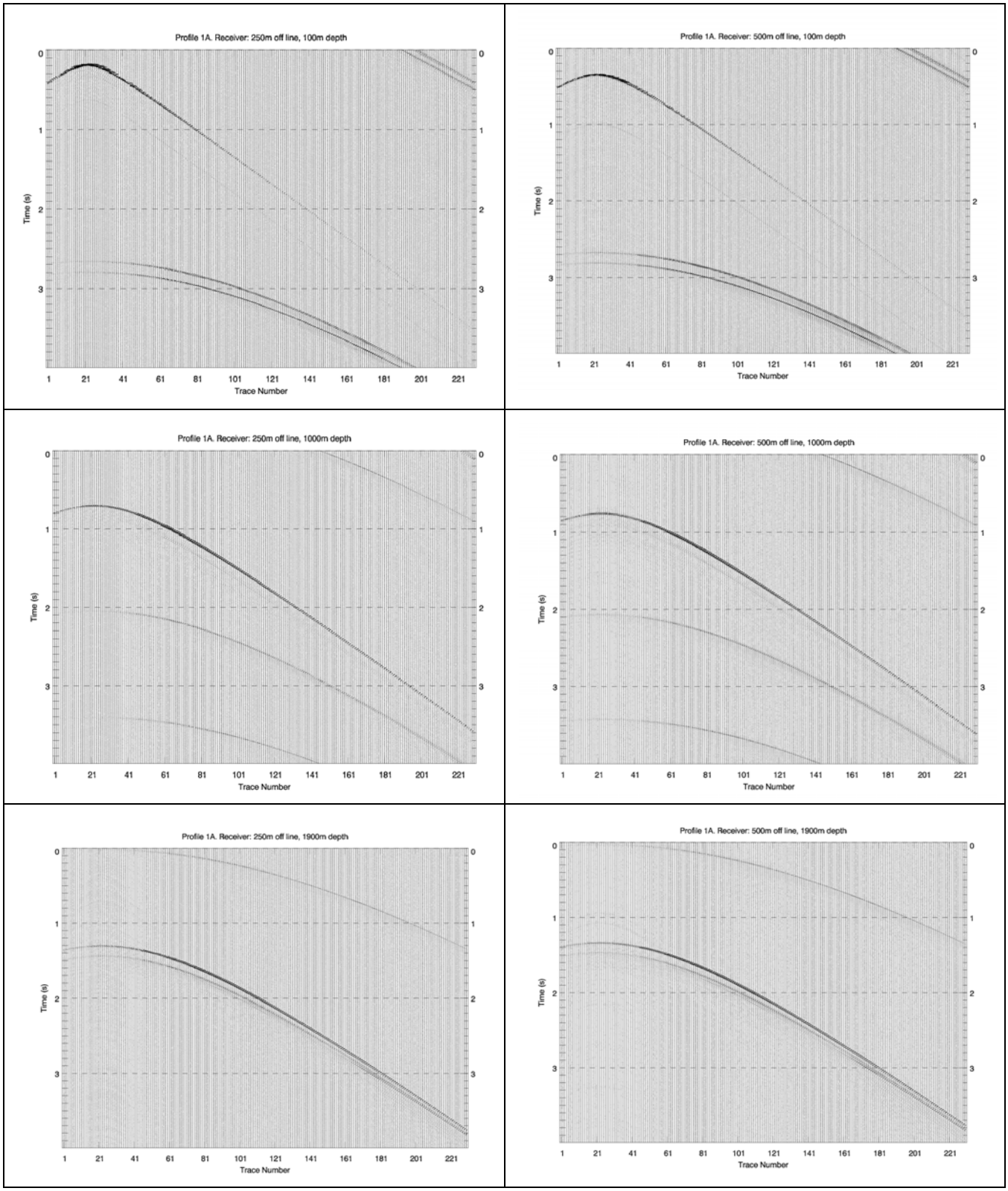

Figure 65: Synthetic pressures for 250 and 500 m off-line receivers of Profile 1A.

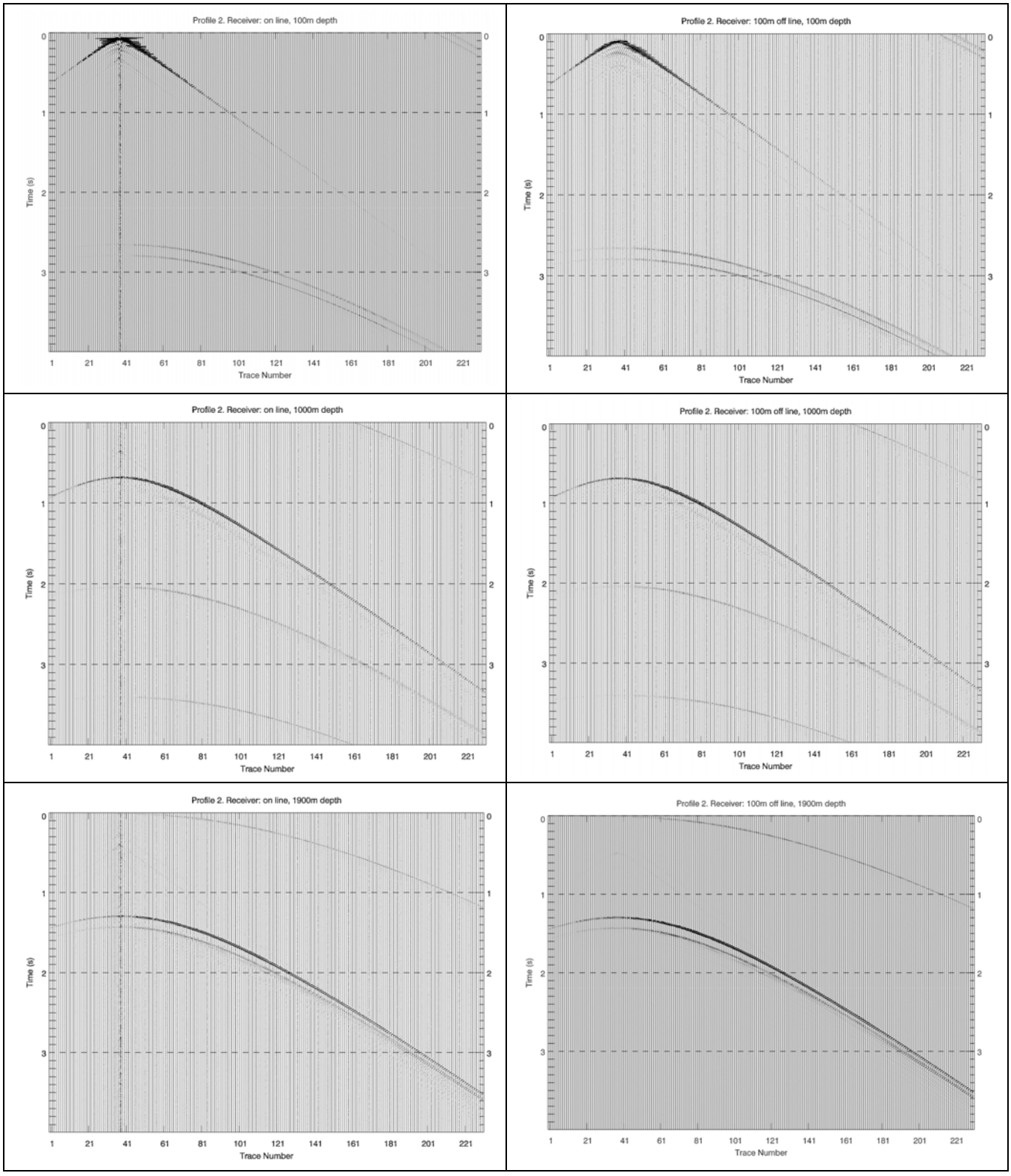

Figure 66: Synthetic pressures for on-line and 100 m off-line receivers of Profile 2.

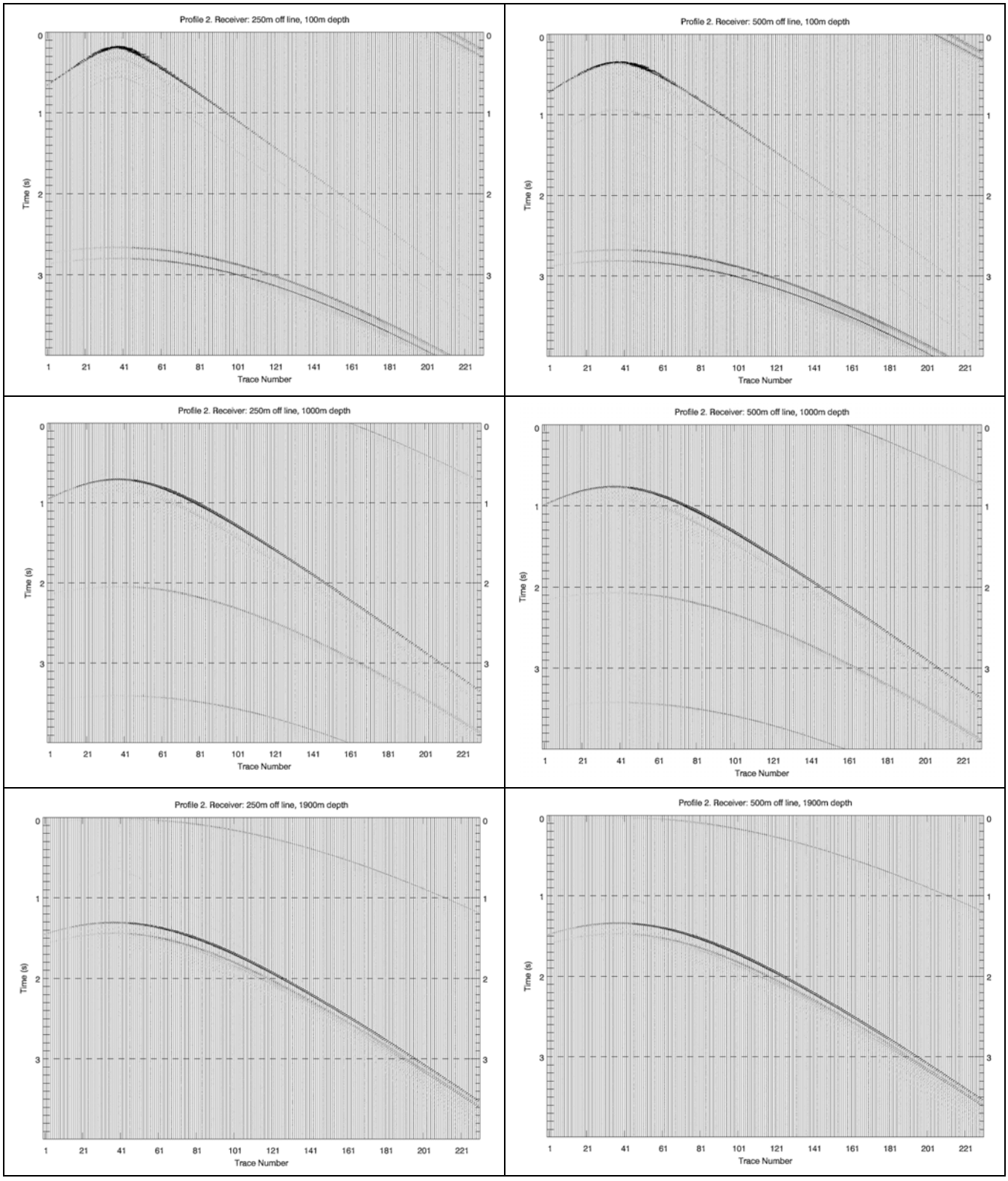

Figure 67: Synthetic pressures for 250 and 500 m off-line receivers of Profile 2.

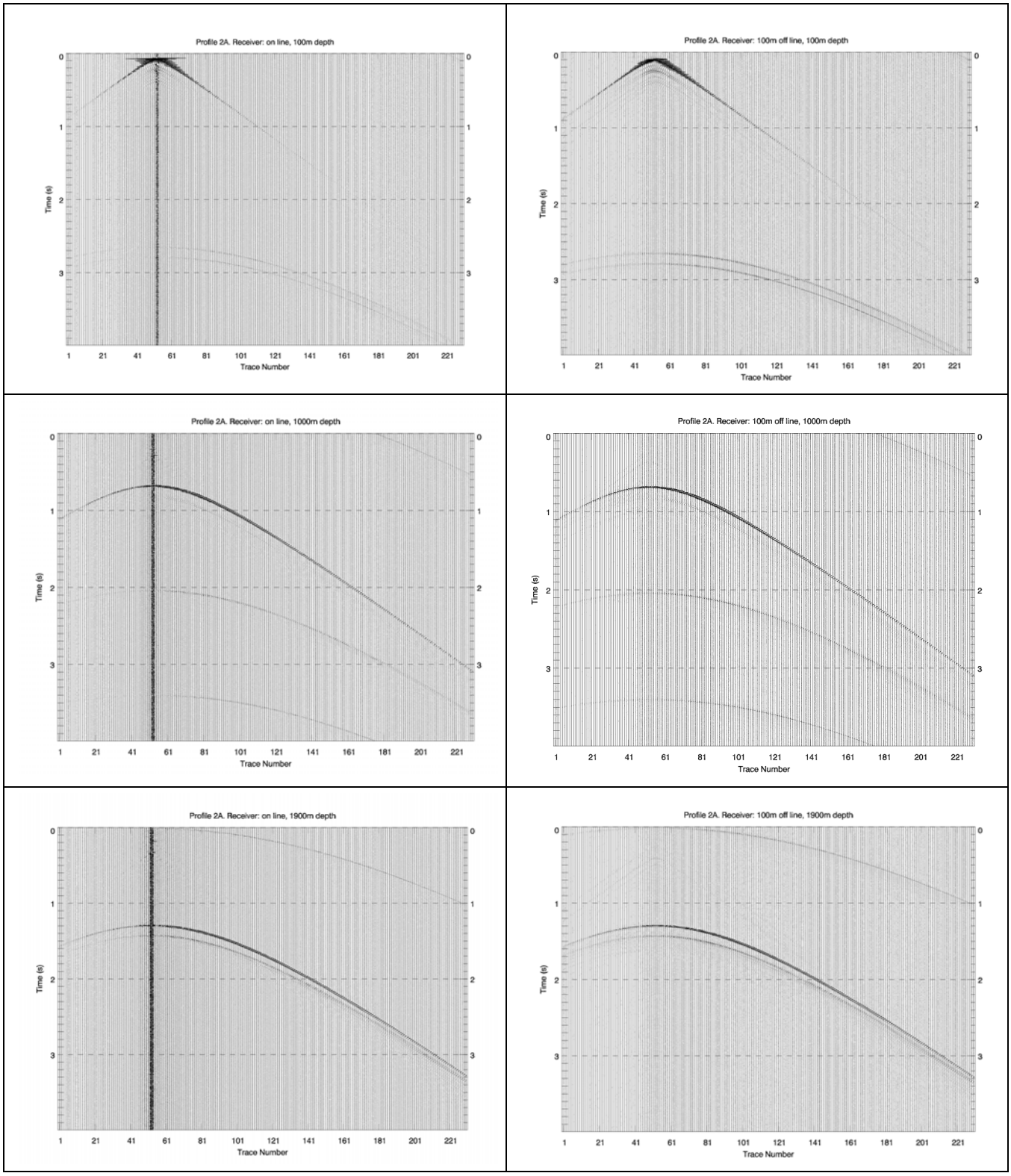

Figure 68: Synthetic pressures for on-line and 100 m off-line receivers of Profile 2A.

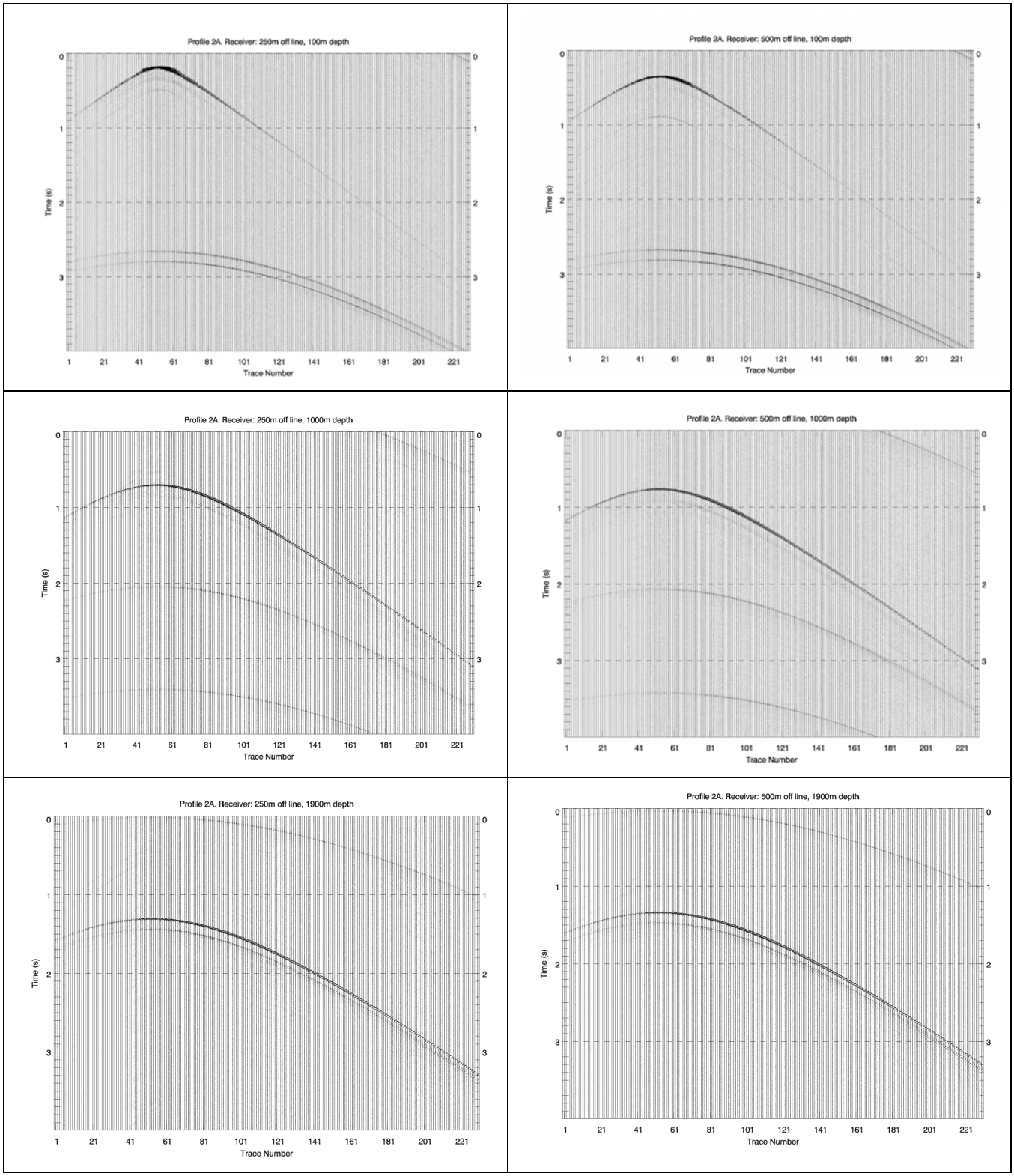

Figure 69: Synthetic pressures for 250 and 500 m off-line receivers of Profile 2A.

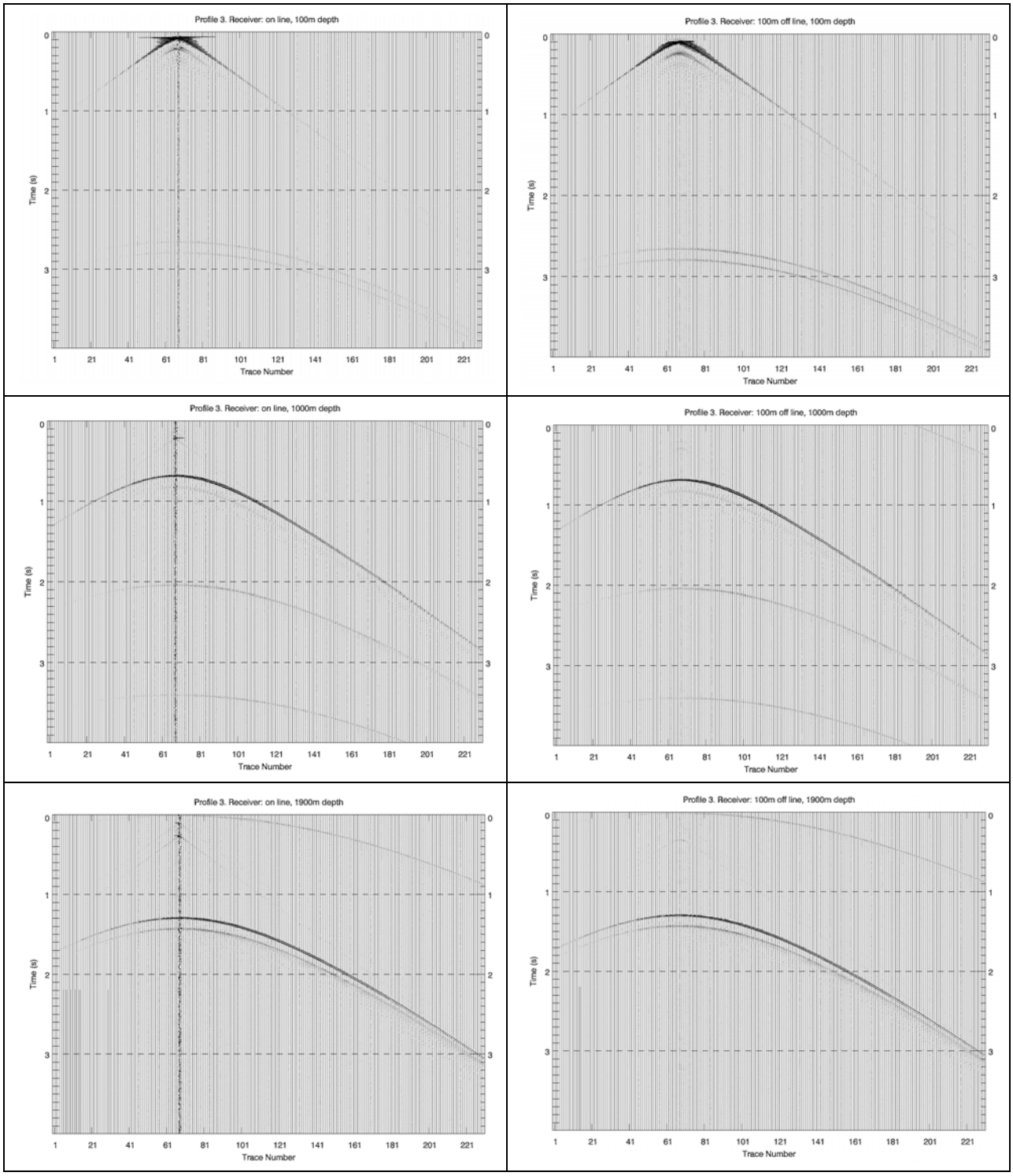

Figure 70: Synthetic pressures for on-line and 100 m off-line receivers of Profile 3.

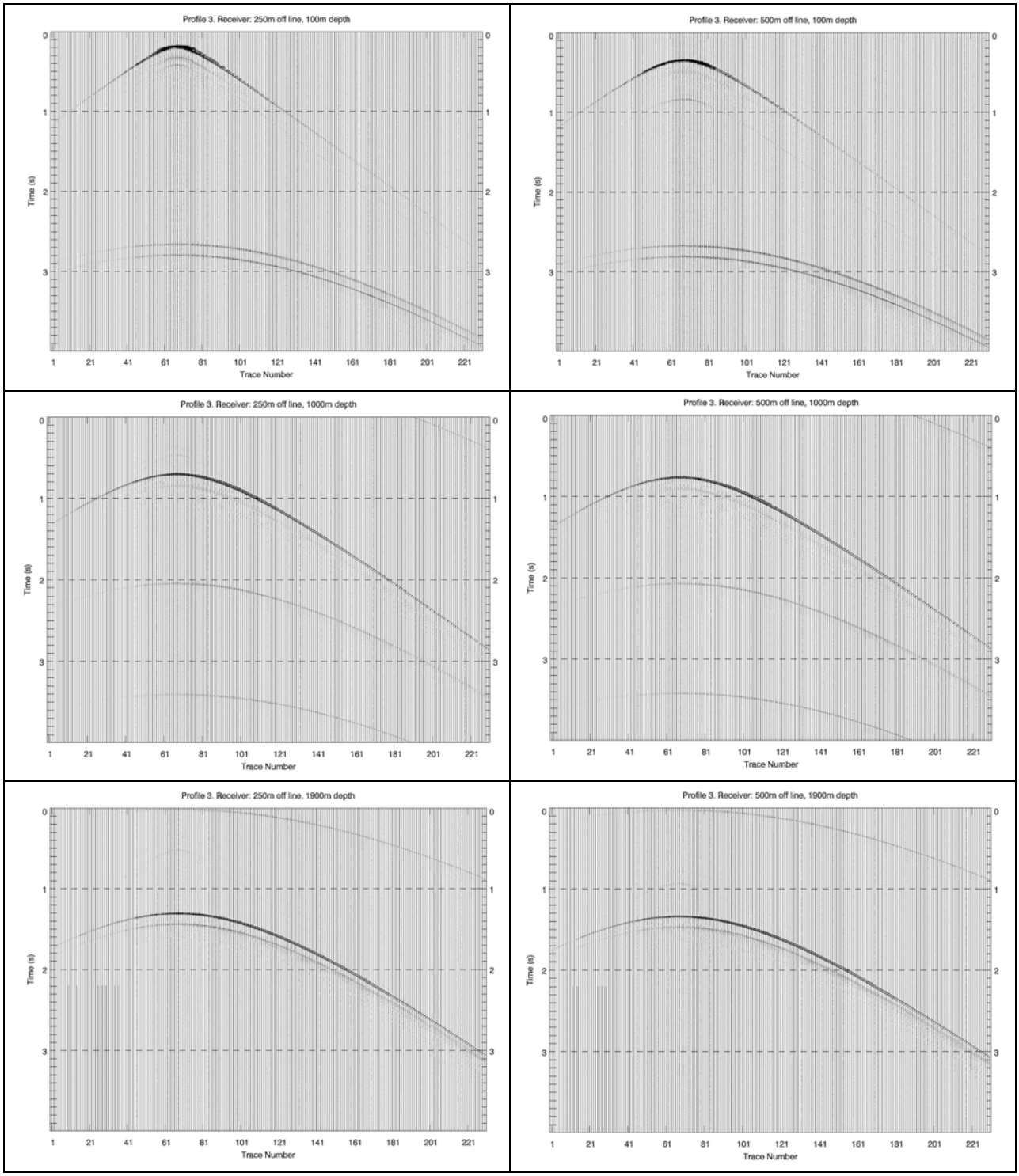

Figure 71: Synthetic pressures for 250 and 500 m off-line receivers of Profile 3.

7.2 Flat-Weighted Sound Exposure Level (SEL) from Wavenumber Integral Model at Deep Site

The synthetic pressure results from the wavenumber integral model shown in Figures 62 through 71 were analysed to directly compute per-pulse SEL and cumulative SEL at the receivers of Profiles 1, 1A, 2, 2A and 3, at depths 100 m, 1000 m and 1900 m over all 230 source points of the

soft-start. These results are presented below in Figures 72 to 86. The 1000 m off-line receivers of these profiles were not included, so the off-line distances are 0 m, 100 m 250 m and 500 m. The wavenumber integral results clearly provide more realistic pressure variation for receivers at steep angles than the parabolic equation results. Compare for example the PE results of Figure 9 with the corresponding wavenumber integral results of Figure 78; the wavenumber integral results show expected maxima directly under the source while the parabolic equation results have flat sections at these locations. The wavenumber integral results also appear to have less scatter. The reason for this behaviour is unknown.

Overall, the wavenumber integral results and parabolic equation results show similar structure of level variation with range. However, the parabolic equation results appear to systematically exceed the wavenumber integral results for the 100 m deep receiver in Profiles 1 and 2 by approximately 3 dB, and at Profile 3 by approximately 1-2 dB. These systematic differences also occur between the predicted cumulative SEL levels over the full source line.

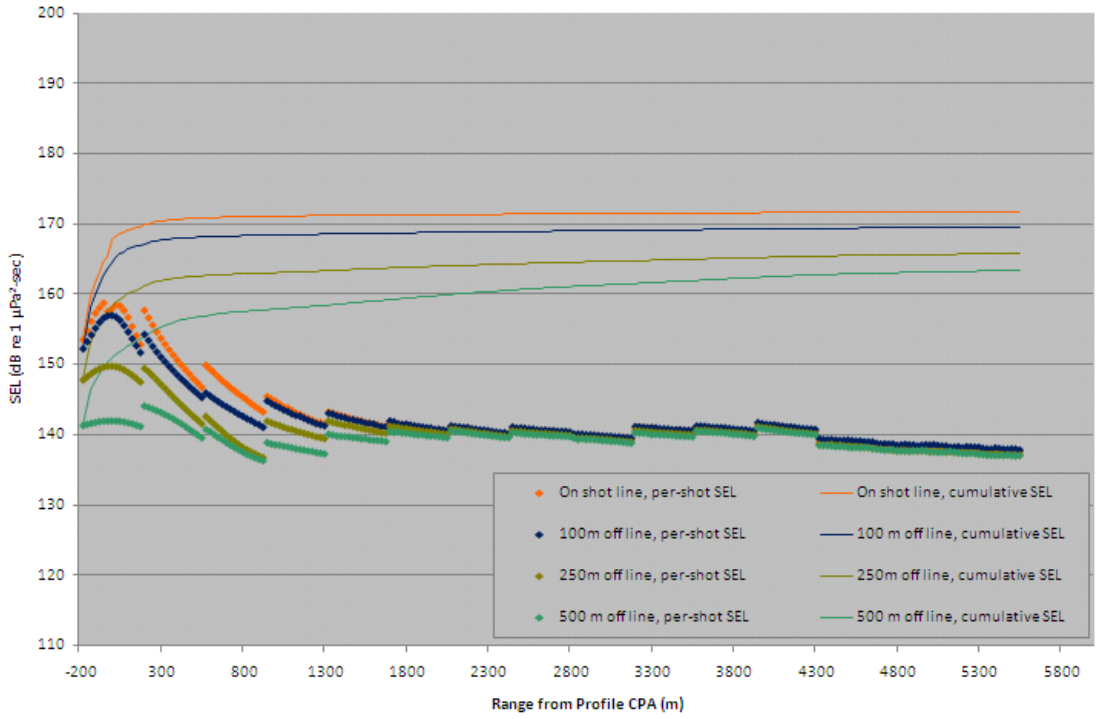

Figure 72: Per-pulse and cumulative SEL at Deep site for receivers on Profile 1 at 100 m depth.

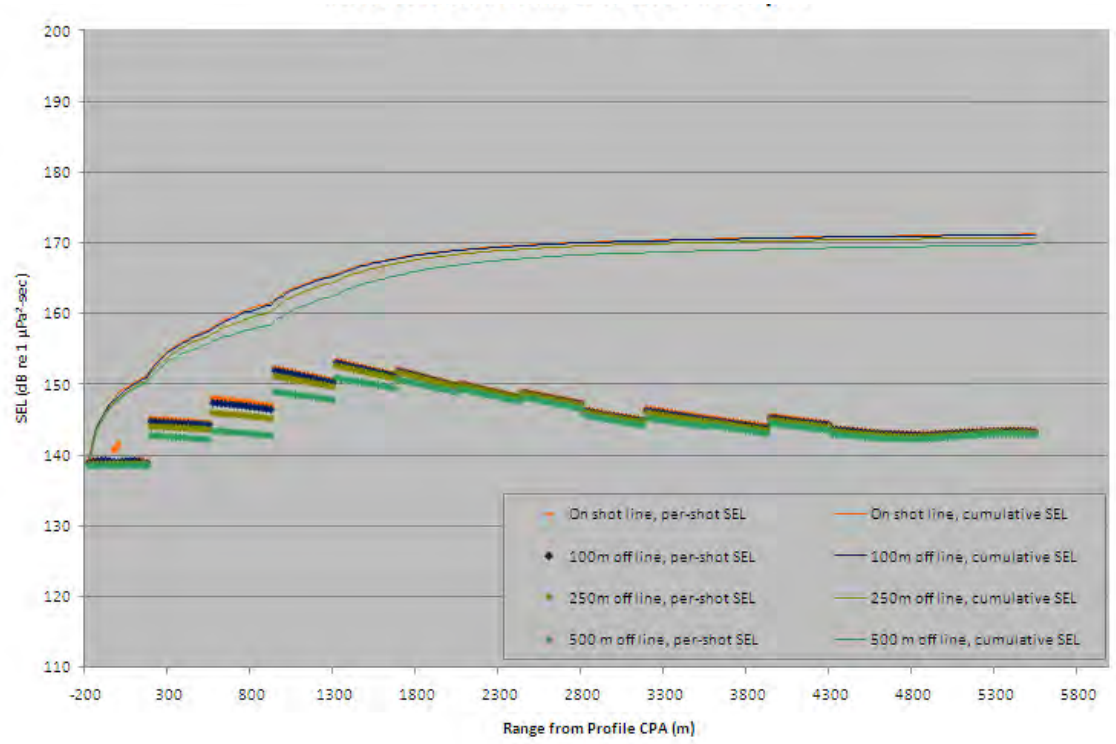

Figure 73: Per-pulse and cumulative SEL at Deep site for receivers on Profile 1 at 1000 m depth.

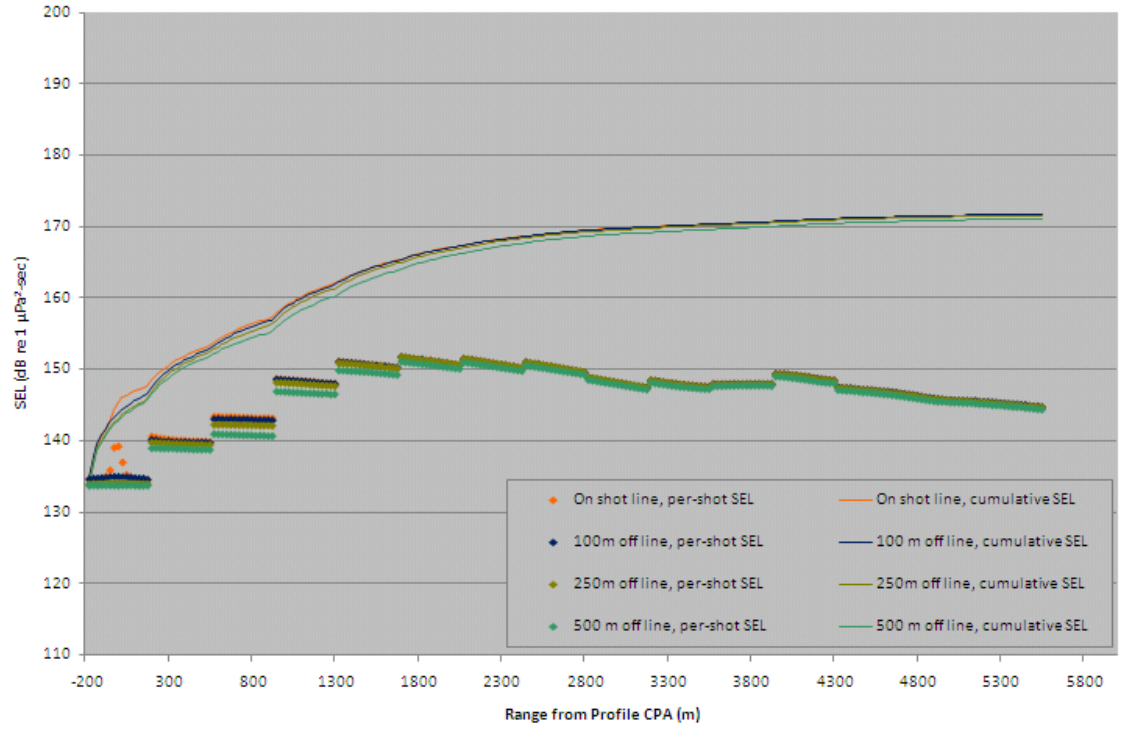

Figure 74: Per-pulse and cumulative SEL at Deep site for receivers on Profile 1 at 1900 m depth.

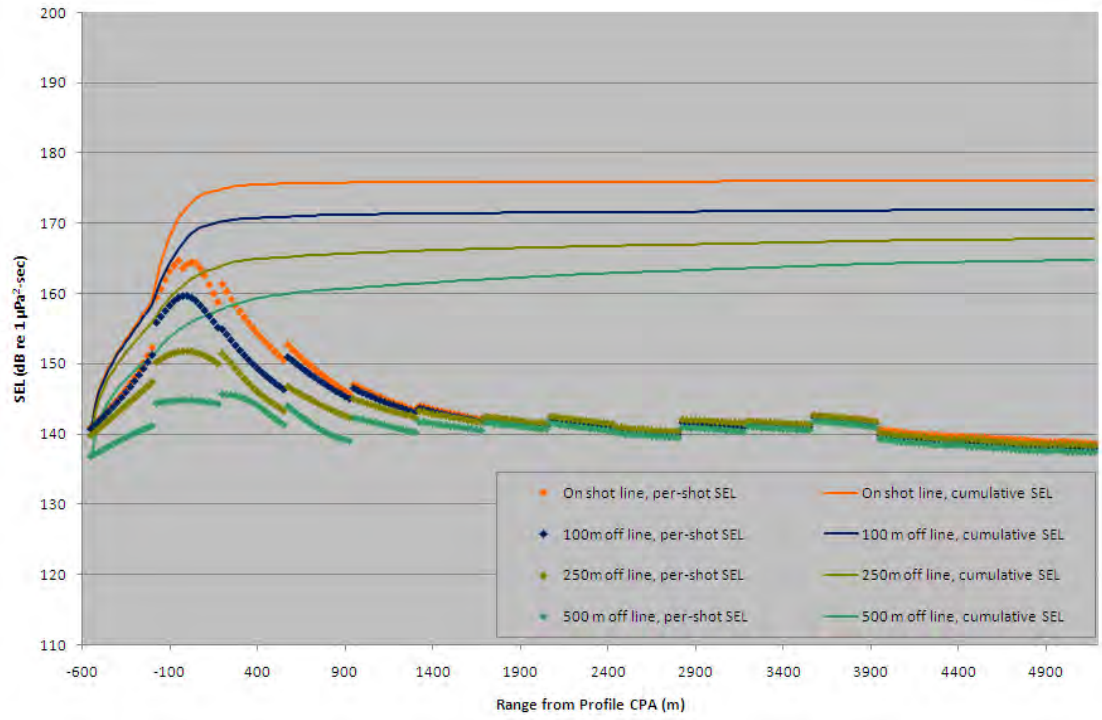

Figure 75: Per-pulse and cumulative SEL at Deep site for receivers on Profile 1A at 100 m depth.

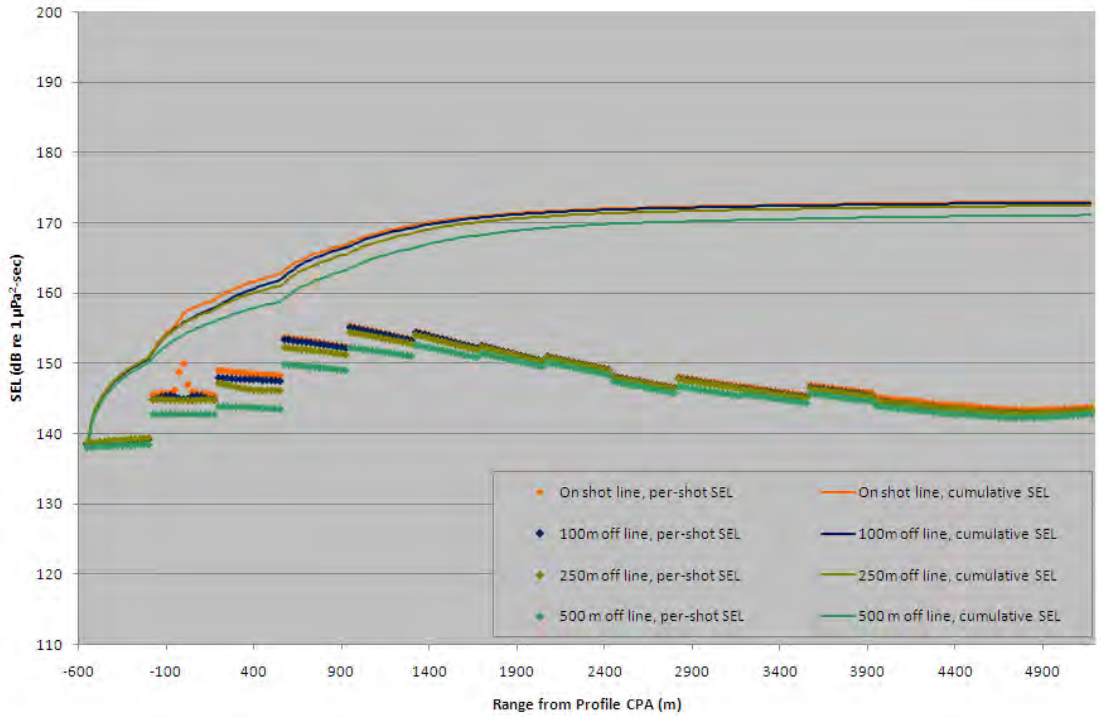

Figure 76: Per-pulse and cumulative SEL at Deep site for receivers on Profile 1A at 1000 m depth.

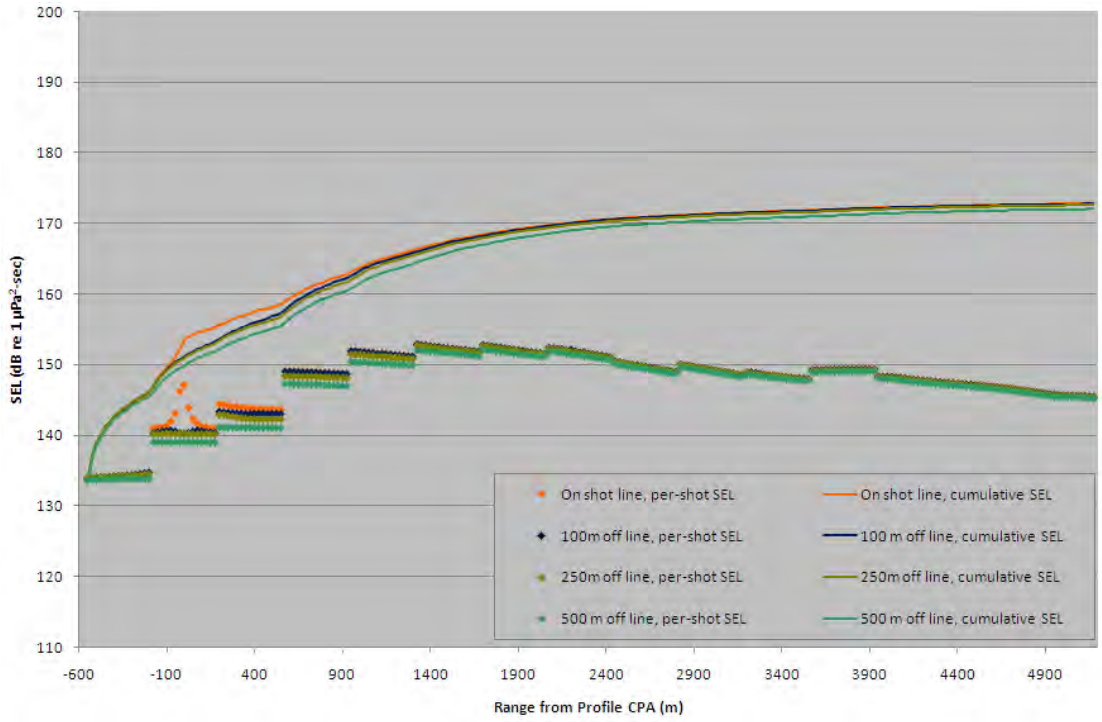

Figure 77: Per-pulse and cumulative SEL at Deep site for receivers on Profile 1A at 1900 m depth.

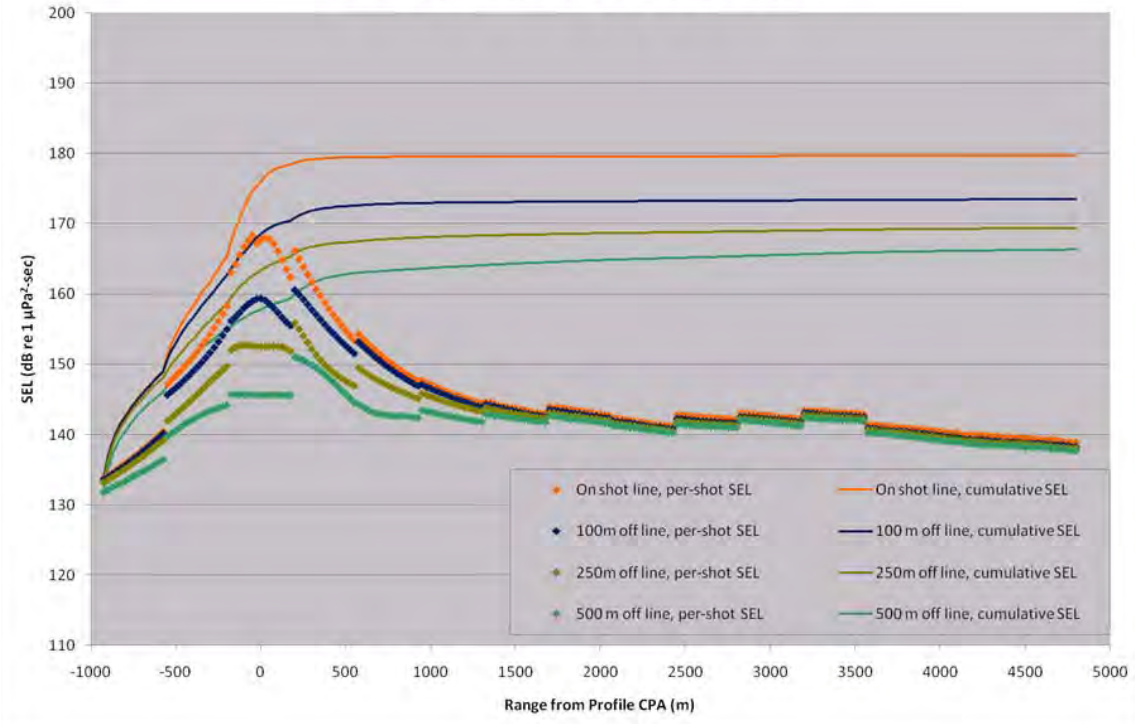

Figure 78: Per-pulse and cumulative SEL at Deep site for receivers on Profile 2 at 100 m depth.

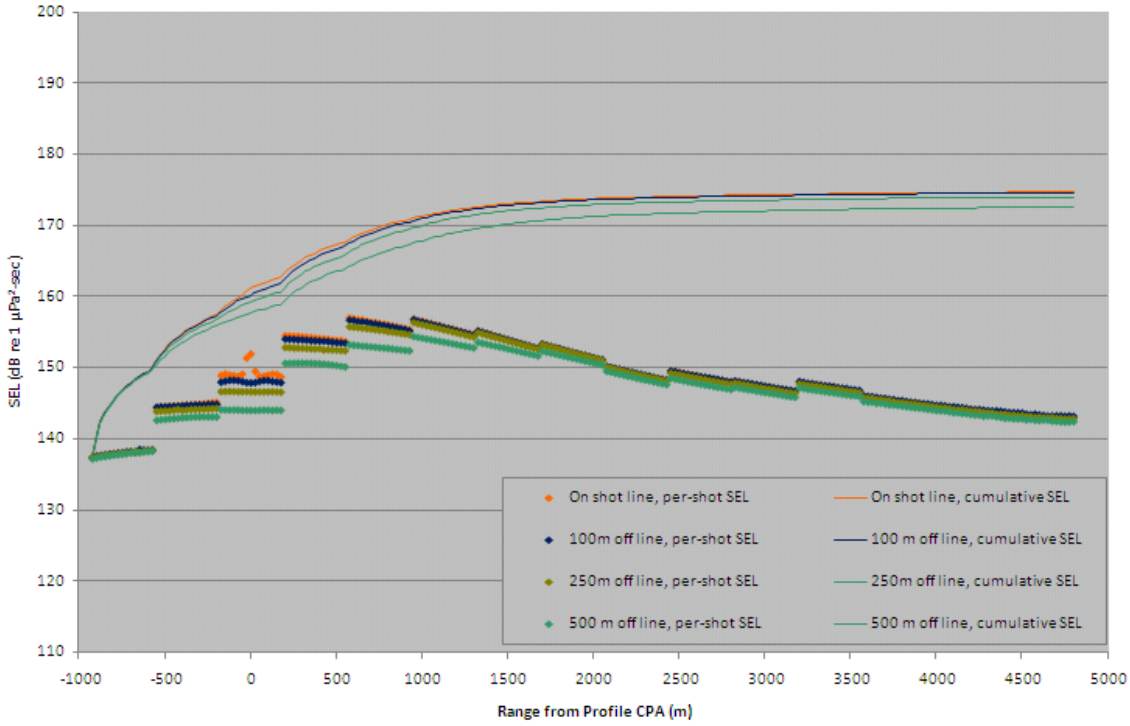

Figure 79: Per-pulse and cumulative SEL at Deep site for receivers on Profile 2 at 1000 m depth.

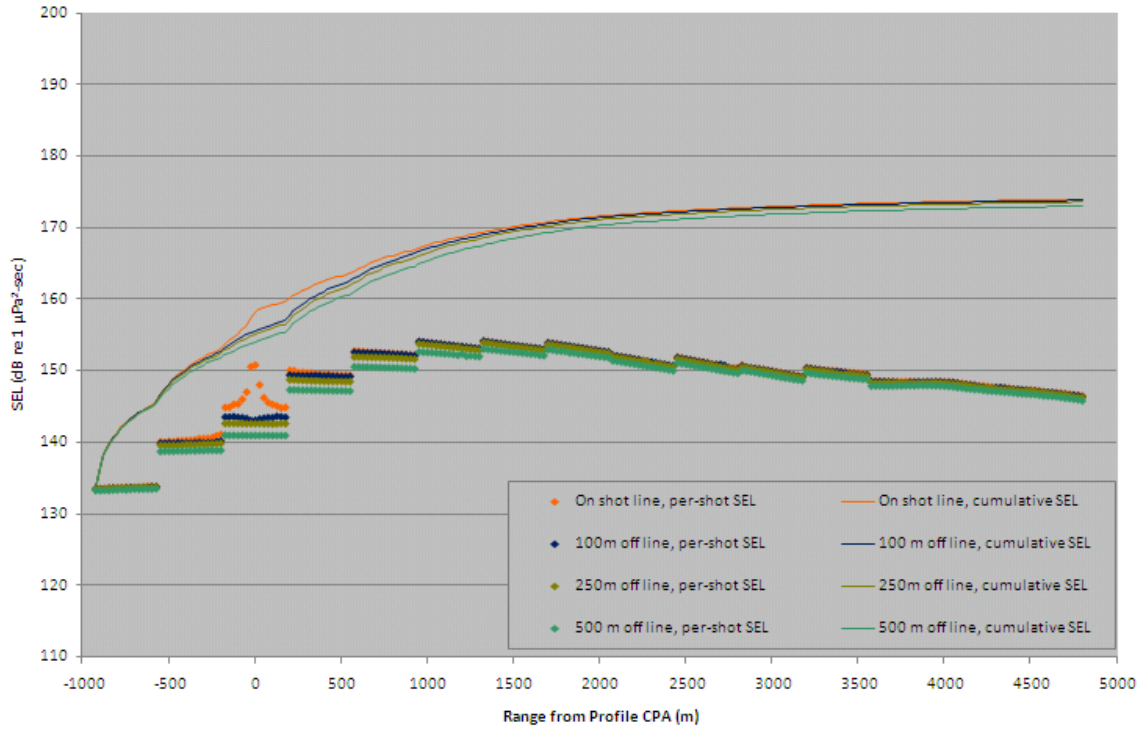

Figure 80: Per-pulse and cumulative SEL at Deep site for receivers on Profile 2 at 1900 m depth.

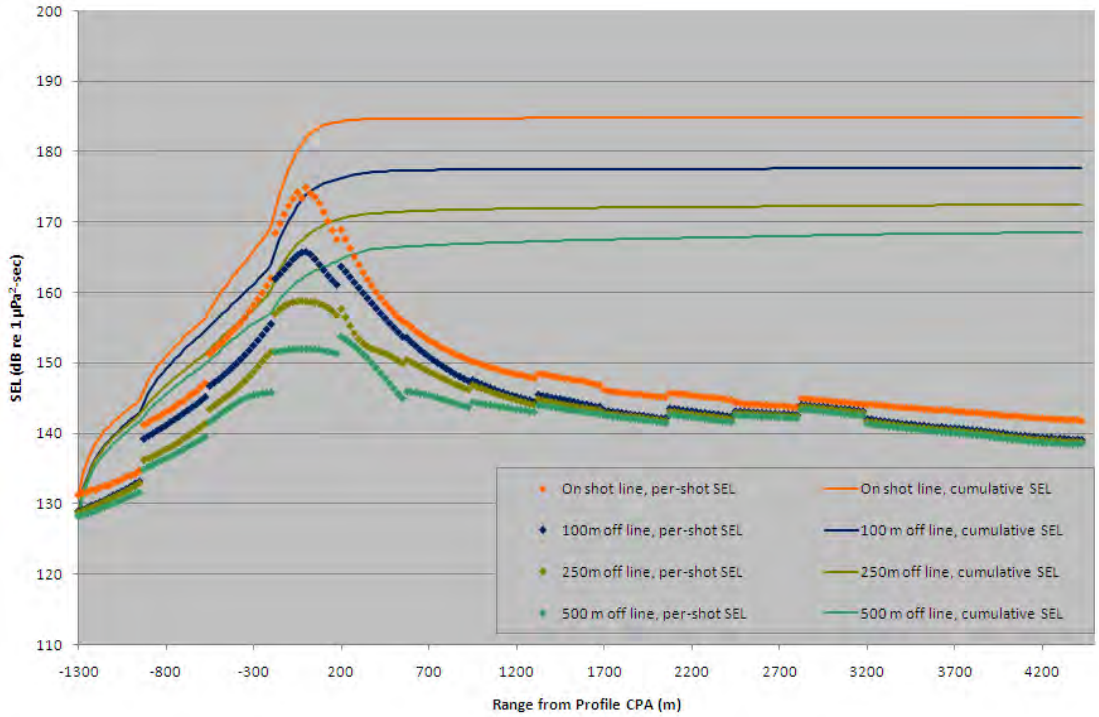

Figure 81: Per-pulse and cumulative SEL at Deep site for receivers on Profile 2A at 100 m depth.

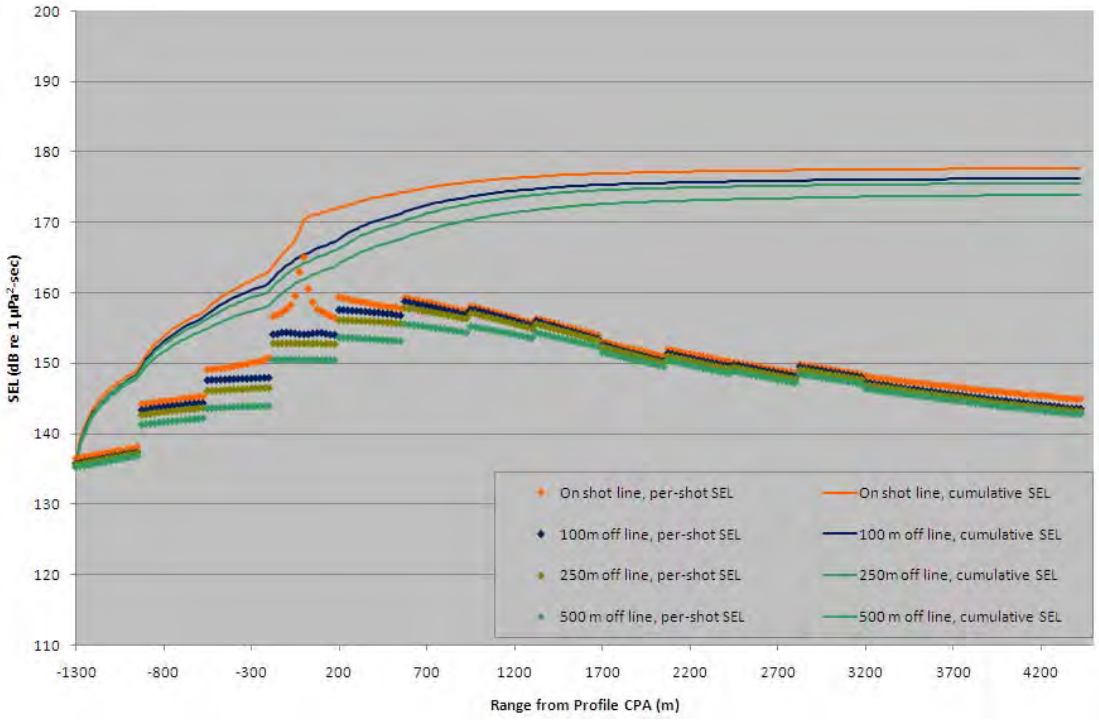

Figure 82: Per-pulse and cumulative SEL at Deep site for receivers on Profile 2A at 1000 m depth.

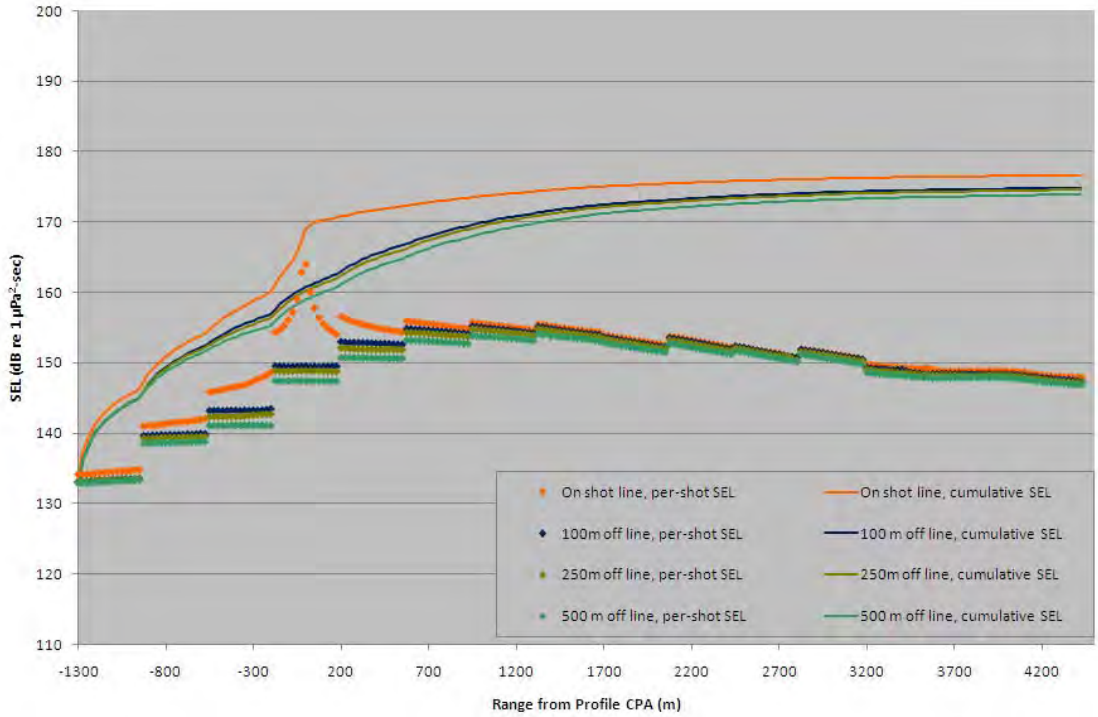

Figure 83: Per-pulse and cumulative SEL at Deep site for receivers on Profile 2A at 1900 m depth.

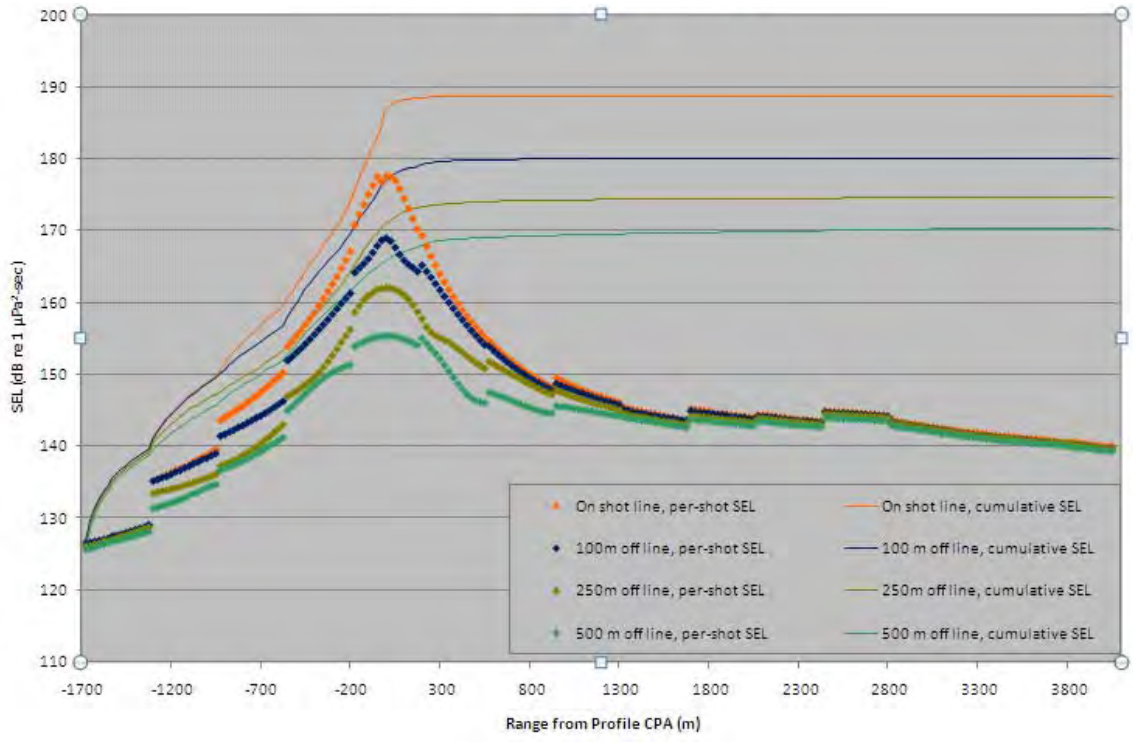

Figure 84: Per-pulse and cumulative SEL at Deep site for receivers on Profile 3 at 100 m depth.

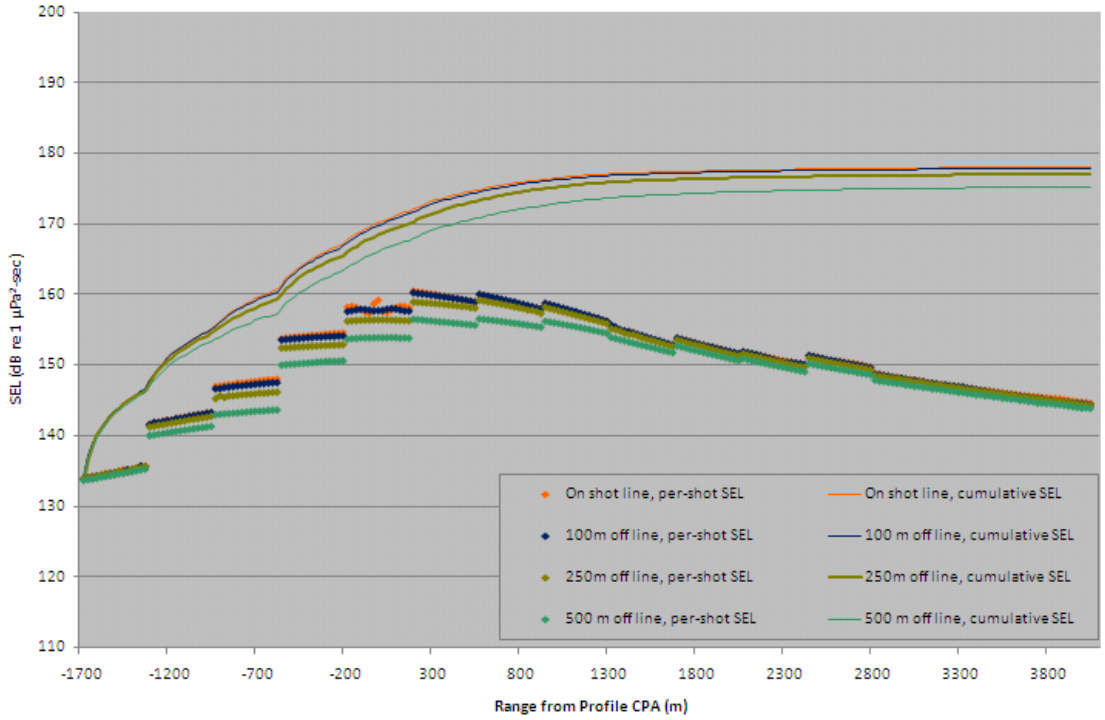

Figure 85: Per-pulse and cumulative SEL at Deep site for receivers on Profile 3 at 1000 m depth.

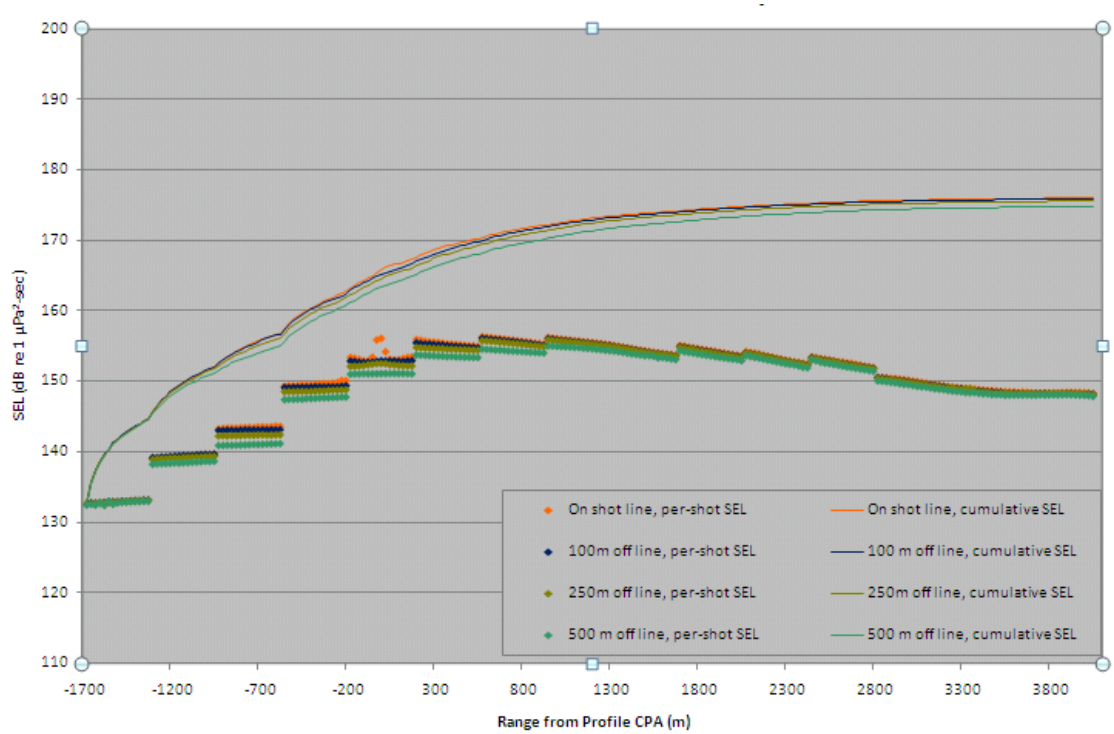

Figure 86: Per-pulse and cumulative SEL at Deep site for receivers on Profile 3 at 1900 m depth.

7.3 M-Weighted Sound Exposure Level (SEL)

The synthetic pressure results shown in Figures 62 through 71 were analysed to directly compute per-pulse M-weighted SEL and cumulative M-weighted SEL over all 230 source points of the soft-start sequence. An example of these results is presented below in Figure 87. The complete set of graphs is in Appendix A, Figure A1 to Figure A36. The M-weighted levels for low frequency

cetaceans are nearly coincident with the unweighted levels. The pinniped, mid-frequency cetacean and high frequency cetacean results respectively are consistently less than the unweighted levels by approximately 3 dB, 7 dB and 9 dB for the 100 m and 1000 m deep receivers. Interestingly the M-weighted cumulative SEL levels for the deepest 1900 m receiver show more difference from the unweighted levels. The high frequency cetacean M-Weighted cumulative SEL level at 100 m off-line and 1900 m depth is 13 dB less than the corresponding unweighted level.

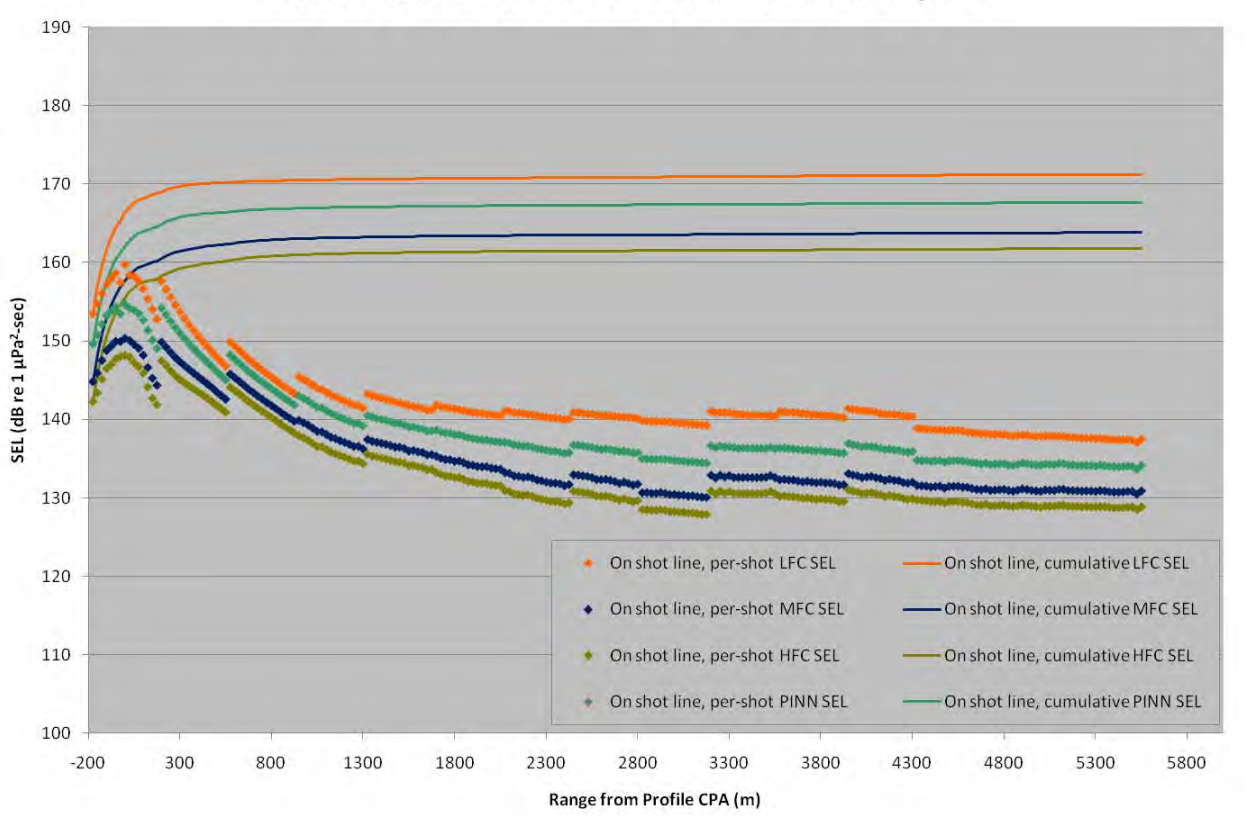

Figure 87: Per-pulse and cumulative M-weighted SEL for on-source-line receivers on Profile 1 at 100 m depth.

7.4 Peak and Rms Sound Pressure Level (SPL)

The synthetic pressure results shown in Figures 62 through 71 were analysed to directly compute per-pulse peak SPL and 90% rms SPL over all 230 source points of the soft-start. These results are presented below in Figures 88 through 102. The peak SPL's are substantially less than the 218 dB re 1 µPa and 230 dB re 1 µPa (flat-weighted) peak level thresholds representative of onset of PTS for pinnipeds and cetaceans respectively. Consequently these are not discussed here further.

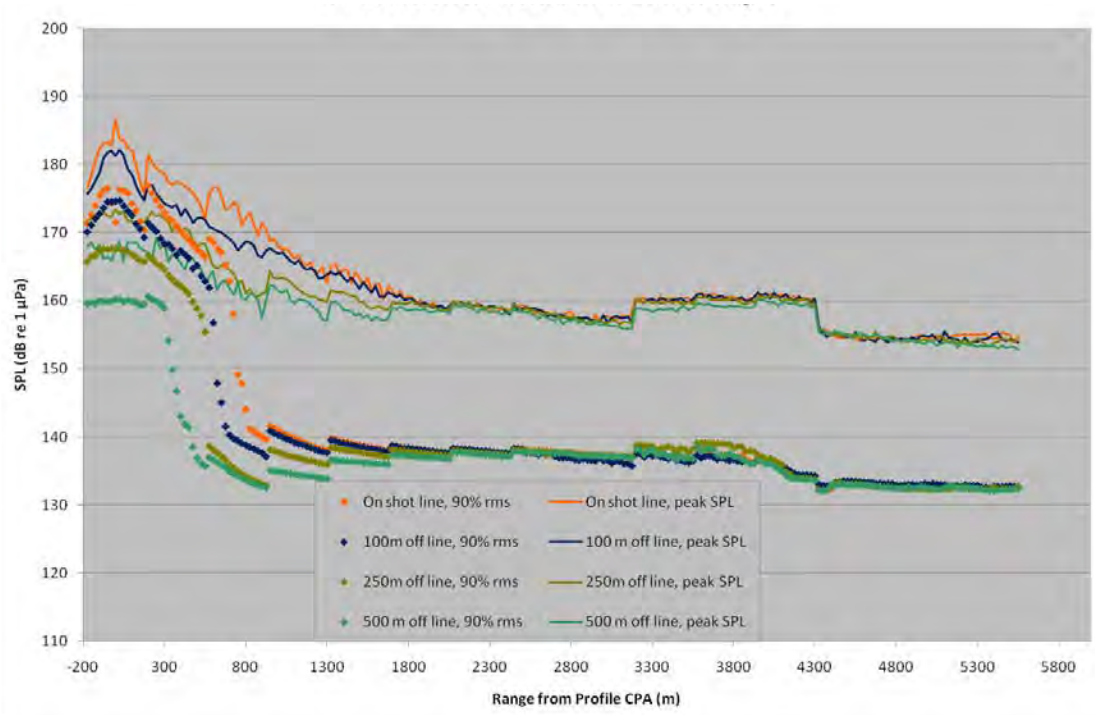

Figure 88: Peak SPL and 90% rms SPL for receivers on Profile 1 at 100 m depth.

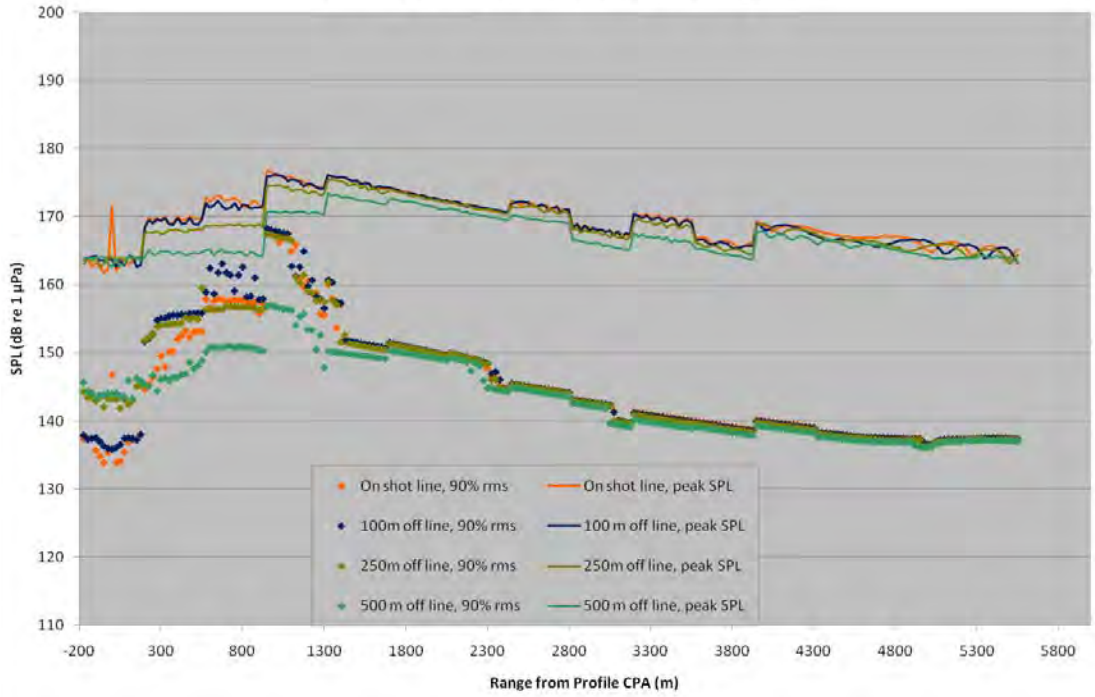

Figure 89: Peak SPL and 90% rms SPL for receivers on Profile 1 at 1000 m depth.

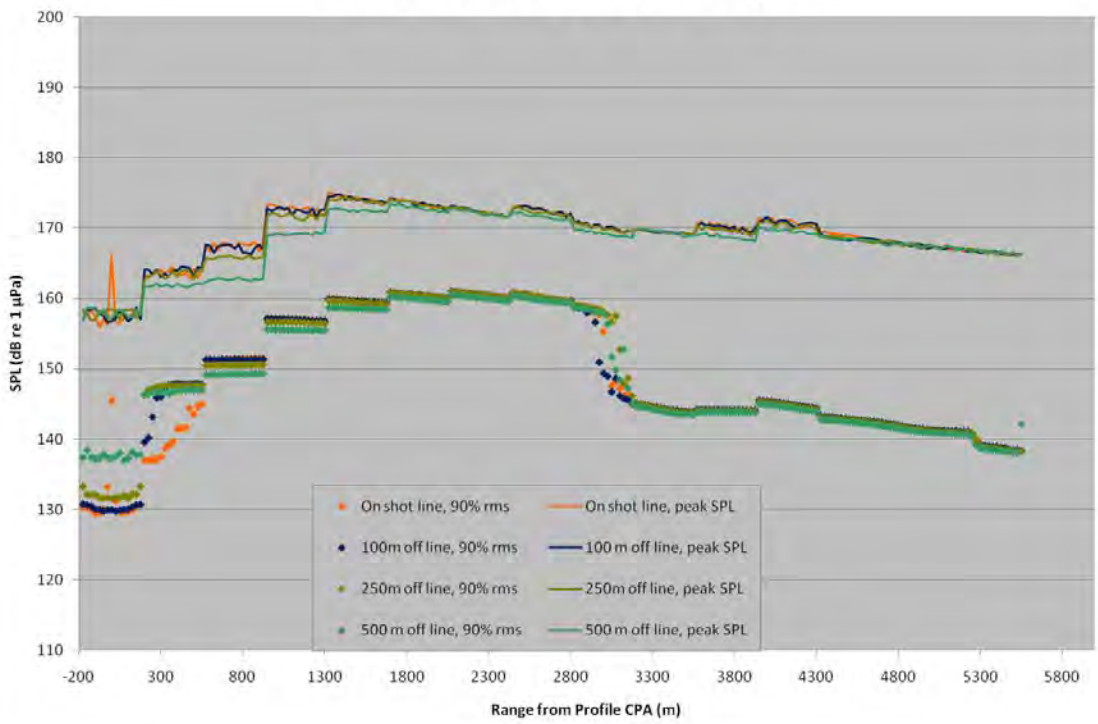

Figure 90: Peak SPL and 90% rms SPL for receivers on Profile 1 at 1900 m depth.

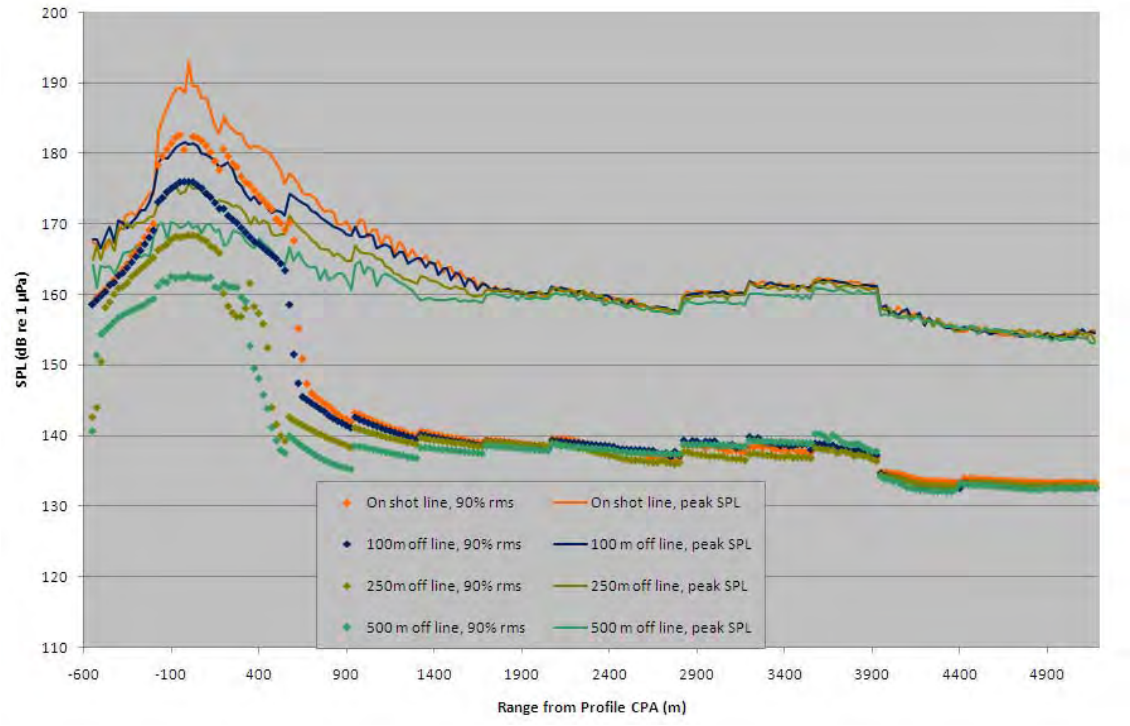

Figure 91: Peak SPL and 90% rms SPL for receivers on Profile 1A at 100 m depth.

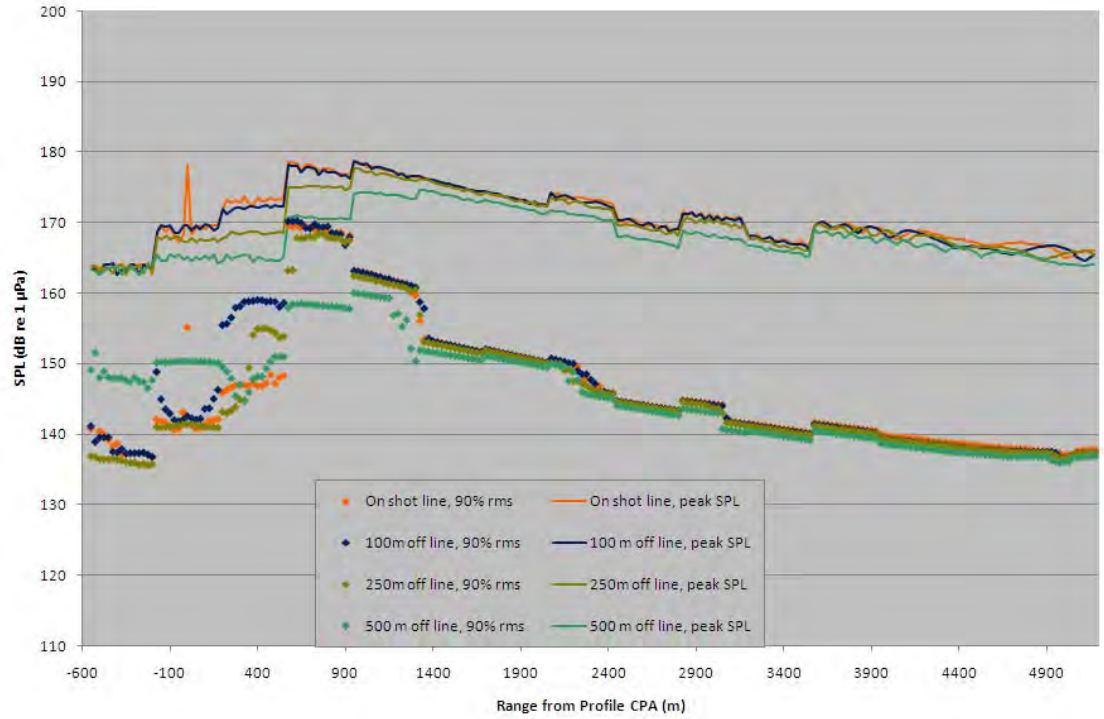

Figure 92: Peak SPL and 90% rms SPL for receivers on Profile 1A at 1000 m depth.

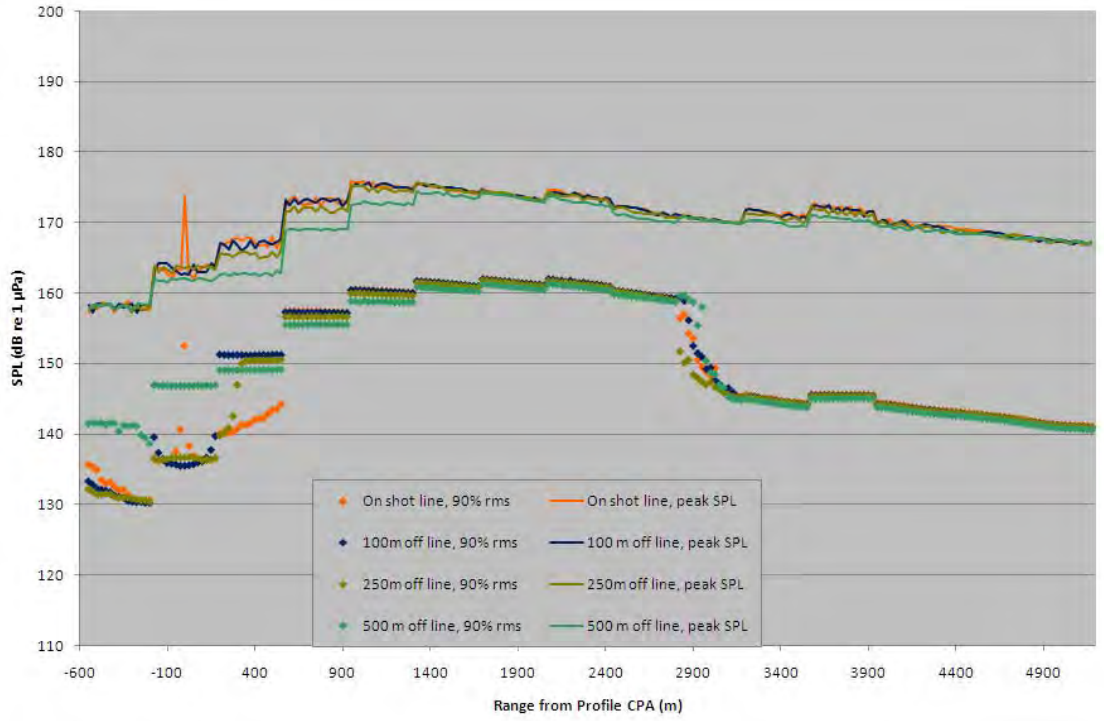

Figure 93: Peak SPL and 90% rms SPL for receivers on Profile 1A at 1900 m depth.

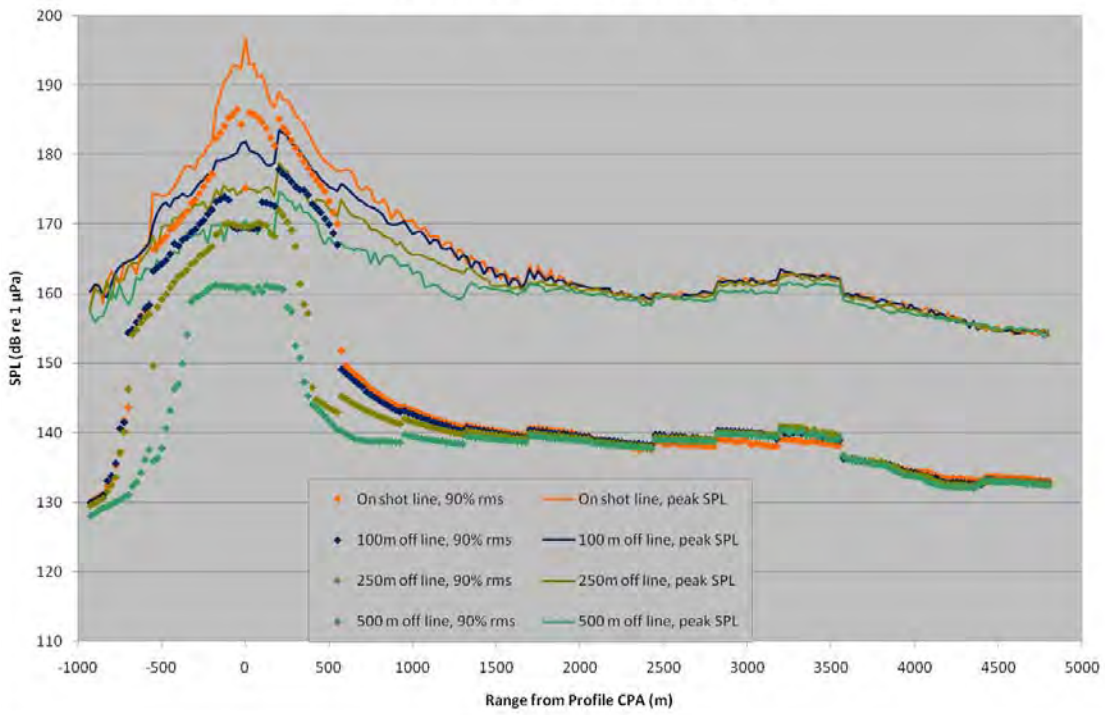

Figure 94: Peak SPL and 90% rms SPL for receivers on Profile 2 at 100 m depth.

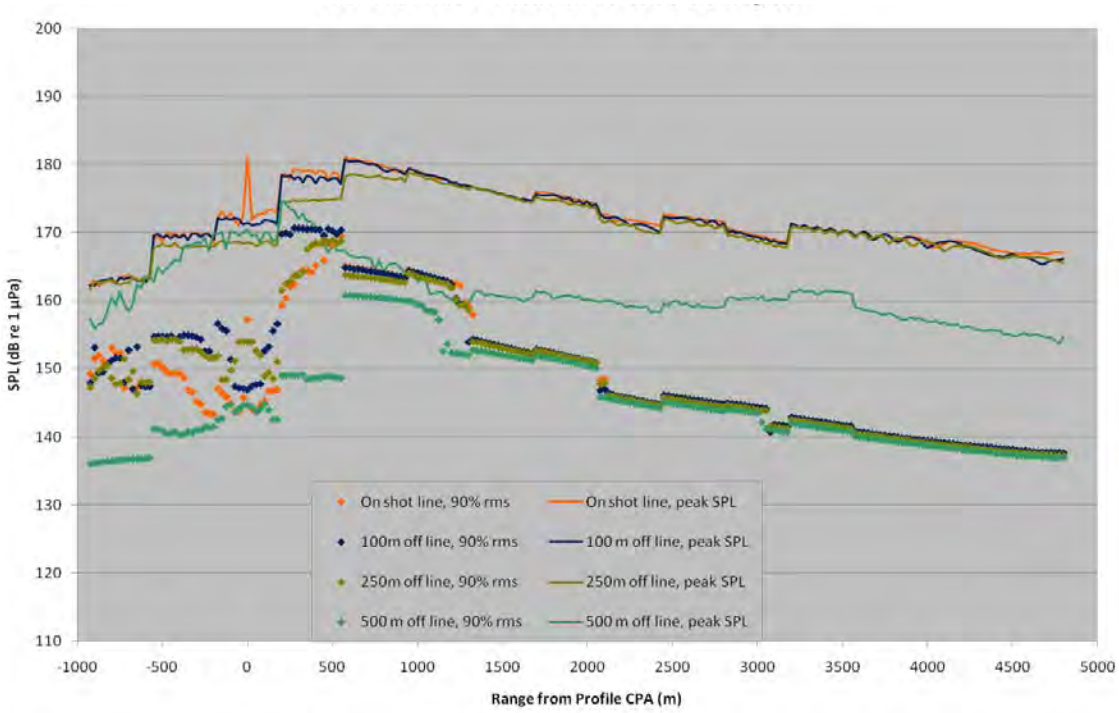

Figure 95: Peak SPL and 90% rms SPL for receivers on Profile 2 at 1000 m depth.

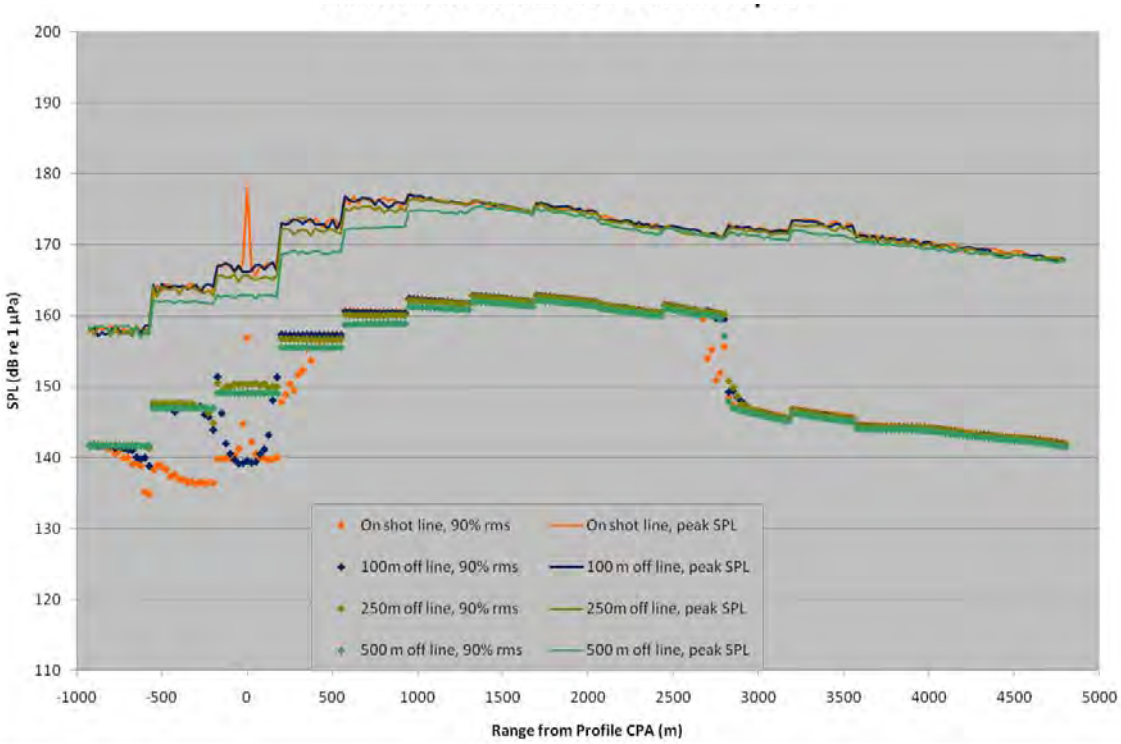

Figure 96: Peak SPL and 90% rms SPL for receivers on Profile 2 at 1900 m depth.

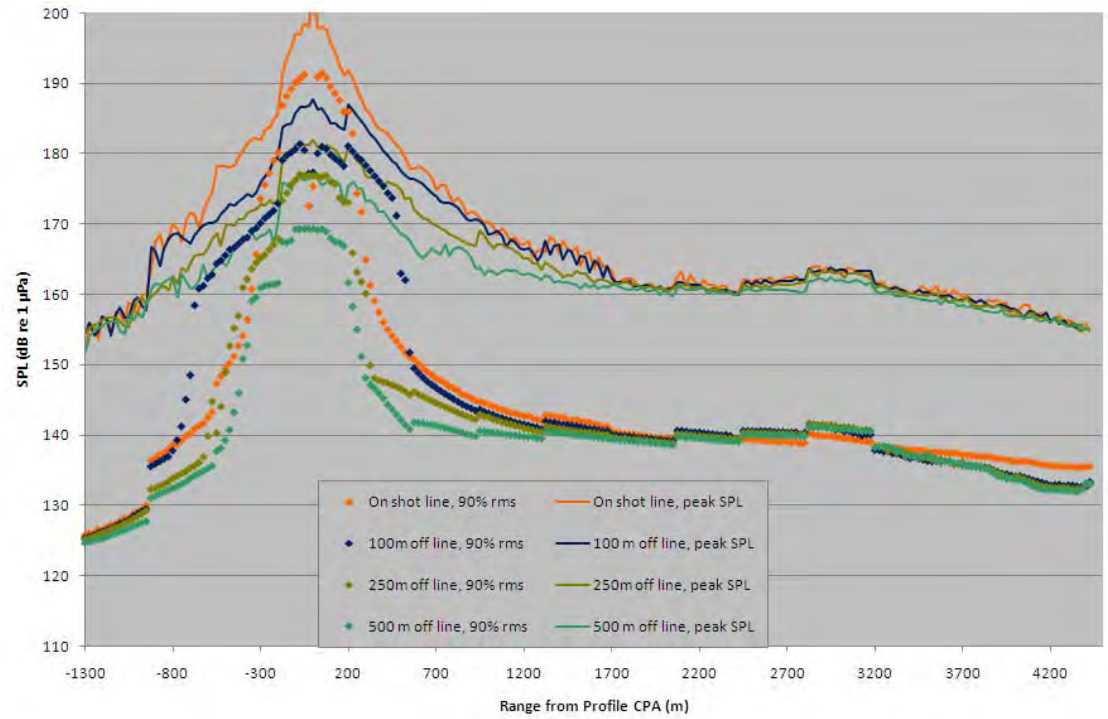

Figure 97: Peak SPL and 90% rms SPL for receivers on Profile 2A at 100 m depth.

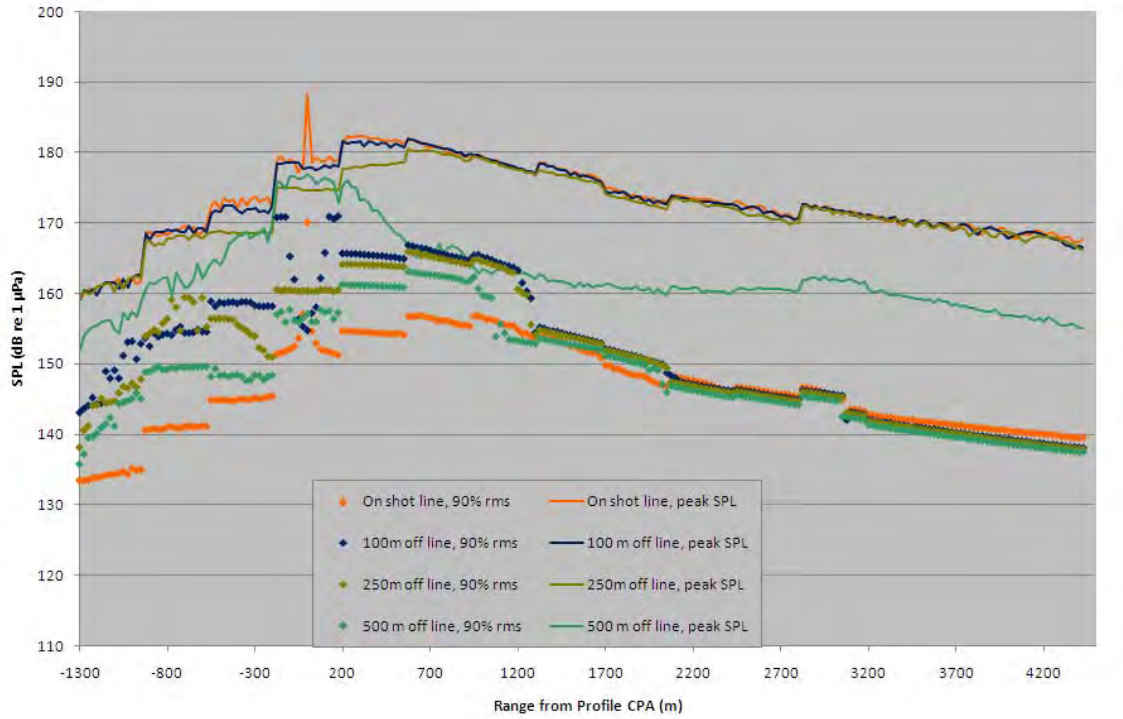

Figure 98: Peak SPL and 90% rms SPL for receivers on Profile 2A at 1000 m depth.

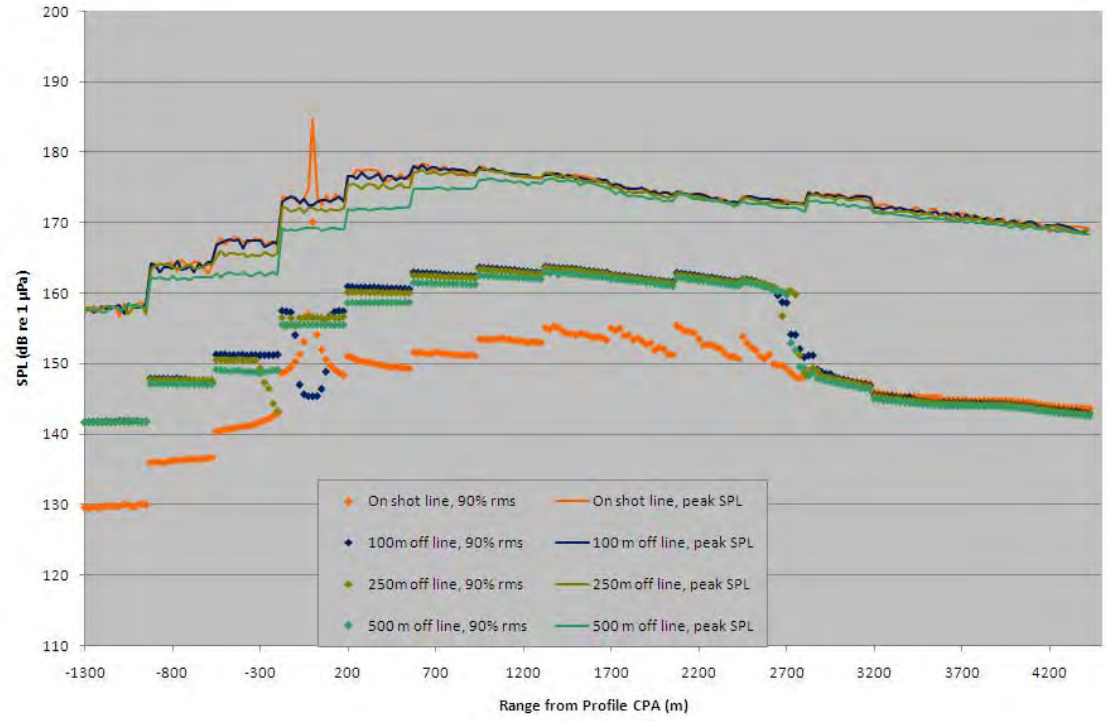

Figure 99: Peak SPL and 90% rms SPL for receivers on Profile 2A at 1900 m depth.

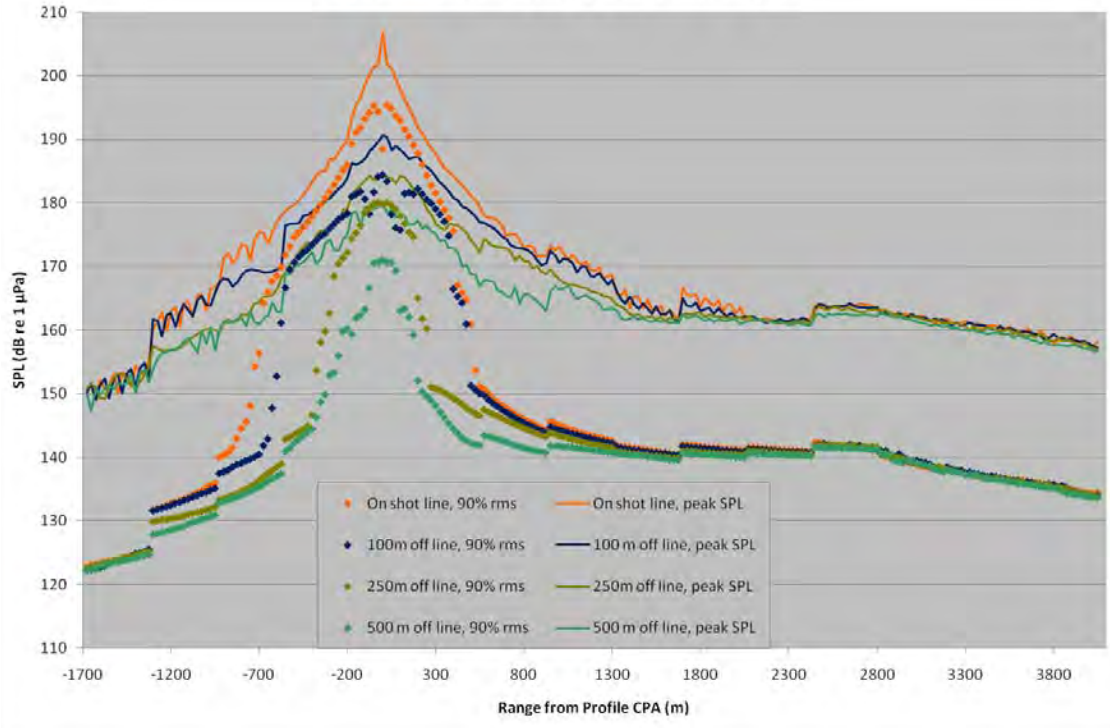

Figure 100: Peak SPL and 90% rms SPL for receivers on Profile 3 at 100 m depth.

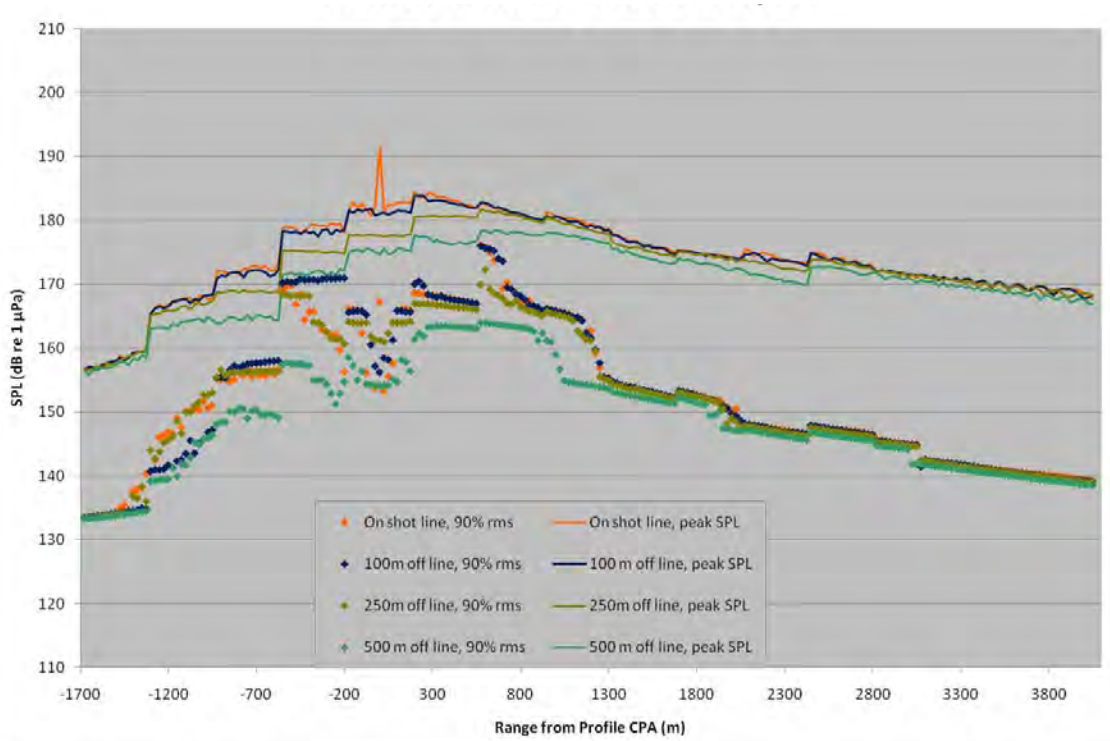

Figure 101: Peak SPL and 90% rms SPL for receivers on Profile 3 at 1000 m depth.

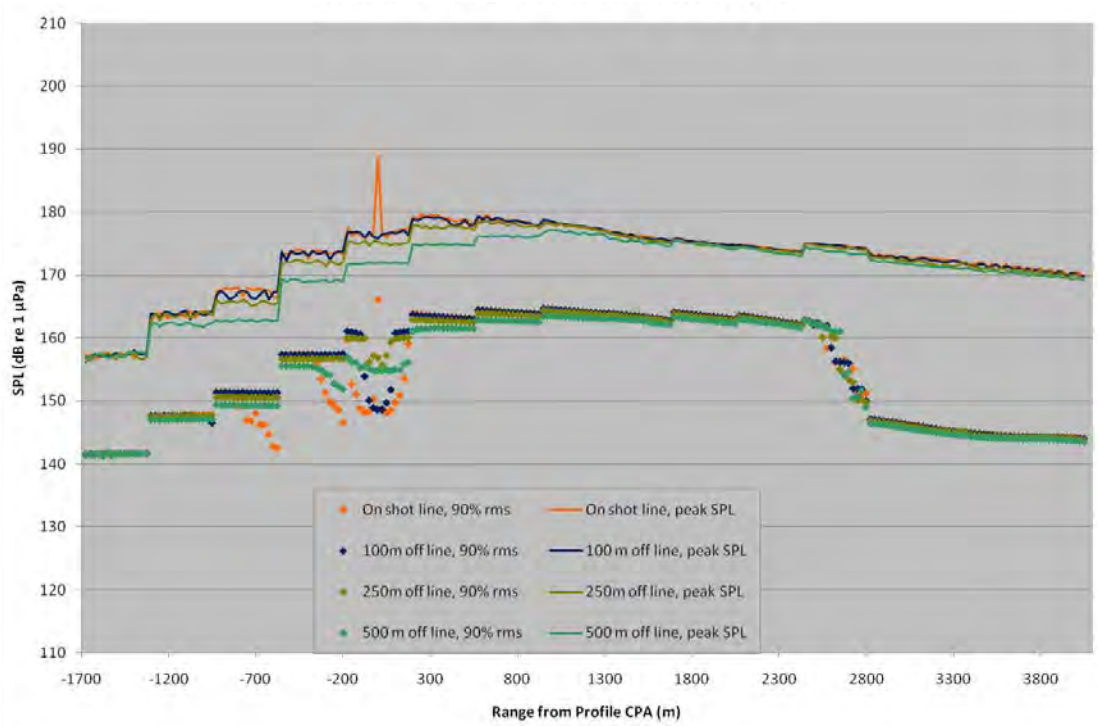

Figure 102: Peak SPL and 90% rms SPL for receivers on Profile 3 at 1900 m depth.

8 Discussion of Results

8.1 Overview of SEL results

The results presented in Section6 from parabolic equation acoustic model runs for receiver points at close lateral range from the source line in deep water are affected by modelling limitations that require them to be taken with caution as indicators of impact for marine mammals. There are caveats associated with their use as they might underestimate the levels that would be observed in practice under equivalent conditions. It is nonetheless possible to draw meaningful conclusions from this modelling study as long as the estimated levels are below the injury criteria by such a margin that it would be very unlikely that they would exceed them even accounting for possible errors. The shallow site results indicate that a greater fraction of cumulative sound exposure arises from source positions further from the receiver, where the parabolic equation model is believed accurate. Therefore the shallow site predictions of the parabolic equation models are thought to be accurate.

In terms of the SEL metric, the estimated cumulative level for an animal located just 100 m to the side of the source line at the midpoint of Step 1 of the soft-start in deep water are 22 dB below the Southall *et al*. (2007) criterion for cetaceans and 10 dB below the criterion for pinnipeds, without even introducing the M-weighting modifier that would decrease the level values.

For an animal that remains in the same fixed location 100 m to the side of the source line at the midpoint of Step 3 of the soft-start in deep water, the estimated cumulative SEL would still leave a margin of 13 dB for cetaceans though it would be just 1 dB below threshold for pinnipeds. Furthermore, these SEL estimates assume a worst-case situation where the animal remains in one geographic location while tracking vertically the maximum sound intensity along the water column. For the peak SPL metric all maxima observed at CPA during Steps 1–3 of the soft-start are below the Southall criteria thresholds by 29 dB for cetaceans and 17 dB for pinnipeds, again assuming a worst-case scenario where the animal is at the most strongly insonified depth. These results only considered contributions to SEL for source points during the soft-start procedure and not during the full array operations following soft-start. However, in deep water most SEL is accumulated from close-range source points so the full array operations, being at distance from the receiver locations considered here, are not expected to raise the total cumulative SEL significantly.

It can therefore be argued from this study that in a deep-water environment a marine mammal in the immediate vicinity of the airgun array in the first three steps of soft-start is unlikely to suffer from auditory injury according to the Southall criteria unless the animal passes within 100 m of the source line as the seismic array passes.

Shallow water sound level predictions at the same distance from the source line are greater than in deep water. The cumulative SEL level 100 m off the mid-point of Step 1 of soft start reaches 182 dB re 1 μPa^2s which is 17 dB below the PTS onset criterion threshold for cetaceans and 4 dB below the threshold for pinnipeds. For an animal that remains fixed at 100 m to the side of the source line at the mid-point of Step 3 of soft-start the maximum cumulative SEL is predicted to reach 185 dB 1 μPa^2s which is still 1 dB below the criterion threshold for PTS onset. As for the deep environment, the shallow site scenario modeling results suggest that PTS would only be exceeded if the animal remains stationary as the airgun array passes within less than 100 m from the animal at the 3rd Step of soft-start and while the vessel continues to complete the soft start procedure. We did not compute the additional SEL that would be received by the animal after the soft-start procedure completed, when full array operations would begin. Those sounds in shallow water could contribute significantly to the overall received cumulative SEL. However the animal would have had time to move away to reduce those exposures if sensed as disagreeable. Only exposures from the start to end of the soft-start procedure are considered in the analysis here.

8.2 Comparison of Parabolic Equation and Wavenumber Integral Model Results

The two acoustic models employed for the present study differ in the approach used to solve the acoustic wave equation but are expected to give near-identical transmission loss estimates for

regions where both are applicable. We do expect some difference in the computed airgun sound levels for the following reasons:

1. Far-field airgun array source levels computed in a horizontal plane were input to the parabolic equation model, while the wavenumber integral model uses individual notional airgun pressure signatures to compute the full 3-D directivity pattern including near-field effects.
2. The parabolic equation model treated a continuous sound speed profile in the water while the wavenumber integral model treated the water as a single homogeneous layer.
3. The parabolic equation model is not expected to produce accurate results for steep propagation angles below the horizontal. This would affect receivers directly below the airgun array and with propagation angles greater than 45° from horizontal.

The per-pulse and cumulative SEL levels can be compared directly for the 100 m depth receivers of Profiles 1, 2 and 3. These results from the parabolic equation model are shown in Figures 7, 9, and 11, respectively, while the corresponding wavenumber integral results are shown in Figures 72, 78, and 84, respectively.

Per-pulse SEL levels on Profile 1 for the on-line receiver at 100 m depth are predicted by both models to be maximal when the airgun array passes directly over the receiver (note this is not necessarily the case for deeper receivers during soft-start). The parabolic equation model predicts the maximum on-line per-pulse SEL at 100 m depth to be approximately 163 dB re 1 μPa^2s while the wavenumber integral predicts 159 dB re 1 μPa^2s. The model differences at 100 m depth decrease with increasing off-line distance; at 500 m off-line the model predictions differ by less than 2 dB. The per-pulse model predictions for Profile 1 at 100 m depth agree fairly well at all off-line distances until the source has moved past Profile 1 by approximately 3 km, with the wavenumber integral model consistently giving levels approximately 2 dB less than the parabolic equation model. The cumulative SEL increases negligibly once the source is beyond 3 km away. At that time the predicted cumulative levels are approximately 175 and 172 dB re 1 $\mu Pa^2 \cdot s$ for the parabolic equation and wavenumber integral models, respectively.

Literature Cited

Brekhovskikh, L.M. 1980, *Waves in Layered Media*, 2nd Edition. Academic Press, New York.

Collins, M.D. 1993. A split-step Padé solution for the parabolic equation method. *J. Acoust. Soc. Am*. 93(4):1736-1742.

Collins, M.D., R.J. Cederberg, D.B. King, and S.A. Chin-Bing. 1996. Comparison of algorithms for solving parabolic wave equations. *J. Acoust. Soc. Am.* 100(1): 178-182.

Dragoset, W.H. 1984. A comprehensive method for evaluating the design of airguns and airgun arrays. *16th Annual Proc. Offshore Tech. Conf*. 3:75-84.

Frisk, G.V. 1994. *Ocean and Seabed Acoustics: A Theory of Wave Propagation*. Prentice Hall, Englewood Cliffs, New Jersey.

Gentry, R., A. Bowles, W. Ellison, J. Finneran, C. Greene, D. Kastak, D. Ketten, J. Miller, P. Nachtigall, W.J. Richardson, B. Southall, J. Thomas and P. Tyack. 2004. Noise exposure criteria. Presentation to U.S. Mar. Mamm. Commis. Advis. Commit

Greene, C.R., Jr. 1997. Physical acoustics measurements. pp. 3-1 to 3-63 *In:* W.J. Richardson (ed.), *Northstar Marine Mammal Monitoring Program, 1996: Marine Mammal and Acoustical Monitoring of a Seismic Program in the Alaskan Beaufort Sea*. LGL Rep. 2121-2. Rep. from LGL Ltd., King City, ON, and Greeneridge Sciences Inc., Santa Barbara, CA, for BP Explor. (Alaska) Inc., Anchorage, AK, and Nat. Mar. Fish. Serv., Anchorage, AK, and Silver Spring, MD. 245 p.

Jensen, F.B., W.A. Kuperman, M.B. Porter and H. Schmidt. 1993. *Computational Ocean Acoustics*. Springer-Verlag, New York.

Landro, M. 1992. Modeling of GI gun signatures. *Geophysical Prospecting*, 40(7):721-747.

Laws, M., L. Hatton, and M. Haartsen. 1990. Computer modeling of clustered airguns. *First Break*, 8(9):331–338.

MacGillivray, A.O. 2006. *An Acoustic Modelling Study of Seismic Airgun Noise in Queen Charlotte Basin.* M.Sc. Thesis. University of Victoria, Victoria, BC.

MacGillivray, A.O., M.M. Zykov, and D.E. Hannay. 2007. Chapter 3: Summary of Noise Assessment. *In: Marine Mammal Monitoring and Mitigation During Open Water Seismic Exploration by ConocoPhillips Alaska, Inc. in the Chukchi Sea July-October 2006*. Report by LGL Alaska Research Associates and JASCO Research Ltd.

Malme, C.I., P.W. Smith, and P.R. Miles. 1986. *Characterisation of Geophysical Acoustic Survey Sounds*. Prepared by BBN Laboratories Inc., Cambridge, for Battelle Memorial Institute to the Minerals Management Service, Pacific Outer Continental Shelf Region, Los Angeles, CA.

McCauley, R.D., M.-N. Jenner, C. Jenner, K.A. McCabe, and J. Murdoch. 1998. The response of humpback whales (*Megaptera novaeangliae*) to offshore seismic survey noise: preliminary results of observations about a working seismic vessel and experimental exposures. *APPEA J.—Austral. Petrol. Prod. & Explor. Assoc. J.* 38:692-707.

Miller, J.H., A.E. Bowles, B.L. Southall, R.L. Gentry, W.T. Ellison, J.J. Finneran, C.R. Greene, Jr., D. Kastak, D.R. Ketten, P.L. Tyack, P.E. Nachtigall, W.J.Richardson and J.A. Thomas. 2005. Strategies for weighting exposure in the development of acoustic criteria for marine mammals. *J. Acoust. Soc. Am*. 118:2019 (Abstract). Presentation available at: http://www.oce.uri.edu/faculty_pages/miller/Noise_Weighting_10_18_2005.ppt

Racca, R.G. and J.A. Scrimger. 1986. *Underwater Acoustic Source Characteristics of Air and Water Guns*. Report by JASCO Research Ltd., Victoria, BC, for DREP Contract No. 06SB 97708-5-7055.

Southall, B.L., A.E. Bowles, W.T. Ellison, J.J. Finneran, R.L. Gentry, C.R. Greene Jr., D. Kastak, D.R. Ketten, J.H. Miller, P.E. Nachtigall, W.J. Richardson, J.A. Thomas, and P.L. Tyack. 2007. Marine Mammal Noise Exposure Criteria: Initial Scientific Recommendations. *Aquatic Mammals* 33(4).

Teague, W.J., M.J. Carron, and P.J. Hogan. 1990. A comparison between the generalized digital environmental model and Levitus climatologies. *J. Geophys. Res.* 95(C5):7167–7183.

Zhang, Z. and C. Tindle. 1995. Improved equivalent fluid approximations for a low shear speed ocean bottom. *J. Acoust. Soc. Am.* 98:3391-3396.

Ziolkowski, A. 1970. A method for calculating the output pressure waveform from an air gun. *Geophys. J. R. Astr. Soc*. 21:137–161.

Appendix A: Per-Pulse and Cumulative M-Weighted SEL from WaveNumber Integral Model at Deep Site

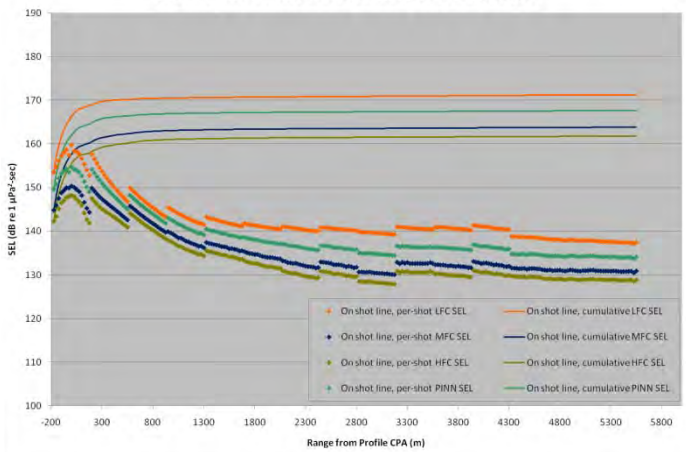

Figure A1: Per-pulse and cumulative M-weighted SEL for on-source-line receivers on Profile 1 at 100 m depth.

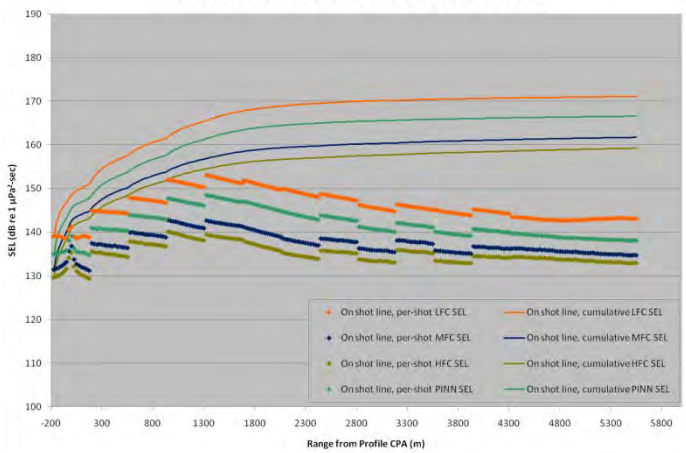

Figure A2: Per-pulse and cumulative M-weighted SEL for on-source-line receivers on Profile 1 at 1000 m depth.

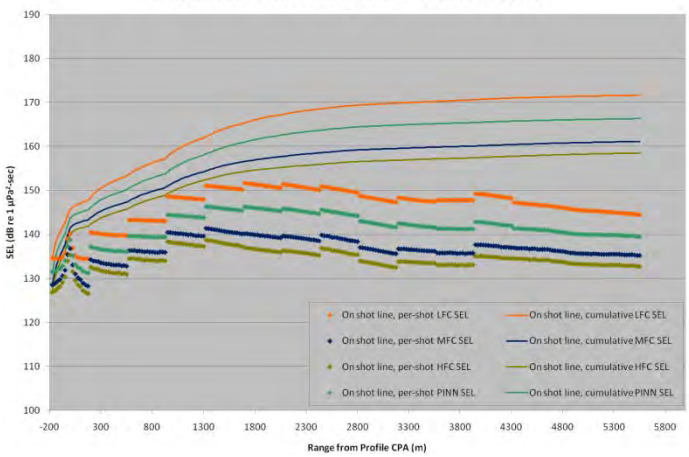

Figure A3: Per-pulse and cumulative M-weighted SEL for on-source-line receivers on Profile 1 at 1900 m depth.

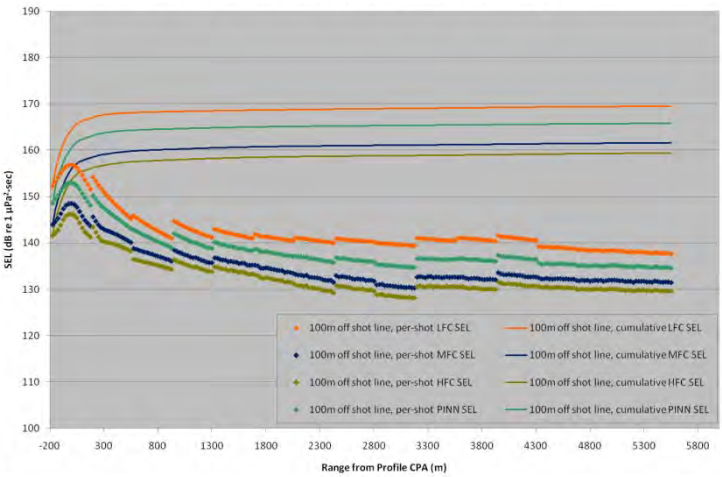

Figure A4: Per-pulse and cumulative M-weighted SEL for 100 m off-source-line receivers on Profile 1 at 100 m depth.

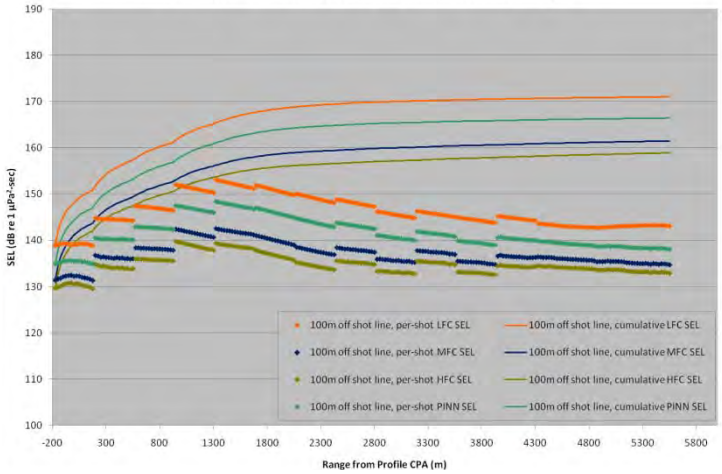

Figure A5: Per-pulse and cumulative M-weighted SEL for 100 m off-source-line receivers on Profile 1 at 1000 m depth.

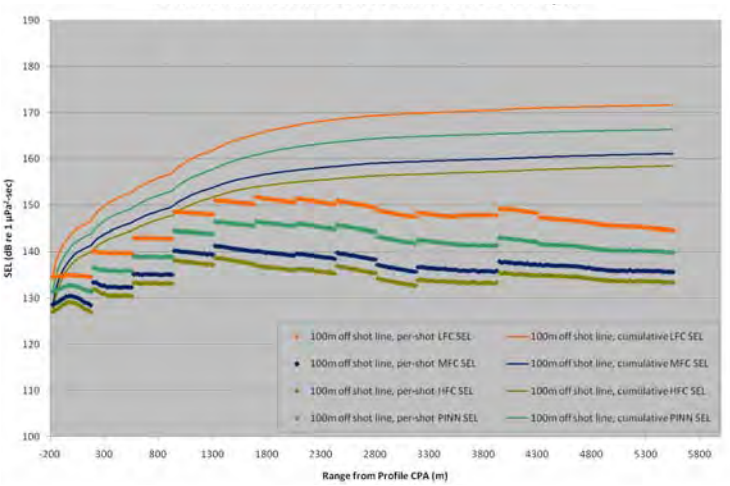

Figure A6: Per-pulse and cumulative M-weighted SEL for 100 m off-source-line receivers on Profile 1 at 1900 m depth.

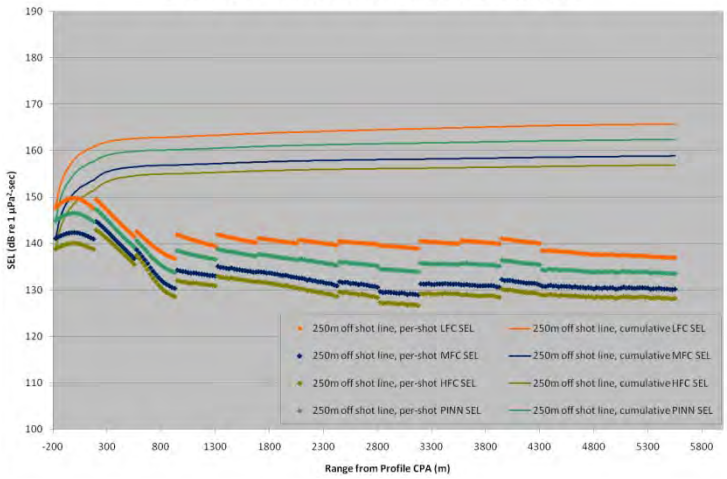

Figure A7: Per-pulse and cumulative M-weighted SEL for 250 m off-source-line receivers on Profile 1 at 100 m depth.

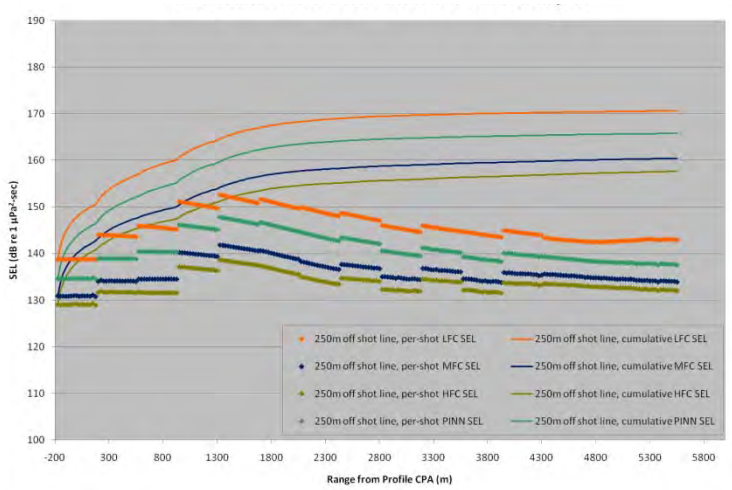

Figure A8: Per-pulse and cumulative M-weighted SEL for 250 m off-source-line receivers on Profile 1 at 1000 m depth.

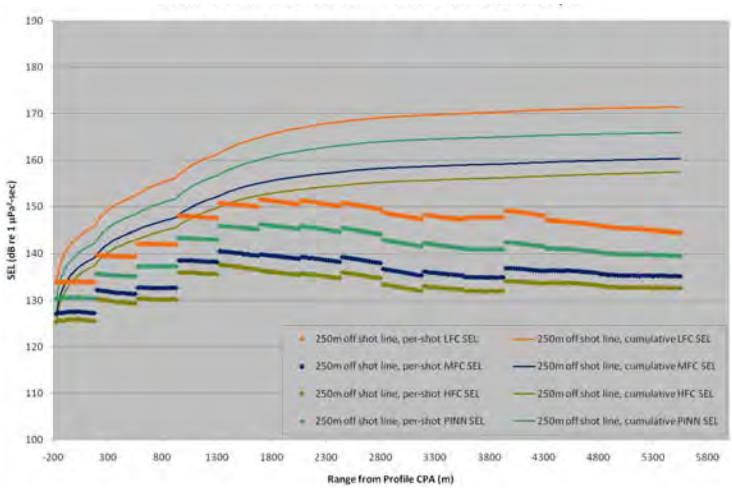

Figure A9: Per-pulse and cumulative M-weighted SEL for 250 m off-source-line receivers on Profile 1 at 1900 m depth.

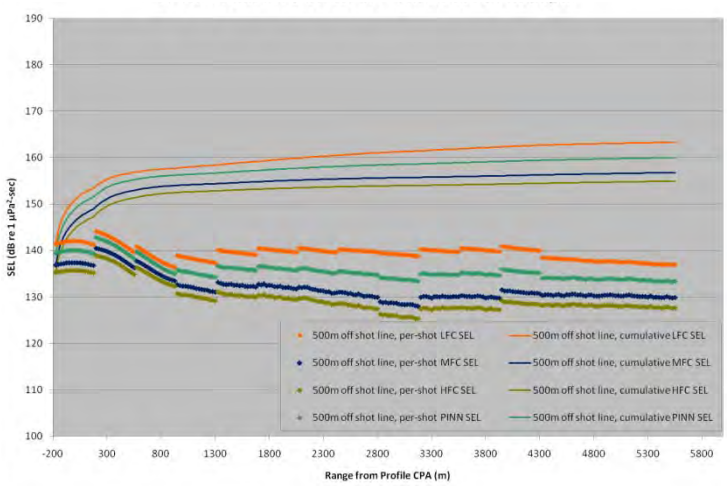

Figure A10: Per-pulse and cumulative M-weighted SEL for 500 m off-source-line receivers on Profile 1 at 100 m depth.

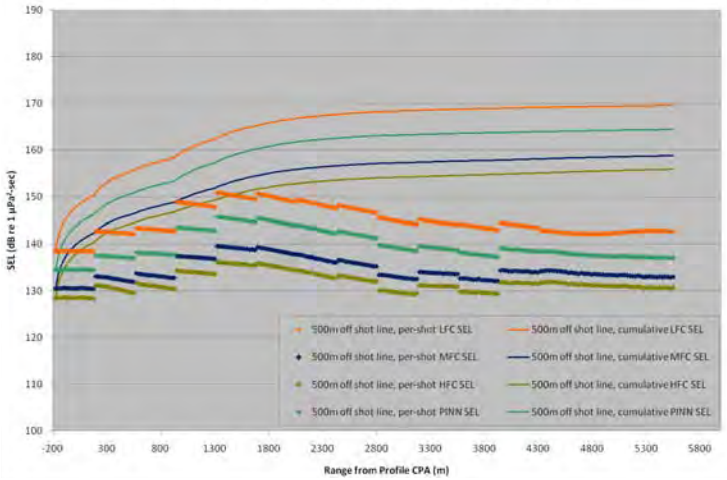

Figure A11: Per-pulse and cumulative M-weighted SEL for 500 m off-source-line receivers on Profile 1 at 1000 m depth.

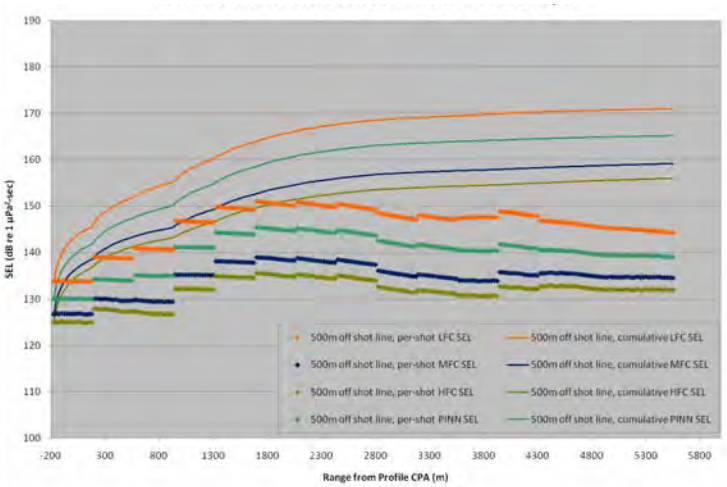

Figure A12: Per-pulse and cumulative M-weighted SEL for 500 m off-source-line receivers on Profile 1 at 1900 m depth.

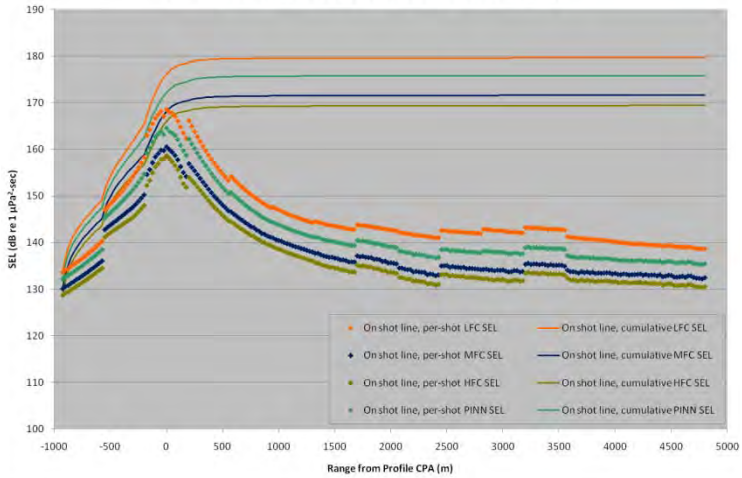

Figure A13: Per-pulse and cumulative M-weighted SEL for on-source line receivers on Profile 2 at 100 m depth.

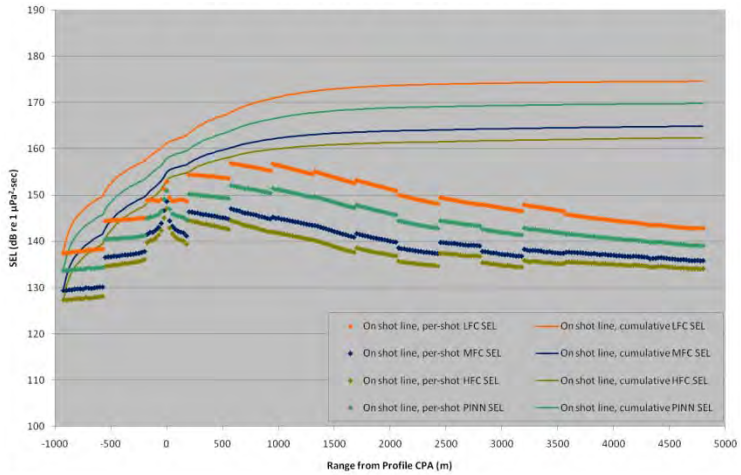

Figure A14: Per-pulse and cumulative M-weighted SEL for on-source-line receivers on Profile 2 at 1000 m depth.

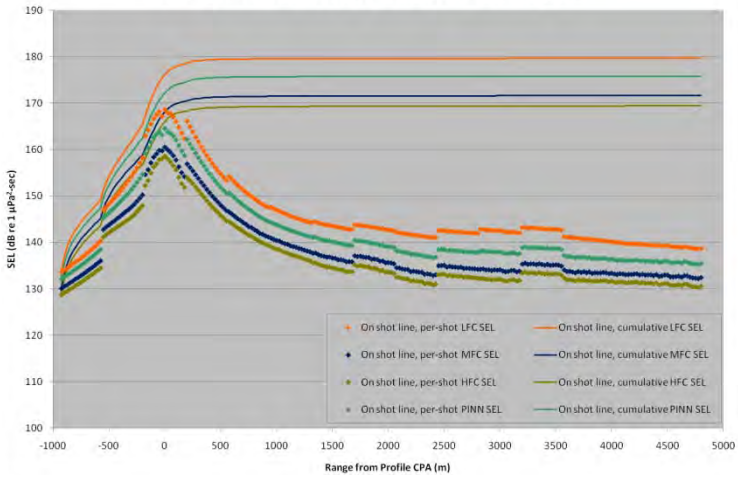

Figure A15: Per-pulse and cumulative M-weighted SEL for on-source-line receivers on Profile 2 at 1900 m depth.

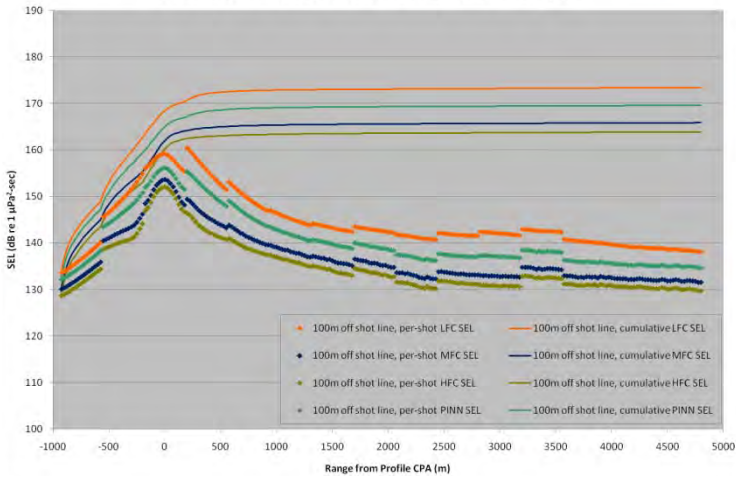

Figure A16: Per-pulse and cumulative M-weighted SEL for 100 m off-source-line receivers on Profile 2 at 100 m depth.

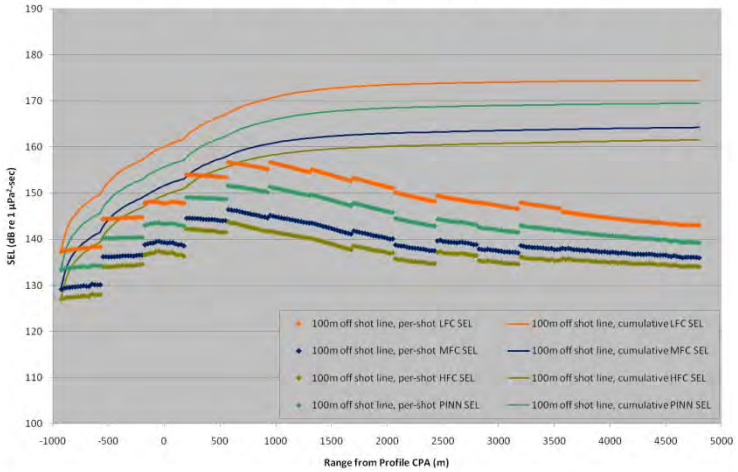

Figure A17: Per-pulse and cumulative M-weighted SEL for 100 m off-source-line receivers on Profile 2 at 1000 m depth.

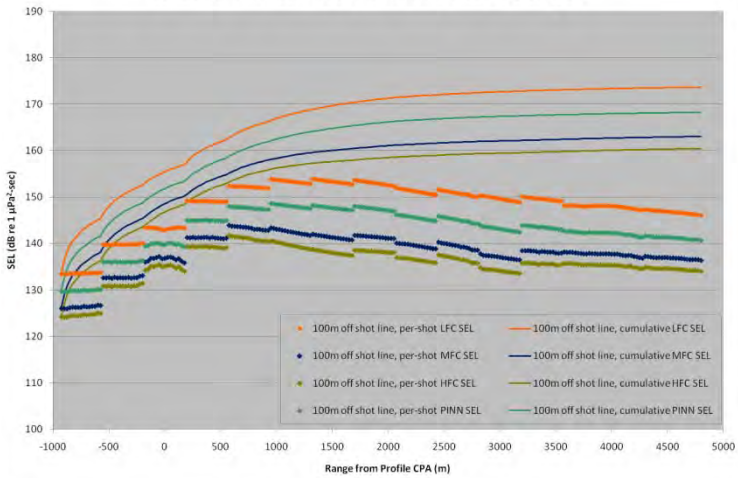

Figure A18: Per-pulse and cumulative M-weighted SEL for 100 m off-source-line receivers on Profile 2 at 1900 m depth.

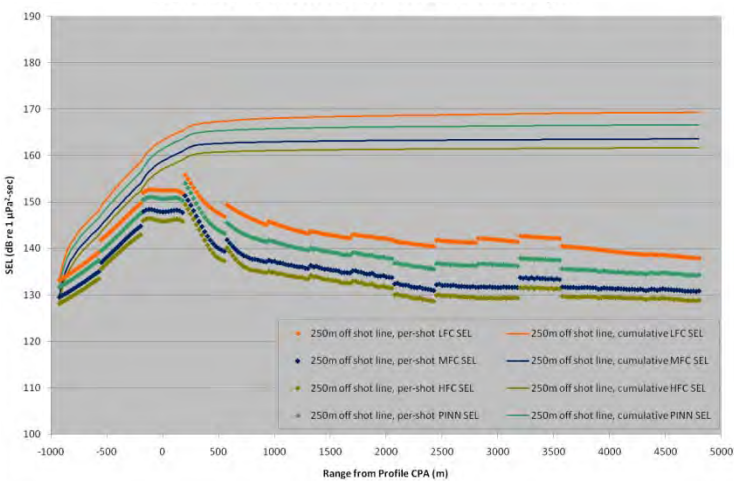

Figure A19: Per-pulse and cumulative M-weighted SEL for 250 m off-source-line receivers on Profile 2 at 100 m depth.

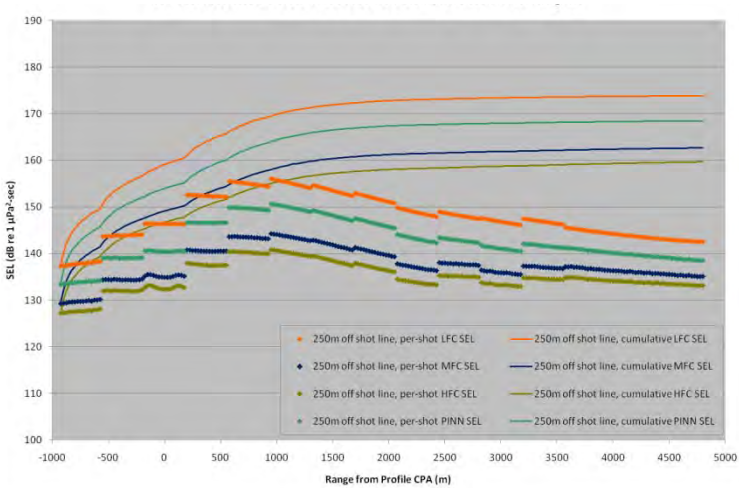

Figure A20: Per-pulse and cumulative M-weighted SEL for 250 m off-source-line receivers on Profile 2 at 1000 m depth.

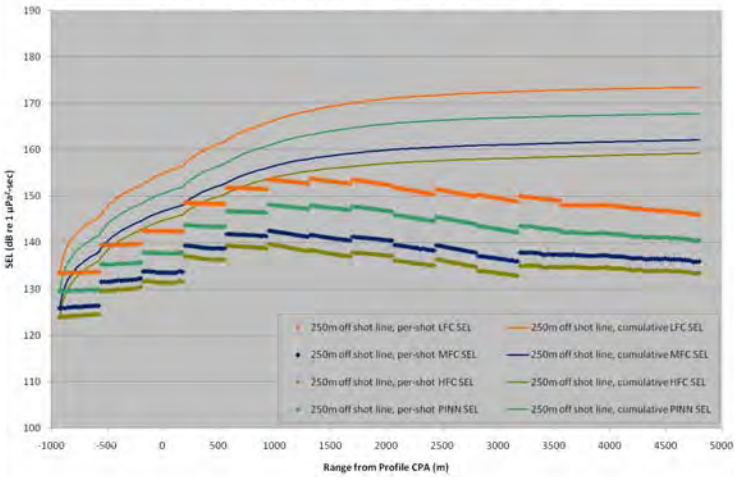

Figure A21: Per-pulse and cumulative M-weighted SEL for 250 m off-source-line receivers on Profile 2 at 1900 m depth.

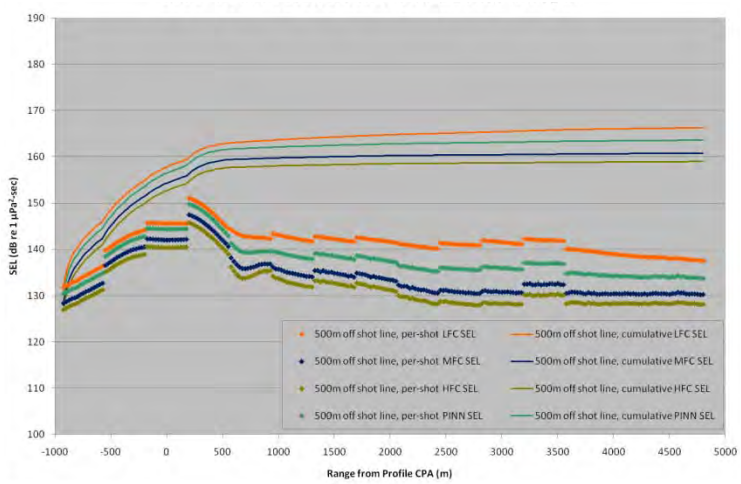

Figure A22: Per-pulse and cumulative M-weighted SEL for 500 m off-source-line receivers on Profile 2 at 100 m depth.

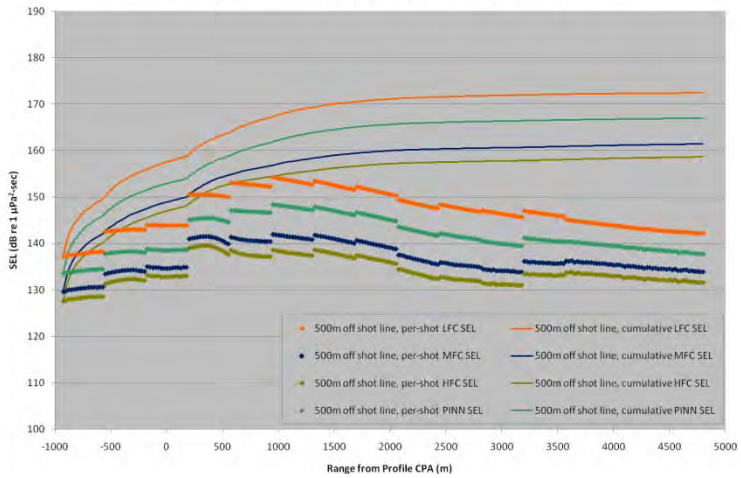

Figure A23: Per-pulse and cumulative M-weighted SEL for 500 m off-source-line receivers on Profile 2 at 1000 m depth.

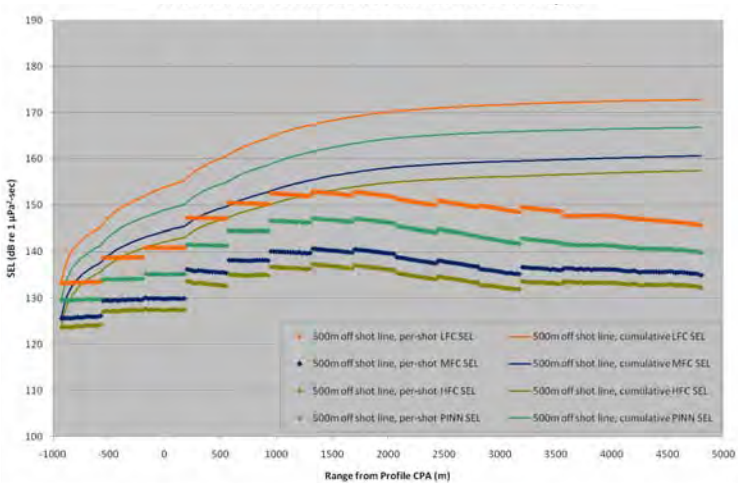

Figure A24: Per-pulse and cumulative M-weighted SEL for 500 m off-source-line receivers on Profile 2 at 1900 m depth.

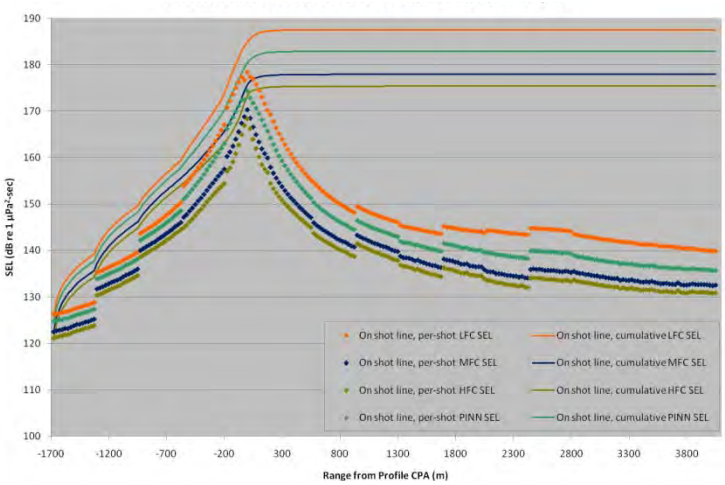

Figure A25: Per-pulse and cumulative M-weighted SEL for on-source-line receivers on Profile 3 at 100 m depth.

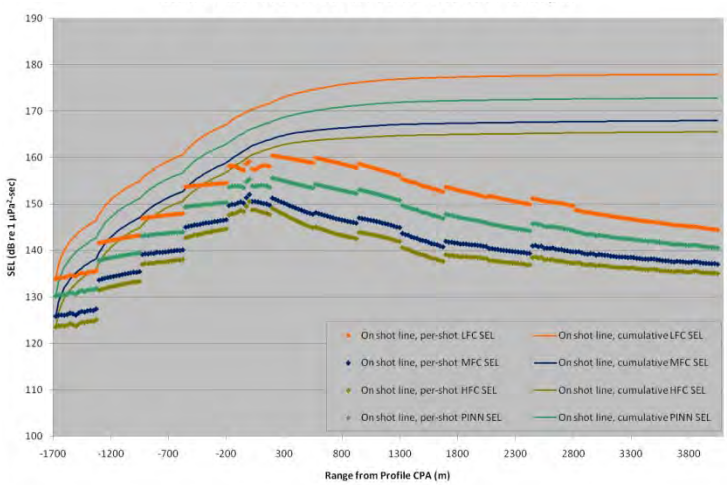

Figure A26: Per-pulse and cumulative M-weighted SEL for on-source-line receivers on Profile 3 at 1000 m depth.

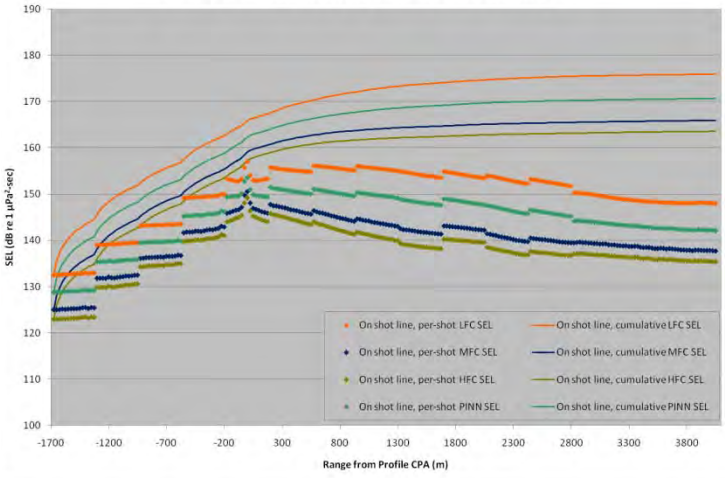

Figure A27: Per-pulse and cumulative M-weighted SEL for on source line receivers on Profile 3 at 1900 m depth.

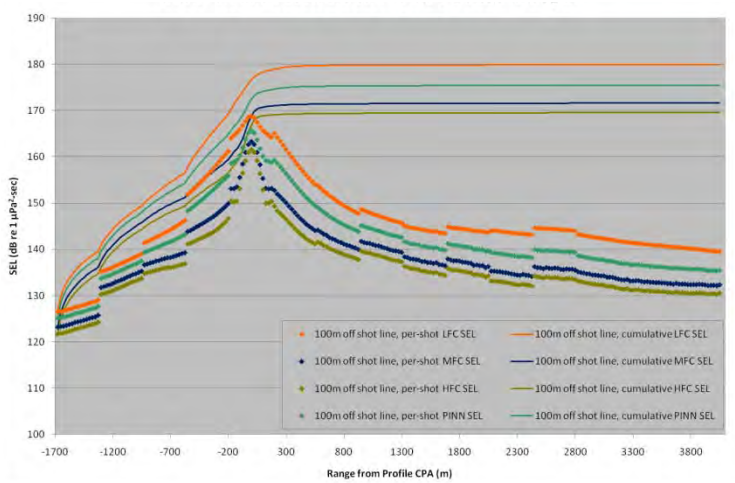

Figure A28: Per-pulse and cumulative M-weighted SEL for 100 m off-source-line receivers on Profile 3 at 100 m depth.

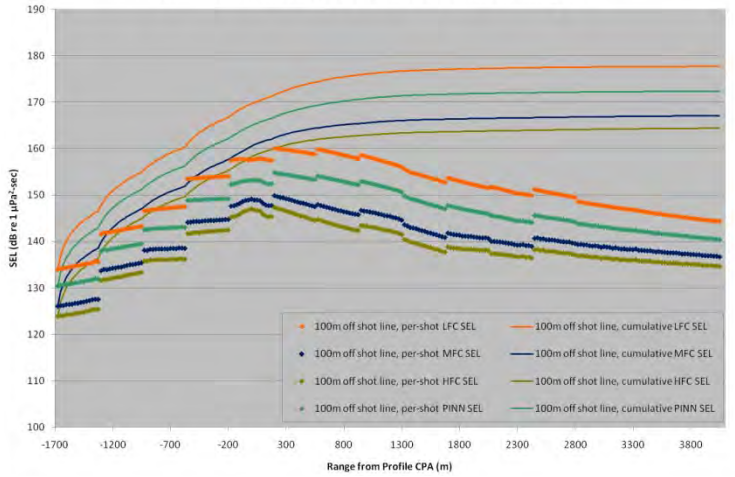

Figure A29: Per-pulse and cumulative M-weighted SEL for 100 m off-source-line receivers on Profile 3 at 1000 m depth.

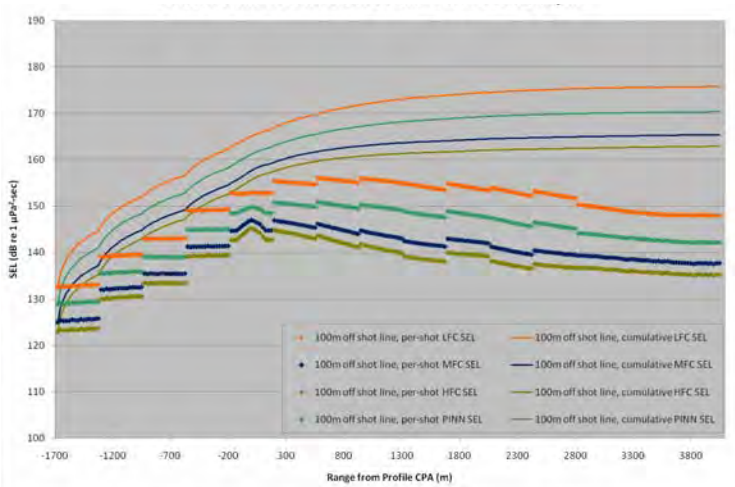

Figure A30: Per-pulse and cumulative M-weighted SEL for 100 m off-source-line receivers on Profile 3 at 1900 m depth.

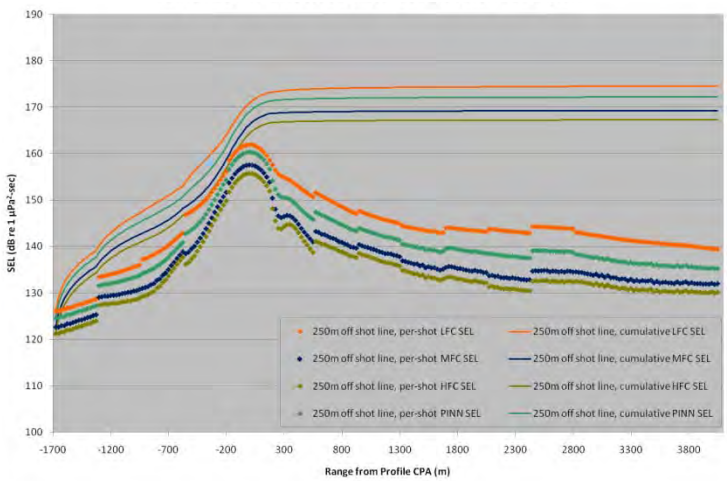

Figure A31: Per-pulse and cumulative M-weighted SEL for 250 m off-source-line receivers on Profile 3 at 100 m depth.

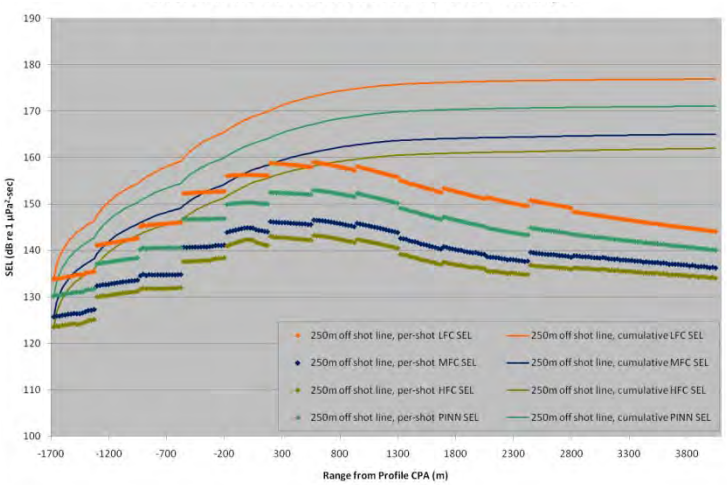

Figure A32: Per-pulse and cumulative M-weighted SEL for 250 m off-source-line receivers on Profile 3 at 1000 m depth.

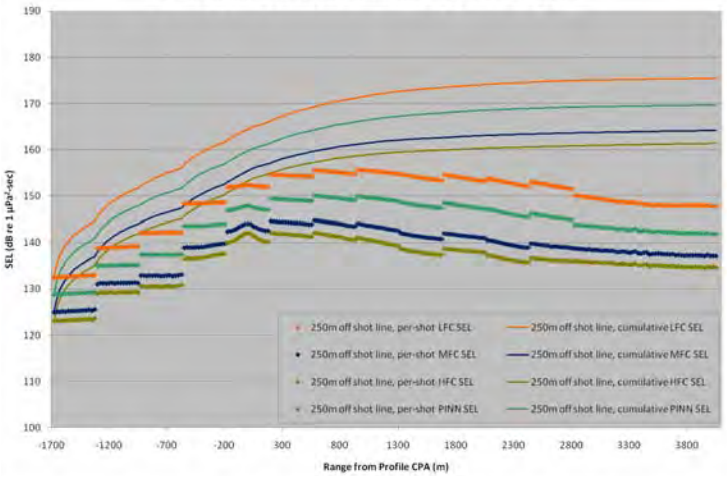

Figure A33: Per-pulse and cumulative M-weighted SEL for 250 m off-source-line receivers on Profile 3 at 1900 m depth.

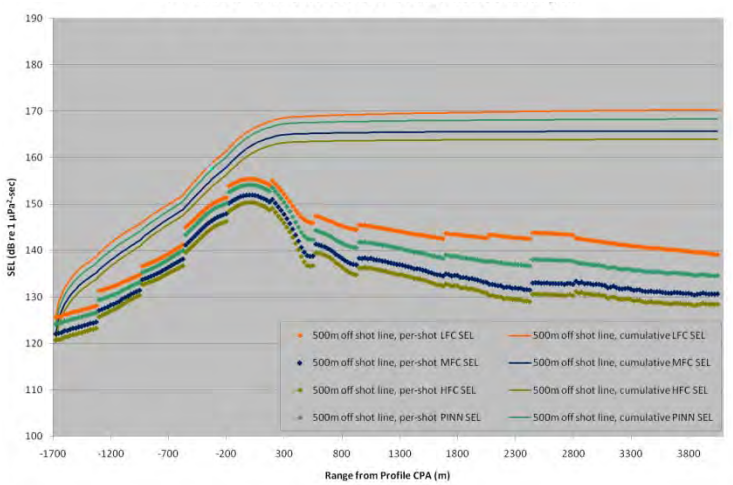

Figure A34: Per-pulse and cumulative M-weighted SEL for 500 m off-source-line receivers on Profile 3 at 100 m depth.

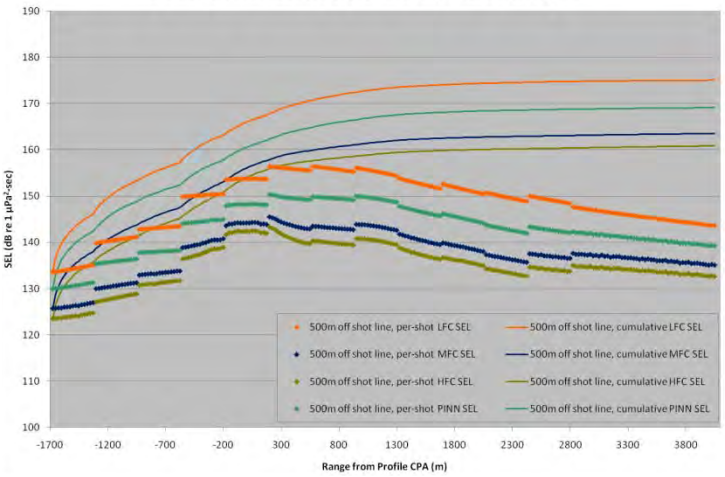

Figure A35: Per-pulse and cumulative M-weighted SEL for 500 m off-source-line receivers on Profile 3 at 1000 m depth.

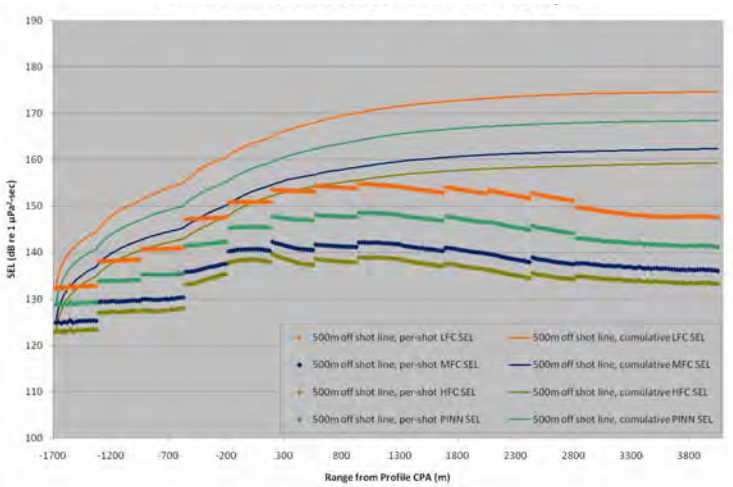

Figure A36: Per-pulse and cumulative M-weighted SEL for 500 m off-source-line receivers on Profile 3 at 1900 m depth.

For further information and publications,
please visit our website at

www.ogp.org.uk

International Association of Oil & Gas Producers

209-215 Blackfriars Road
London SE1 8NL
United Kingdom
Telephone: +44 (0)20 7633 0272
Fax: +44 (0)20 7633 2350

165 Bd du Souverain
4th Floor
B-1160 Brussels, Belgium
Telephone: +32 (0)2 566 9150
Fax: +32 (0)2 566 9159

Internet site: www.ogp.org.uk
e-mail: reception@ogp.org.uk